Aalborg Universitet

AALBORG UNIVERSITY

Photovoltaic Array Reconfiguration under Partial Shading Conditions for Maximum Power Extraction

A State-of-the-Art Review and New Solution Method

Rezazadeh, Sevda ; Moradzadeh, Arash ; Pourhossein , Kazem ; Akrami, Mohammadreza ; Mohammadi-Ivatloo, Behnam ; Anvari-Moghaddam, Amjad

Published in:
Energy Conversion and Management

DOI (link to publication from Publisher):
10.1016/j.enconman.2022.115468

Creative Commons License
CC BY-NC-ND 4.0

Publication date:
2022

Document Version
Accepted author manuscript, peer reviewed version

Link to publication from Aalborg University

Citation for published version (APA):
Rezazadeh, S., Moradzadeh, A., Pourhossein , K., Akrami, M., Mohammadi-Ivatloo, B., & Anvari-Moghaddam, A. (2022). Photovoltaic Array Reconfiguration under Partial Shading Conditions for Maximum Power Extraction: A State-of-the-Art Review and New Solution Method. *Energy Conversion and Management*, *258*, 1-36. Article 115468. https://doi.org/10.1016/j.enconman.2022.115468

General rights
Copyright and moral rights for the publications made accessible in the public portal are retained by the authors and/or other copyright owners and it is a condition of accessing publications that users recognise and abide by the legal requirements associated with these rights.

- Users may download and print one copy of any publication from the public portal for the purpose of private study or research.
- You may not further distribute the material or use it for any profit-making activity or commercial gain
- You may freely distribute the URL identifying the publication in the public portal -

Take down policy
If you believe that this document breaches copyright please contact us at vbn@aub.aau.dk providing details, and we will remove access to the work immediately and investigate your claim.

Downloaded from vbn.aau.dk on: May 23, 2026

Photovoltaic Array Reconfiguration under Partial Shading Conditions by Novel 8-Queen's Technique to Maximum Power Extraction: A State-of-the-Art Solution

Sevda Rezazadeh[1], Arash Moradzadeh[2], Kazem Pourhossein[1], Mohammadreza Akrami[1], Behnam Mohammadi-Ivatloo[3,4*], Amjad Anvari-Moghaddam[3]

[1]Department of Electrical Engineering, Tabriz Branch, Islamic Azad University, Tabriz, Iran
[2]Faculty of Electrical and Computer Engineering, University of Tabriz, 5166616471 Tabriz, Iran
[3]Department of Energy (AAU Energy), Aalborg University, 9220 Aalborg, Denmark
stu.sevdarezazadeh@iaut.ac.ir, arash.moradzadeh@tabrizu.ac.ir, k.pourhossein@iaut.ac.ir, akrami.mreza.eng@gmail.com, mohammadi@ieee.org, aam@energy.aau.dk
[*]Corresponding author: Behnam Mohammadi-Ivatloo

Abstract: Non-uniform irradiance due to partial shading conditions (PSCs) reduces the power delivered by the photovoltaic (PV) cell. The output power reduction in the PV arrays directly depends on the shading pattern and type of array configuration which is selected. So far, many dynamic and static reconfiguration methods have been used for maximum power point tracking under PSCs in the PV arrays. However, most conventional methods suffer from some major problems such as the need for additional equipment and sensors, complex wiring, the use of expensive sensors, production of complex switching matrices, high costs, and inability to reconfigure PV arrays with very small, large, and non-square sizes. Accordingly, this paper, after reviewing the dynamic and static PV array reconfiguration methods, presents a novel static-based technique called 8-Queen's for reconfiguring the PV modules corresponding to the Total-Cross-Tied (TCT) inter-connection PV array. The 8-Queen's technique has a great ability to apply on high dimensions and rectangular shapes PV arrays and is based on the movement of 8 queens on the chessboard so that none of the queens can attack the others. The effectiveness of the suggested method is expressed by implementing it on 7 cases of the TCT PV array in different sizes and various PSCs. In a comparative scenario, the performance and effectiveness of the proposed 8-Queen's technique are evaluated compared to other conventional methods. Indicators of global maximum power point (GMPP), fill factor, power efficiency, and mismatch losses evaluate the results of the employed methods. The evaluation of results and reaching the high values of the GMPP i.e. $22.2V_mI_m, 22.2V_mI_m, 67.5V_mI_m, 66.6V_mI_m, 126V_mI_m, 346V_mI_m$, and $8.1V_mI_m$, respectively, for cases 1 to 7 represent the effectiveness of the 8-Queen's technique compared to other used methods. In addition, the performance evaluation of the proposed technique in real-world PV arrays is performed by modeling a sample PV array taking into account measurement errors. The results in this step also show that the proposed technique can also provide acceptable performance for solving problems related to maximum power point tracking under PSCs in PV systems.

Keywords-Photovoltaic array, maximum power point tracking (MPPT), reconfiguration, partial shading condition (PSC), 8-Queen's technique

Abbreviations		n	Number of columns
PV	Photovoltaic	u_{m-n}	Ascending diameters
PSC	Partial shade condition	d_{m+n}	Descending diameters
MPPT	Maximum power point tracking	$U_{cnt(p)}$	Queen's in ascending diameters
TCT	Total-Cross-Tied	$D_{cnt(q)}$	Queen's in descending diameters
GMPP	Global maximum power point	j	Column index, and
S	Series	$G_{1,j}$	Irradiance in the panel labeled $1j$
P	Parallel	G_0	Full irradiance
SP	Series-Parallel	I_{1j}	Limited current for full irradiance of the panel labeled $1j$
EAR	Electrical array reconfiguration	I_m	The PV module's current
FF	Fill factor	P_m	Maximum extracted power
BL	Bridged-Linked	V_{OC}	Open-circuit voltage
ANNs	Artificial neural networks	I_{SC}	Short circuit current
STC	Standard test condition	η	Power efficiency
ML	Mismatch loss	P_{in}	Solar energy input
Variables		MPP_{uni}	Maximum power under uniform radiation
R_m	Queen in the m^{th} row	$GMPP_{PSCs}$	GMPP under PSCs
C_n	Queen in the n^{th} column	I_{1n}	The current limit in full radiation
m	Number or rows		

1. Introduction

Increasing energy demand and environmental awareness have led to increased electricity generation from renewable energy sources in recent years [1]. In many developed countries, renewable energy has become a very suitable replacement for fossil fuels. Global statistics represent that the average global energy growth rate in the past decade has been 5.4% [2]. Among renewable energy sources, solar energy is one of the most important energies that in addition to sustainability, is also environmentally compatible. Thus, the production of electricity from solar energy on a large scale has become one of the important goals of the 21st century [3]. This can be achieved by a technology that converts sunlight directly into electrical

energy. This process is done through a photoelectric effect technology in the Photovoltaic (PV) array [4]. The technology of using the PV panels to generate energy over other renewable energy sources has advantages such as low installation costs, easy transportation, usable in various places, and most importantly without environmental pollution [5]. Despite these advantages, a PV system sometimes suffers from physical and electrical defects such as arc faults, hot spots, line-to-line faults, open circuit faults, converter switch faults, and shaded faults [6]. In the meantime, the mismatch phenomena is a common damage condition in most PV systems that causes to reduce the extraction of productive power in the PV array. The mismatch phenomenon is caused by cracking of the module or due to the difference in radiation received by the PV modules [7]. The occurrence of this phenomenon in a PV array can have losses such as the difference between the maximum power of a PV array and the sum of the maximum power of its modules [8]. Given that solar energy is received by one surface per square meter, the mismatch caused by changes in the radiation level in the PV array is called partial shading. Static and dynamic shadows are considered as two types of shadow conditions. Static shading occurs due to the accumulation of dust, tree leaves, floating clouds, and birds sitting on glass. But, permanent conditions such as the shade of trees and surrounding buildings are creating a dynamic shade. Figure 1 illustrates examples of partial shading on the PV arrays. As shown in Figure 2, the occurrence of either of these two states over time has unique effects on the characteristic curves of the PV array and maximum power point. In addition, the stability of partial shade condition (PSC) can cause other serious damage to internal equipment such as open or short-circuited diodes in the PV array [9]. Thus, when a string is subjected to PSC, the modules that cannot supply the string current are short-circuited by bypass diodes. In terms of PSC losses, for example, a loss of 5-10% of PV energy in countries such as Germany and Japan, and also about 4% for Spain has been reported in [10].

Figure 1. PV arrays under PSC

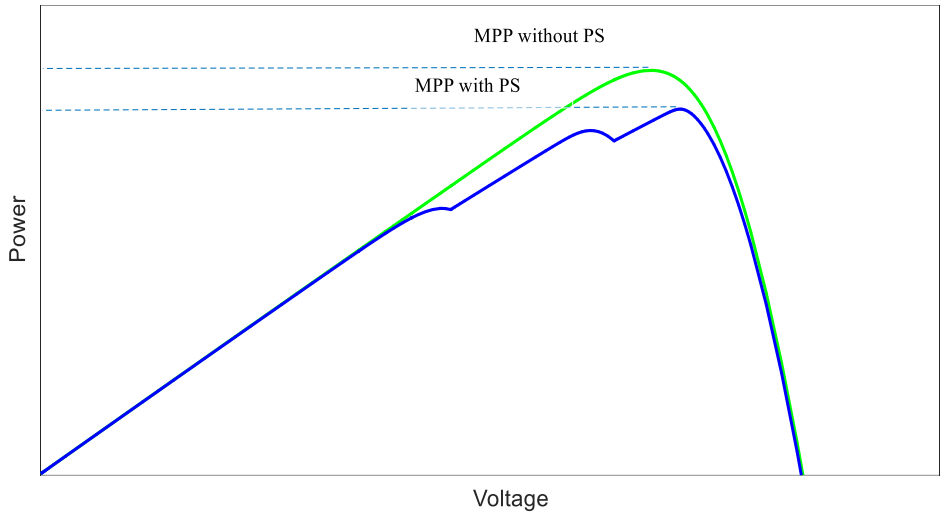

Figure 2. Effect of PSC on the maximum power point

Today, maximum power point tracking (MPPT) and achieving the maximum power output of the PV arrays in dealing with these issues have posed many challenges in this field for researchers and craftsmen. Solutions to deal with the aforementioned problems caused by the PSC in the PV arrays are divided into two categories of passive and active techniques. Each of these techniques has details that have been studied in various studies. In the description of the passive technique, can be referred to the use of the bypass diodes and different types of connections for PV modules for reducing the partially shaded losses. Total-Cross-Tied (TCT), Honey Comb, Bridge-Link (BL), and Series-Parallel (SP) are some of the most common types of connection models for the PV modules [11,12]. Figure 3 shows the interconnections between PV modules by each of these models. The results presented in various studies have shown the ability and efficiency of the TCT model connection in extracting maximum power compared to other connection models [13].

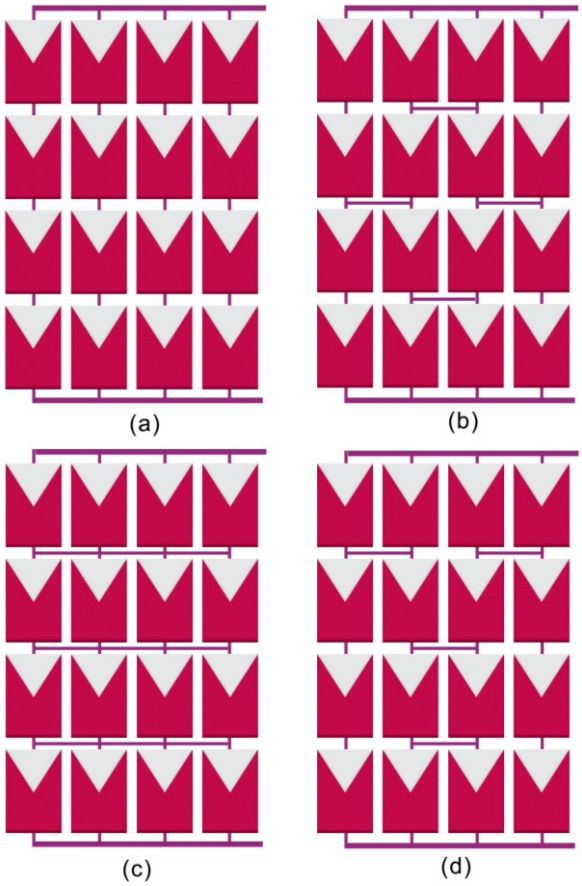

Figure 3. Various interconnections between PV modules: (a) SP arrangement; (b) BL arrangement; (c) TCT arrangement; (d) Honey Comb arrangement

Active techniques for PSC fall into three categories, each with its advantages and disadvantages:

- Utilizing multi-tracker converters
- Utilizing micro converters
- Reconfiguration of PV arrays

The technique of utilizing multi-track converters tracks the maximum power point with the same shading independently for each set of the PV arrays. The use of a large number of converters in this technique makes it expensive [14]. The technique of utilizing micro converters is also an expensive method, but employing this solution leads to the high energy efficiency of the PV array [15]. Finally, utilizing the PV array reconfiguration method, modules related to a PV array can be configured by the switches between them. This method can be mainly employed for the TCT and SP connection models. This method is economically viable and has been able to extract high energy efficiency in the PSC of the PV array. Reconfiguration of the PV array eliminates the effect of mismatch losses under partial shadow conditions of the PV array in extracting maximum power and also achieving maximum energy efficiency [16]. In general, reconfiguration techniques are divided into two categories: dynamic and static techniques. In dynamic or electrical array reconfiguration (EAR) techniques, the modules are dynamically configured inside the PV array to extract the maximum output power under PSC. Static techniques that refer to the physical displacement of modules follow a fixed connection scheme, in which the modules are displaced in the PV array without changing the electrical connections. Static techniques do not require any sensors or switching matrices. Applying these

techniques to distribute shadows on a PV array is possible by using a reconfiguration pattern [13,17].

So far, many valuable studies have been performed to track the maximum power point of a PV array under PSCs using these techniques. In [18], authors have reviewed all the static and dynamic techniques related to PV panels reconfiguration under PSCs and provided an overview of them. Performance evaluation of each of the available methods is one of the obvious achievements of that study. The valuable work of [19] based on a thorough review of 125 recently published papers provides a comprehensive figure of new PV array reconfiguration methods. In the same study, a comprehensive classification has been performed in which sixty-four methods are fully classified into nine groups and nine evaluation criteria are summarized. In addition, a comprehensive comparison based on ten specific indicators, such as complexity, response speed, monitor variables, shadow dispersion rate, and range of application is presented. Finally, the optimal performance and effectiveness of static methods are shown due to faster response speed and high compatibility. For example, concerning dynamic techniques, one can refer to the basic studies such as [20] and [21] that have provided an EAR controller for changing the electrical connections between PV modules based on the radiation level to provide input current to the motor. In [22], an irradiance equalization algorithm has been utilized to control a PV system by the EAR technique. Based on the proposed algorithm, each PV module can connect with any of the array rows. The technique proposed in that paper was performed on a small-scale grid-connected PV system of 1.65 kWp, which shows the results of the feasibility of the approach and also the ideal power delivery under PSCs in the PV array. In [23], the increase in energy conversion for a 4×4 PV array under PSCs has been performed by reconfiguration of shaded arrays using a novel dynamic-based reconfiguration method called the L-shaped propagated array configuration. In [24], an analytical procedure for tracking the real MPP under Uniform Irradiance Condition (UIC) and PSC has been introduced. The basis of the proposed method is through the use of analytical formulas for the behavior of the PV system. In another study [25], achieving maximum output power under PSC has been performed by shifting shaded PV modules within the PV array via a reconfiguration procedure based on the reduction of irradiance mismatch index. In [26], a new EAR-based reconfiguration technique has been proposed, consisting of a fixed part, an adaptive part, and a switching matrix. In this technique, the switching matrix plays an essential role by connecting compatible PV cells to fixed cells in order to compensate for radiation drop in each row. An adaptive reconfiguration solution has been proposed in [27] to reduce the effect of shadows on PV panels. In this study, a switching matrix connects a solar adaptive bank to a fixed part of a solar PV array. According to a model-based control algorithm, the output power of the solar PV array increases. In [28], an adaptive bank scheme has been proposed based on the bubble sort method for shadow dispersion, which requires a continuous change to identify the best-configured array. This method switches the adaptive PV arrays one time and after each switching, the power of the whole system is analyzed. The simulation and experimental results presented in this study emphasized a 13% improvement in efficiency compared to the performance of the central inverter topology. The method presented in [29] is an important step to determine the optimal connection structure. In this method, different applications of a fuzzy technique have been suggested. Typically, fuzzy logic which is used in situations such as uncertainty is utilized to determine the optimal layout of the PV array in the reconfiguration problem. The reconfiguration performed in this study makes it possible to achieve the maximum power point and, based on the real-time adaptation of a switch matrix to self-ability,

maintains a constant load voltage. In [30], the scanning algorithm has been employed to reconfigure PV arrays with partial shadows. This algorithm only uses the short-circuit current value measured in certain parts of the PV array. In [31], a shadow dispersion model based on a two-phase reconfiguration method has been proposed to reduce mismatch losses. The results of the proposed method in that study are compared to the results of the traditional physical relocation (SuDoKu), electrical reconfiguration, and TCT interconnection schemes. Evaluation of the results shows the achievement of the Fill Factor (FF) metric values for the proposed method in short wide case, long wide, short narrow, and long narrow cases PV arrays of 72%, 62%, 81%, and 75%, respectively, which shows the superiority of the proposed technique over the mentioned conventional methods. In [14], a reconfiguration method based on dynamic programming and the Munkres algorithm has been employed for extracting the maximum output power of the PV array. In this method, the control system runs a simple dynamic programming algorithm to modify the switch design. In [32], the iterative and hierarchical sorting algorithm has been selected for solving the reconfiguration problem. In this study, hierarchical sorting is performed on an iterative basis, but continuous switching and complex computation reduce the overall system reliability. Potential performance improvements of more than 10% in some cases, and between 4% and 10% in a large number of cases under random and sudden PSCs, were the achievements of the method proposed in this study. As mentioned in the literature, the use of dynamic techniques requires additional peripherals such as sensors and switches, which are not economically viable and complicate the system configuration [16]. Table 1 lists the studies related to reconfiguration of the PV modules by dynamic techniques with a description of the advantages and disadvantages.

Table 1. A comprehensive review of studies related to reconfiguration of PV modules by dynamic methods

Subcategory	Ref.	Used method	Advantages	Disadvantages
Adaptive-bank based	[28]	Bubble-sort model-based control algorithm	– Identifies the best panel for proper distribution of the shadows	– Requires continuous switching – Complex and time-consuming switches – Requires separate sensors implementation.
	[29]	Fuzzy logic	– Determines the optimal connection structure – Accurate and fast, Suitable for systems of different sizes	– Determining radiation based on the amount of short-circuit currents is a difficult and expensive task
	[30]	Scanning algorithm	– Increases efficiency significantly – Selects the best configuration – Runs on panels with different levels and features	– Getting the short circuit current of all the rows is a difficult task – Can't be applied for large dimensions of PV arrays
	[33,34]	Elastic photovoltaic structure	– Select the best configuration	– It requires many switches (complex) – Unable to provide TCT
	[35]	Shading degree model-based reconfiguration	– Reduces computing time – Reduces mismatch	– Frequent short circuit errors

		algorithm	– Reduces hot spots		
	[36,37]	Artificial Neural Network	– Has great effectiveness – Strength and accuracy	–	Has many connections
	[38,39]	Image processing	– Reduces the effects of partial shadows – Reduces energy loss for installations in small systems – Ability to improve output power in case of partial shadows and module failure in commercial systems	–	Obtaining voltage and current gives more complexity – Requires long time (Proposed image processing algorithm takes one frame every two minutes)
Irradiance equalization based	[14]	Munkres Assignment Algorithm	– Reduces the effects of mismatch – Minimizes aging of switches in the switching matrix – Minimizes the number of switching operations	–	Can't render for large dimensions – There are more replacements
	[40]	Random search algorithm	– Fast	–	It provides different results for input data due to randomness – The complexity of control algorithms – It requires a large number of switching devices
	[33]	Best-Worst storing	– Fast and in some cases provides the optimal solution	–	Needs a lot of switching devices – Contains sophisticated control algorithms – In most cases, do not have the desired result
	[41]	Greedy algorithm	– Optimal configuration in low computing time – Optimal configuration without the need for heavy programming – It can be used for large dimensions	–	Need a lot of switching actions – Contains sophisticated control algorithms
	[42]	Reconfiguration algorithm	– Simplicity – Providing important improvements in array's power production alongside a reduced number of switching action	–	Expensive – Numerous wiring – Complex to control

On the other hand, some studies have physically reconfigured the PV modules using static techniques to extract maximum output power. In [43], the distribution of shadow effects on a 3×3 PV array has been performed using an interconnection scheme. The results of

comparisons in this study show the superiority of the proposed scheme compared to the SP, TCT, and BL PV settings. A magic square arrangement for the TCT PV array has been presented in [44] to extract maximum output power under PSC. In the same study, the results of reconfigurations were evaluated based on the P-V characteristics curve, power loss, FF, and the effect of shadow scatter on the maximum power point. Evaluations showed that the power at the maximum power point of the Magic Square and Re-arranged TCT configurations was 2279 watts more, and the FF was 9.91 higher than the TCT configuration. In another study [45], two shadow distribution models in an asymmetric PV array have been proposed for the TCT PV array. The compounds proposed in this paper significantly reduce the drop in mismatch. A PV array reconfiguration method called SuDoKu has been introduced in [46] to increase the maximum output power under PSC in the PV TCT array. In this study, the physical position of the PV modules in the TCT PV array is rearranged based on the SuDoKu scheme and the results show that placing the PV array modules based on the SuDoKu puzzle pattern improves performance under PSCs. In valuable studies [47] and [13], optimal SuDoKu and improved SuDoKu methods for distributing partial shadow effects in the PV TCT array have been suggested, respectively. In the evaluation of these studies, it has been concluded that the improved SuDoKu performed better than the SuDoKu and the optimal SuDoKu. In [48], a new procedure, namely the skyscraper puzzle, has been employed for enhancing output power production in PSCs. In this study, the employed procedure is implemented for reconfiguration of two 9×9 and 5×5 PV arrays. In this study, various evaluation indicators have analyzed the results of the proposed method and various techniques such as TCT, dominance square, and Sudoku. Finally, evaluations have shown that the skyscraper procedure provides better shadow scattering throughout the PV array and improves the power reduction by reducing the mismatch loss. Reducing the effects of PSC on the power generation of TCT PV arrays has been done in [49] using a new reconfiguration method called Odd-Even configuration. In [50], a novel Magic-Square puzzle PV module reconfiguration technique has been introduced to reduce mismatch losses under PSC and applied on a 9×9 TCT PV array. The reconfiguration of the PV arrays used in this study was also performed with some conventional techniques to provide a comparative approach to analyze the results. The evaluations emphasized the high performance of the Magic-Square method compared to other conventional SuDOKu-based methods. In [51], decreasing partial shading losses and increasing power generation have been done by a static PV module reconfiguration technique called the Zig-Zag method. The reconfiguration of PV array modules has been done by presenting a new static-based method called prime numbers in [52]. In this study, 6 PV panels with different shading conditions have been used to implement the proposed technique. In addition, in order to express the effectiveness of the proposed method, other conventional methods have been used and the results have been evaluated using various evaluation indicators. In [53], a static based array configuration method under the spiral step pattern has been developed to configure 4×4 and 9×9 PV arrays under PSCs. The proposed method in this study has a high resistivity to generating mismatch losses compared to other conventional solutions. In [54], a 4×4 TCT PV array has been reconfigured under PSC by introducing a static-based reconfiguration approach called the Ken-Ken puzzle. In another research [55], a physical array configuration scheme called Lo Shu has been proposed to distribute shadows and to reduce mismatch losses while being implemented on a 9×9 TCT PV array with different shading conditions. The results presented in the same study showed that for the shadow patterns considered in all seven models, the proposed Lo Shu technique performed better than the TCT and Dominance Square

methods. As it was observed, the I-V and P-V characteristic curves of proposed method were smoother and more reasonable than the curves related to other mentioned methods. A novel optimal mileage-based PV array reconfiguration technique in a PV power plant under PSCs has been suggested in [56]. In this study, in order to implement an efficient exploration and exploitation with several cooperative factors instead of a single learning factor, the discrete optimization of the upper layer is performed by the suggested swarm reinforcement learning. The presented results show that the proposed technique increases the PV output power increment from 2.12% to 10.62%. Table 2 lists the studies related to reconfiguration of the PV modules by static techniques with a description of the advantages and disadvantages.

Table 2. A comprehensive review of studies related to reconfiguration of PV modules by static methods

Ref.	Technique	PV array size	Advantages	Disadvantages
[46]	Sudoku puzzle	A 9 × 9 TCT connected PV array	– Can be used for large dimensions	– The first column is left without rearrangement – Creating a shadow on the left side – Unsuitable for small size PV arrays – It is difficult to find the optimal pattern
[47]	Optimal SuDoKu	A 9 × 9 TCT connected PV array	– The reduction of mismatch due to the Sudoku method – Reduce wiring – Effective distribution of shadow	– Requires a lot of mathematical formulation
[13]	Improved SuDoKu	A 9 × 9 TCT connected PV array	– Reduces mismatch in comparison to Sudoku and Sudoku optimization methods – Has an effective shadow dispersion	– Suitable for PV arrays up to size of 9 × 9
[57]	Futoshiki puzzle	A 5 × 5 TCT connected PV array	– Increases output power – Reduces mismatch losses – Fast to implement	– Complexity and lots of wiring – Can't be used for large dimensions
[58]	Based on calculated displacement distance "d" between adjacent panels	A 6 × 6 TCT connected PV array	– Increases output power – Reduces mismatch losses – Shadows are positioned at an appropriate distance	– Unsuitable for large size PV arrays
[50]	Magic Square Puzzle	A 9 × 9 TCT connected PV array	– Minimize the difference between the maximum value of Sum of Irradiances (SIR) and the minimum value of SIR	– Reduces reliability – Unsuitable for large size PV arrays – It only performs column scattering
[59]	Dominance Square	A 5 × 5 TCT connected PV array	– Can be used for large size PV arrays	– Long wires (complex connection) – It follows a custom reset process that is not appropriate in real-time situations

[51]	Zig-Zag scheme	A 4×3 connected array	TCT PV	–	No need to change the electrical connection of the modules	–	Unsuitable for large arrays
				–	Performs row and column reset	–	Plenty of wiring and extended connections
						–	Costly
[55]	Lo Shu	A 9×9 connected array	TCT PV	–	Applicable for a variety of shading conditions with large and various dimensions	–	Inability to apply on the large and rectangular size PV arrays
				–	Very fast performance		
				–	No need for complex circuits		

The literature review was also performed for static techniques of reconfiguring the PV arrays. The literature indicates the cost-effectiveness and simplicity of the static techniques. In addition, these techniques do not require additional peripherals such as sensors and switches. It can be seen that the static techniques used to reconfigure the PV modules have not been applied to large dimension and rectangular PV arrays.

In this paper, a novel reconfiguration technique named 8-Queen's is introduced and employed to distribute shadows on the PV array. The proposed solution is based on static techniques and changing the physical location of the modules in the TCT PV arrays reduces the losses due to non-compliance and leads to the extraction of maximum power from the PV array. The 8 Queen's scheme has significant advantages over other reviewed techniques, such as the ability to apply on the PV arrays in various dimensions, especially large size and even rectangular arrays. Also, the selected algorithm for solving the n-Queen's problem in this paper has significant capabilities such as the ability to run for large dimensions up to 1000 Queen's and very fast execution such as the run time for 500 Queen's is about 2 seconds.

In this paper, the 8-Queen's method is applied to 7 cases of PV arrays in the sizes of 4×4, 6×6, 6×6, 9×9, 9×9, 10×12, and 20×20 with different shading conditions, respectively. Finally, in order to demonstrate the efficiency of the proposed method, the results of the 8 Queen's technique are compared to the TCT arrangement, Sudoku, Optimal Sudoku, Improved Sudoku, Square Magic, and d Distance schemes. Comparisons and evaluations are performed using evaluation indicators of Fill Factor (FF), Power efficiency (η), and Mismatch Losses (ML).

The novelty and contributions of this paper are listed as follows:

- Ability to implement the proposed method without the need for sensors and switches in the PV system, which in this regard is very cost-effective compared to other conventional techniques.
- Improving the reconfiguration process without the need for high connections and the complex wiring that classical and EAR methods suffer from, is a prominent feature of the 8-Queen's procedure.
- The proposed procedure has no dependence on PV dimensions and shadow size in the reconfiguration process, which is an ideal performance for the proposed technique.
- Despite other conventional EAR techniques, the proposed method can be implemented on rectangular and very small size PV arrays such as 4×4.

- The proposed technique, unlike other conventional methods, can be implemented on the PV system in a short time, such as a few microseconds, which is a very short time in contrast to the behavior of PV.
- Implementing other conventional methods called Magic Square Puzzle, d Distance, SuDoKu, Optimal SuDoKu, and improved SuDoKu on the studied PV panels and presenting a comparative approach are other contributions of this study. The results of evaluations and comparisons emphasize the effectiveness and superiority of the 8-Queen's technique compared to other mentioned methods.

The continuation of this paper is organized as follows: Section 2 introduces the 8 Queen's technique and how to apply it on PV arrays. The studied cases and simulation results are presented in Section 3. Section 4 describes the performance indicators and evaluates the results. Finally, Section 5 concludes the paper.

2. 8-Queen's technique

As shown in Figure 4, the 8 Queen's puzzle is an example of the general problem n-Queen's, with an arrangement on the $n \times n$ chessboard that the Queens cannot attack each other. This problem can be solved for all natural numbers for n except n=2 and n=3 [60,61] where one solution is to have no two Queens in the same row, column, or diameter.

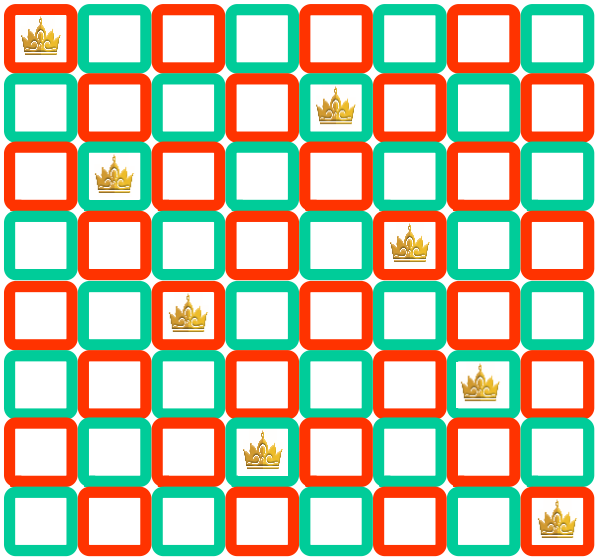

Figure 4. Example of 8-Queen's puzzle

Getting back to the 8-Queen's problem, the output matrix can be presented as follows upon arranging the Queens on the chessboard:

Input:

In general, it is 8. (8×8 is the size of a regular chessboard.)

Output:

A matrix that shows the Queen's position in each row and column.

{1,0,0,0,0,0,0,0}

{0,0,0,0,1,0,0,0}

{0,1,0,0,0,0,0,0}

{0,0,0,0,0,1,0,0}

{0,0,1,0,0,0,0,0}

{0,0,0,0,0,0,1,0}

{0,0,0,1,0,0,0,0}

{0,0,0,0,0,0,0,1}

In this output, the represented number 1 indicates the Queen's position and the number 0 indicates the empty positions on the chessboard.

Algorithm [62]**:**

Input: Chessboard, rows, and column boards.
Output: Placement of each Queen in a row or column that is not attacked by any other Queen.

Start:
if there is a Queen on the left of the current col, then
return false
 	
if there is a Queen on the left upper diagonal, then
return false
 	
if there is a Queen on the left lower diagonal, then
return false;
 	
return true //otherwise it is a valid place
End

Solve N Queen (board, column) [62]**:**

Input: The chessboard, the column that the Queen is trying to put on.
Output: The position matrix where the Queens are located.

Start:
if all columns are filled, then
return true
for each row of the board, do
if is Valid (board, i, col), then
set Queen at a place (i, col) in the board
if solve N Queen (board, col+1) = true, then
return true
otherwise remove Queen from a place (i, col) from the board.

```
  done
  return false
End
```

The main objective of the n-Queen's method is to find the best reconfiguration for the modules in the PV arrays so that the shadow is distributed in the array so that the GMPP is obtained. In using the n-Queen's technique to reconfigure modules in the PV array, any shadowed module in the PV array is considered as a queen on a chessboard. By solving the algorithm, when each Queen on the board is arranged so that it is not attacked by another Queen, in principle, the shadowed modules are reconfigured in such a way that they spread the shadow with the greatest distance from each other in the PV array. In this paper, the n-Queen's problem is solved by considering n=8, and the proposed technique is called 8-queen's. Figure 5 shows the 12 solutions for the placement of all eight queens on a chessboard without attacking each other. Figure 6 shows the flowchart of the proposed 8-Queen's method. This figure shows how to implement the 8-Queen's method step by step.

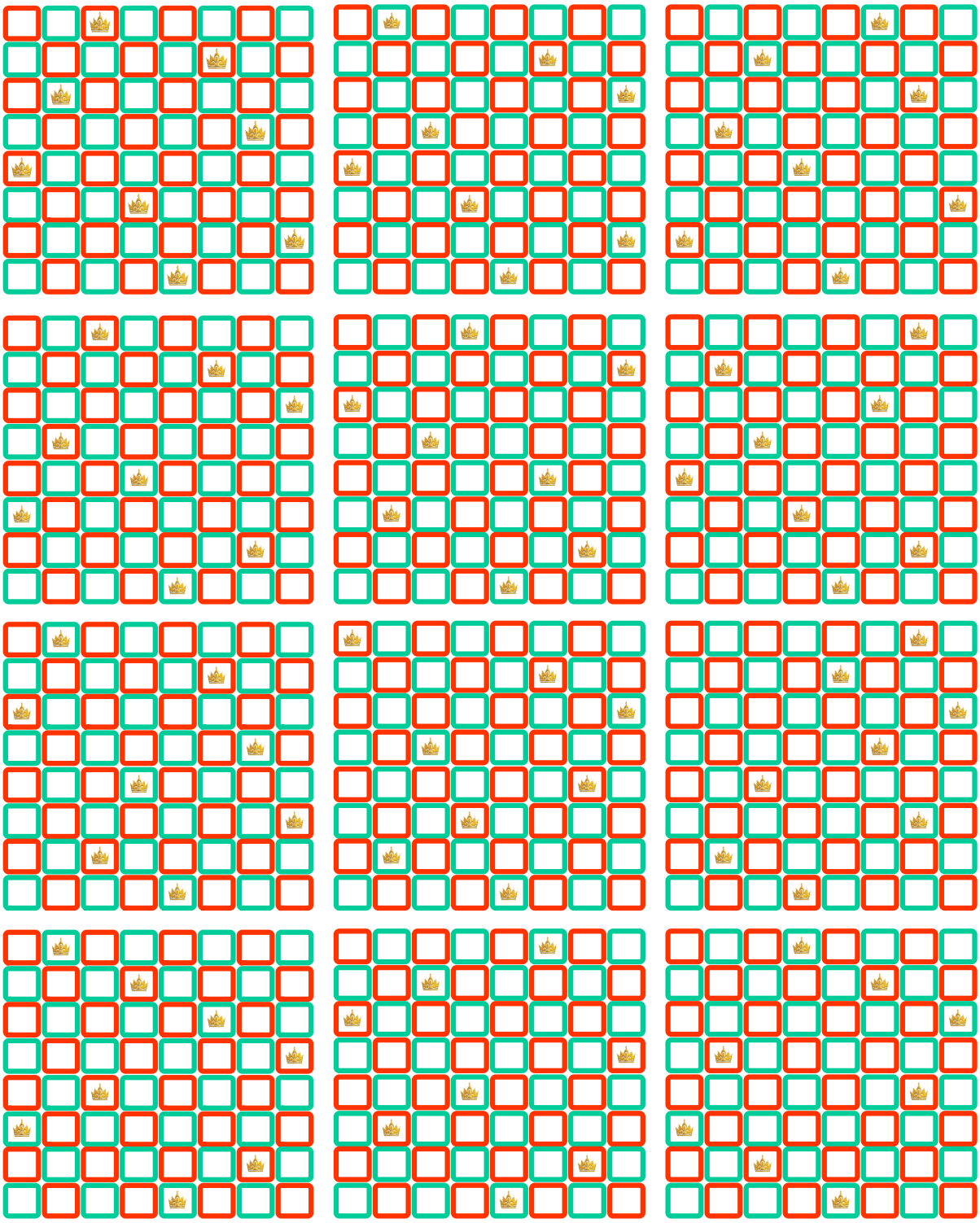

Figure 5. 12 solutions for placing 8-Queen's on the chessboard without any attack on each other

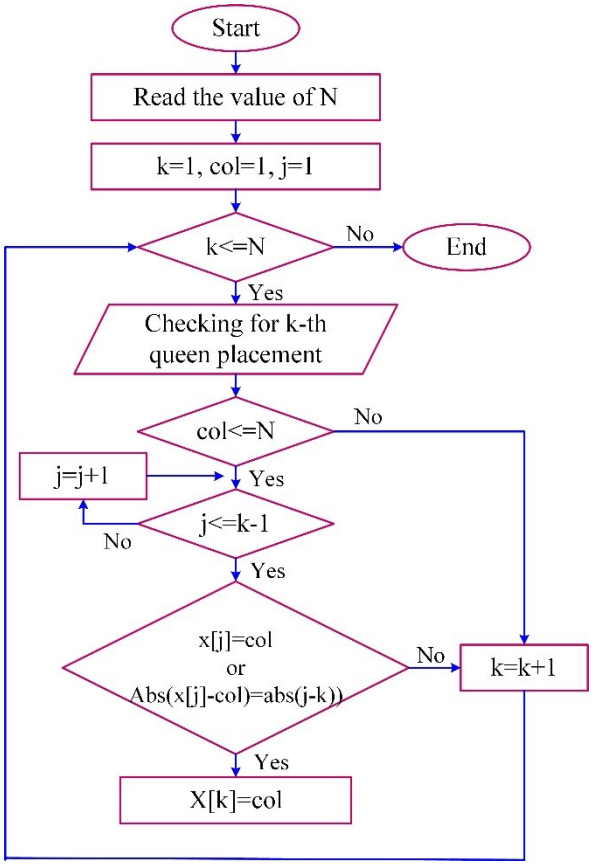

Figure 6. Flowchart of the proposed 8-Queen's procedure

So far, various methods have been employed to solve the n-Queen problem. These methods are divided into four categories as heuristic methods, backtracking, Artificial Neural Networks (ANNs), and local search methods. Each of these categories has solved the n-Queen problem with its algorithms. Table 3 lists the studies related to solving the n-Queen problem using the mentioned techniques, mentioning the advantages and disadvantages of each method.

Table 3. Review of studies related to the presentation of n-Queen's problem solving techniques

Method	Ref.	Solving Algorithm	Advantage	Disadvantage
Backtracking	[63]	Iterative compression	Generates all the answers to the problem and improves the runtime by eliminating incorrect answers.	It does not apply to a large number of Queens. As the number of Queens increases, the execution time also increases, and the efficiency of the method decreases.
	[64]	Parallel hardware scheme		
	[65]	-		
	[66]	A group-based search		
Heuristic	[67–69]	Genetic	Finds the right solutions in less time. Their coding is very easy compared to other algorithms that do the same thing.	In all cases, it may not be the best solution to the problem. It is difficult to select parameters such as the number of generations, population size, and etc.
	[70]	Particle swarm optimization		
	[69]	Simulated Annealing		
	[69]	Tabu Search		
	[71]	Ant colony optimization		
ANNs	[72,73]	Hopfield	They have very high accuracy and speed in	Given that the methods are data-based; they can provide
	[74]	Quantum computing		

	[75]	Chaotic	solving the problem. Also, they can find the most appropriate answers to the problem.	the worst answer with the least flaws in the input information. Not suitable to solve the problems with a small number of Queens.
	[76]	Self-feedback controlled chaotic		
Local search	[77–79]	P system with active membranes	For some problems are the best functional algorithms. They can test many solutions in a short computation time. Most of them can easily adapt to a variety of problems and are therefore flexible.	They cannot reduce the search space.
	[80]	Finite Euclidean plane geometry of p points		
	[81]	Queen Search 2, Queen Search 3		
	[82]	Strategy game		
	[83]	Closed-Form expressions		

The results presented in various studies show that among the presented methods, the local search methods have been able to provide the best results with its high capabilities [60,77,78,84]. Accordingly, in this paper, a P system with active membranes is used to solve the 8-Queen's problem. In the continuation of this section, the P system with an active membrane scheme of the group of local search techniques is introduced.

2.1.P System with active membrane:

The local search method is a powerful tool to solve real problems like n-Queen. Figure 7 provides a schematic of how the n-Queen problem is solved by local search techniques. As Figure 7 shows, this process starts with a random state and continues by selecting a neighbor with the highest target value for jumping. Then, step 2 is repeated until a goal is found among all the neighbors with the highest value and then enters step 4. The P system is a class of distributed computing devices of a biochemical type that can be utilized as a general computing architecture in which various types of objects are processed by different operations. The P system with the membrane is capable of solving linear and non-linear problems in fast time [78]. Active membrane systems for n-Queens have several individual membranes that include an object and no inner rule in each membrane, as well as several communication rules in membranes that reduce the speed of execution. Therefore, the average time to find successful calculations is reduced [77].

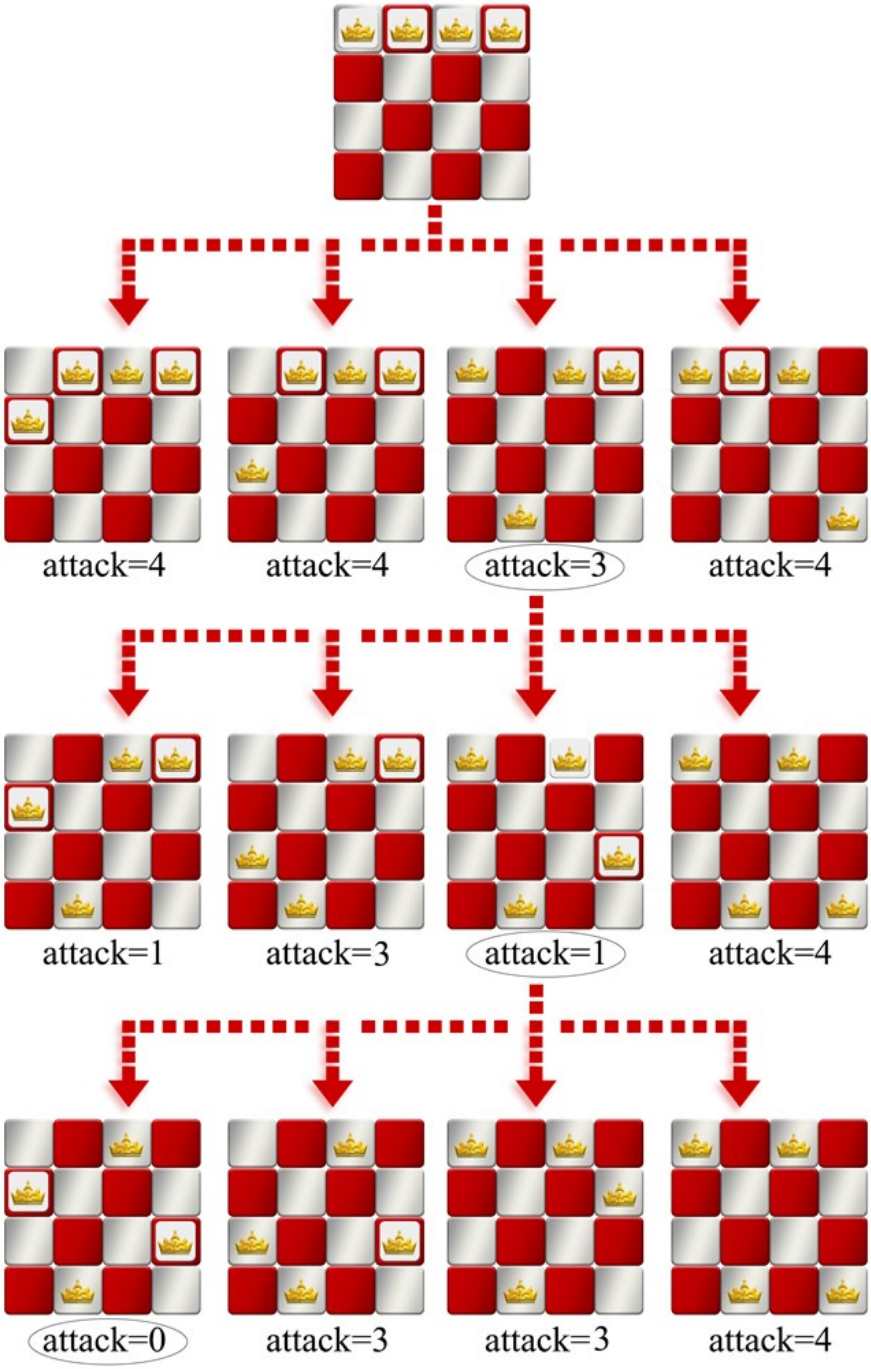

Figure 7. Solve the N-Queen puzzle by local search method

The membrane can be represented by +, -, or 0, and this is interpreted as an electric charge. Figure 8 shows the membrane structure of the P system in solving an n-Queen problem. According to the P system membrane structure as seen in Figure 8, the 3, 5, 6, and 8 membranes are the primary membranes. The string of parentheses that characterize this structure is as follows [84,85]:

$$\mu = [\,_1\,[\,_2\,[\,_5\,]_5\,[\,_6\,]_6\,]_2\,[\,_3\,]_3\,[\,_4\,[\,_7\,[\,_8\,]_8\,]_7\,[\,_8\,]_8\,]_7\,]_4\,]_1$$

As mentioned, the purpose of this method is to move an object or objects from the surface of the membrane into the membrane or nucleus, where we make changes to it and then send it

back to the surface of the membrane. In the above equation, the object enters layer (1) from the surface of the membrane or core and from there enters layer (2), from layer (2) to layer (5), from layer (5) to layer (6), and then exits layer (6) and re-enters layer (2). It then exits layer (2), which contains layers (5) and (6), and enters layer (3). It exits layer (3) and enters layers (4), (7), and (8), respectively, and then exits layer (8) and enters layer (7). Finally, it enters layer (4) from layer (7) and exits there, and with the changes made, it reaches the surface of the membrane, i.e. layer (1).

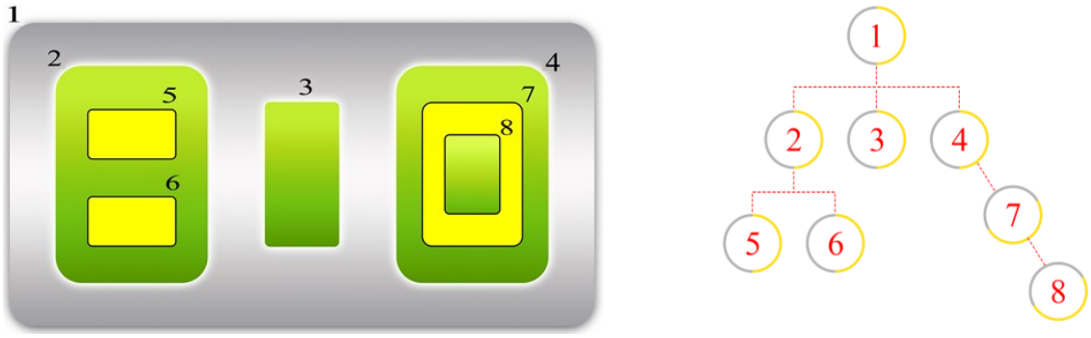

(a) (b)

Figure 8. P system membrane structure; (a) Computing block diagram of the P system, (b) Tree diagram of the P system membrane

Figure 9 represents an example of the membrane structure of the active P system. A P system with an active membrane that has various elements and a set of different rules is shown in Figure 10. As Figures 9 and 10 show, a membrane structure used in membrane computing is based on biological cells, and each membrane may contain objects and other membranes. In other words, the membranes are formed in a layer-to-layer (nested) structure [86]. The active membrane P system indicates the elements in the P structure that pass through the membrane in order to reach the surface of the skin, respectively. However, the authors in [78,79,84] provide further information and explanations on the active membrane p system.

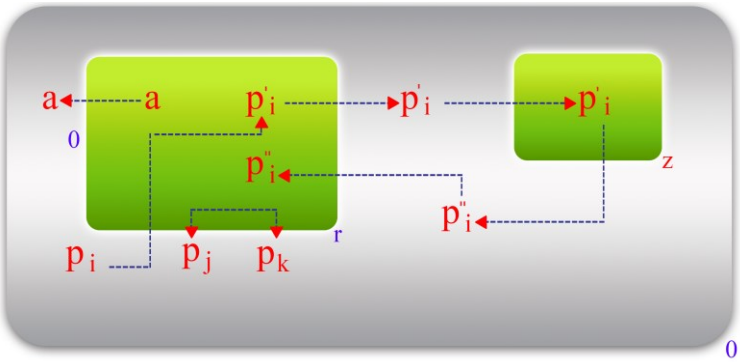

Figure 9. An example of the active structure of the P system

(1)

$P_i[\,]_r^o \rightarrow [P'_i]_r^o$

$[P'_i \rightarrow aP"_i]_r^o$

(2)

$[P"_i]_r^o \rightarrow [\,]_r^x P_j$

$P_i[\,]_r^o \rightarrow [\,P'_i]_r^o$

$[a]_r^- \rightarrow [\,]_r^o a$

(3)

$[P'_i]_r^x \rightarrow [\,]_r^x P'_i$

$P'_i[\,]_z^o \rightarrow [\,P'_i]_z^o$

$[P'_i]_z^o \rightarrow [\,]_z^o P"_i$

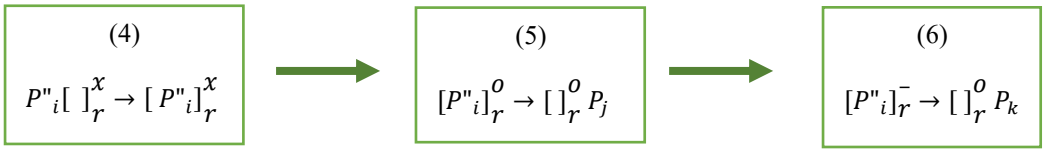

Figure 10. P systems with active membrane have elements and a set of different rules

The solution of the n-Queen problem is done by the P system with active membrane method in 5 steps as follows:

Step 1:

The Queen's are based on a portfolio of 10 different homes that differ in rows and columns. An object from a membrane is used by at most one rule (selected uncertainly).

$$[\ R_m C_n \rightarrow R_m . C_n]_1^0 \ ;\ m\ =\ 1\ ,\dots\ ,N \qquad n\ =\ 1\ ,\dots\ ,N$$

where R_m represents the Queen in the m^{th} row and, C_n represents the Queen in the n^{th} column.

Step 2:

At this stage $R_m C_n$ is sent to the surface membrane and produces u_{m-n} and d_{m+n} which shows ascending and descending diameters, respectively, and creates incremental counters $(+U_{cnt(p)} + D_{cnt(q)})$, where $U_{cnt(p)}$ shows the Queen's in ascending diameters and $D_{cnt(q)}$ demonstrate the Queen's in descending diameters. Each of p and q is represented as $p = m - n \leftarrow U_{cnt(p)}$, $q = m + n \leftarrow D_{cnt(q)}$.

$$[\ R_m . C_n\ ]_1^0 \ \rightarrow\ [\ ]_1^0\ R_m . C_n\ u_{m-n}\ d_{m+n} + D_{cnt(q)} + U_{cnt(p)};$$

$$\mathrm{m}\ =\ 1, \dots, \mathrm{N}, \mathrm{n}\ =\ 1, \dots, \mathrm{N}$$

Step 3:

At this stage, any possible exchange of (m, n) and (w, v) is applicable at any time, where (w, v) is the coordinates of the new point with respect to the (m, n). Due to the principle of active membrane systems at this stage, the rows, columns, and diameters of ascending and descending use more than one rule, and these exchanges cause changes in rows, columns, and diameters, and of course, these exchanges do not affect over other exchanges and they increase overall performance. The mathematical model for implementing this step is as follows:

$$R_t . C_c u_{t-c}\ d_{t+c}\ R_s . C_a\ u_{s-a}\ d_{s+a}\ R_r . C_b\ u_{r-b} d_{r+b}\ R_q\ . C_e\ u_{q-e}\ d_{q+e}\ R_p\ . C_f\ u_{p-f}\ d_{p+f}$$

$$R_o\ . C_h\ u_{o-h}\ d_{o+h}\ R_n . C_g\ u_{n-g} d_{n+g}\ R_m . C_i\ u_{m-i} d_{m+i}\ \ R_l . C_j\ \ u_{l-j}\ d_{l+j}\ R_k . C_d\ u_{k-d} d_{k+d}$$

$$U_{cnt(c-t)}\ D_{cnt(s+a)}\ U_{cnt(s-a)}\ D_{cnt(r+b)}\ U_{cnt(r-b)}\ D_{cnt(q+e)}\ U_{cnt(q-e)}\ D_{cnt(p+f)}\ U_{cnt(p-f)}$$

$$D_{cnt(o+h)}\ U_{cnt(o-h)}\ D_{cnt(n+g)}\ U_{cnt(n-g)}\ D_{cnt(m+i)}\ U_{cnt(m-i)}\ D_{cnt(l+j)}\ U_{cnt(l-j)}\ D_{cnt(k+d)}$$

$$U_{cnt(k-d)} \rightarrow R_t . C_a\ u_{t-a}\ d_{t+a}\ R_s . C_c\ u_{s-c}\ d_{s+c}\ R_r . C_e\ u_{r-e}\ d_{r+e}\ R_q . C_b\ u_{q-b}\ d_{q+b}\ R_p . C_h$$

$$u_{p-h}\ d_{p+h}\ R_o.C_f\ u_{o-f}\ d_{o+f}\ R_n.C_i\ u_{n-i}\ d_{n+i}\ R_m.C_g\ u_{m-g}\ d_{m+g}\ R_l.C_d\ u_{l-d}\ d_{l+d}\ R_k.C_j$$

$$u_{k-j}\ d_{k+j}\ -D_{cnt(t+c)} - U_{cnt(t-c)} - D_{cnt(s+a)} - U_{cnt(s-a)} - D_{cnt(r+b)} - U_{cnt(r-b)} -$$

$$D_{cnt(q+e)} - U_{cnt(q-e)} - D_{cnt(p+f)} - U_{cnt(p-f)} - D_{cnt(o+h)} - U_{cnt(o-h)} - D_{cnt(n+g)} -$$

$$U_{cnt(n-g)} - D_{cnt(m+i)} - U_{cnt(m-i)} - D_{cnt(l+j)} - U_{cnt(l-j)} - D_{cnt(k+d)} - U_{cnt(k-d)} +$$

$$D_{cnt(t+a)} + U_{cnt(t-a)} + D_{cnt(s+c)} + U_{cnt(s-c)} + D_{cnt(r+e)} + U_{cnt(r-e)} + D_{cnt(q+b)} +$$

$$U_{cnt(q-b)} + D_{cnt(p+h)} + U_{cnt(p-h)}\ + D_{cnt(o+f)} + U_{cnt(o-f)} + D_{cnt(n+i)} + U_{cnt(n-i)}$$

$$+D_{cnt(m+g)} + U_{cnt(m-g)}\ + D_{cnt(l+d)} + U_{cnt(l-d)} + D_{cnt(k+j)} + U_{cnt(k-j)}]_1^0$$

As Figure 11 shows the implementation of this step on the chessboard, it can be seen that in the first stage of the p active membrane system with the displacement of the Queens, the number of attacks will be as minimal as possible. As a result, the Queen with the least attack is selected to continue.

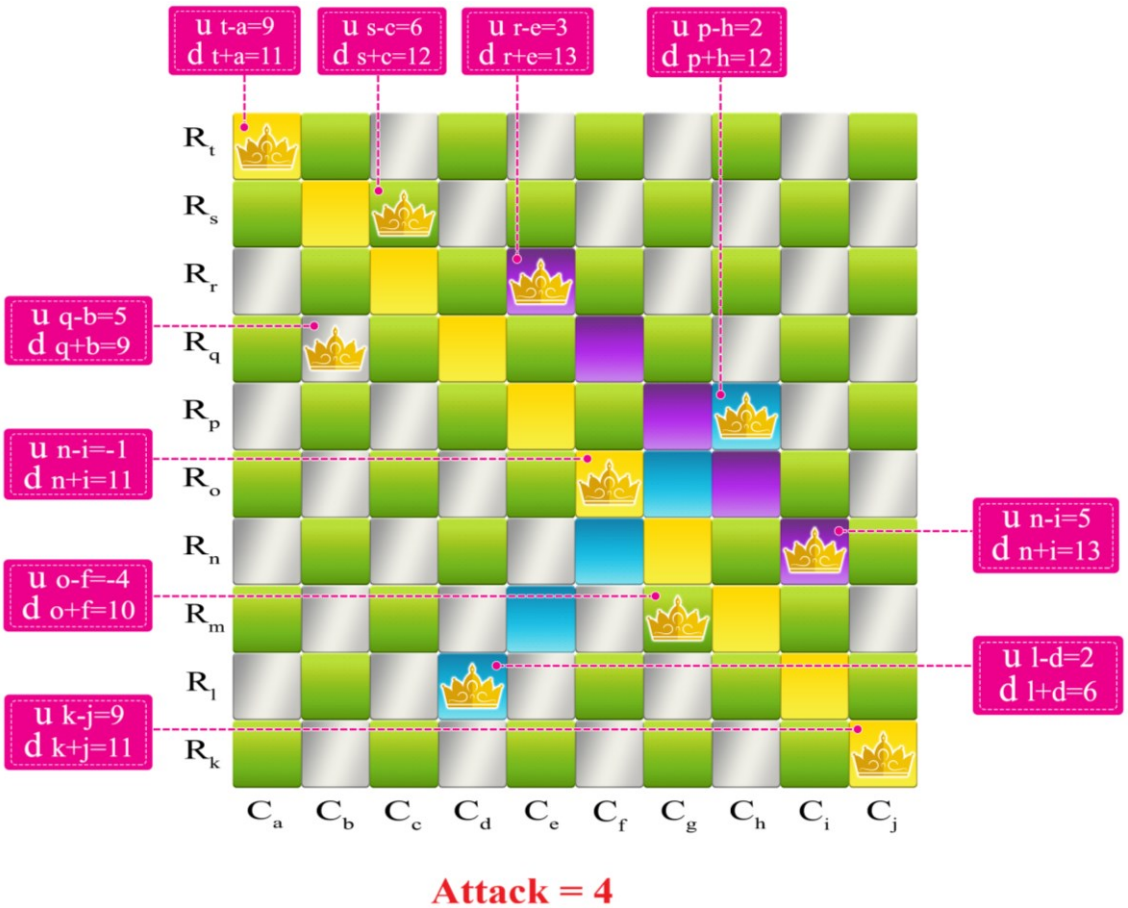

(a)

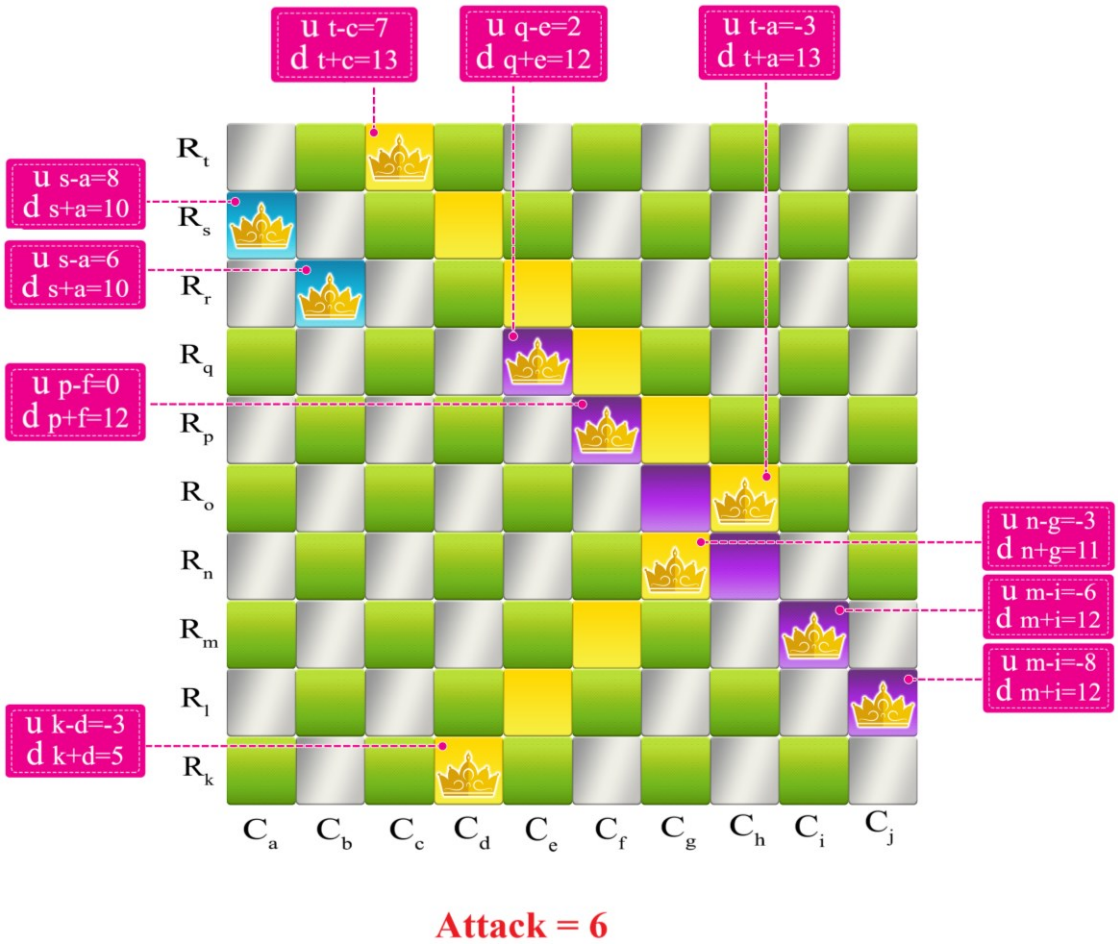

(b)

Figure. 11. Move the Queen's on the chessboard based on step 3; (a) Move the Queens together (b) Without moving the Queens together

In Figure 11, the Queen's are illustrated in $R_{10}C_1, R_9C_3, R_8C_5, R_7C_2, R_6C_8, R_5C_6, R_4C_9, R_3C_7, R_2C_4, R_1C_{10}$ and considering the following relationship:

$$Colli_{Removed}(R_t.C_a) + Colli_{Removed}(R_r.C_e) + Colli_{Removed}(R_p.C_h) + Colli_{Removed}(R_n.C_i) + Colli_{Removed}(R_l.C_d) \geq Colli_{Placed}(R_s.C_c) + Colli_{Placed}(R_q.C_b) + Colli_{Placed}(R_o.C_f) + Colli_{Placed}(R_m.C_g) + Colli_{Placed}(R_k.C_j).$$

where

$$R_{10}C_1 + R_8C_5 + R_6C_8 + R_4C_9 + R_2C_4 \geq R_{10}C_5 + R_8C_1 + R_6C_9 + R_4C_8 + R_1C_{10}$$

$R_{10}C_1 \rightarrow R_{10}C_5$ $\quad R_8C_5 \rightarrow R_8C_9$
$R_6C_8 \rightarrow R_6C_9$ $\quad R_4C_9 \rightarrow R_4C_8$

or

$R_tC_a \rightarrow R_tC_e$ $\quad R_pC_h \rightarrow R_pC_i$
$R_rC_e \rightarrow R_rC_a$ $\quad R_nC_i \rightarrow R_nC_h$

After implementing the above equations, the Queen displacement based on the selected location in the first step is described as in Figure 12.

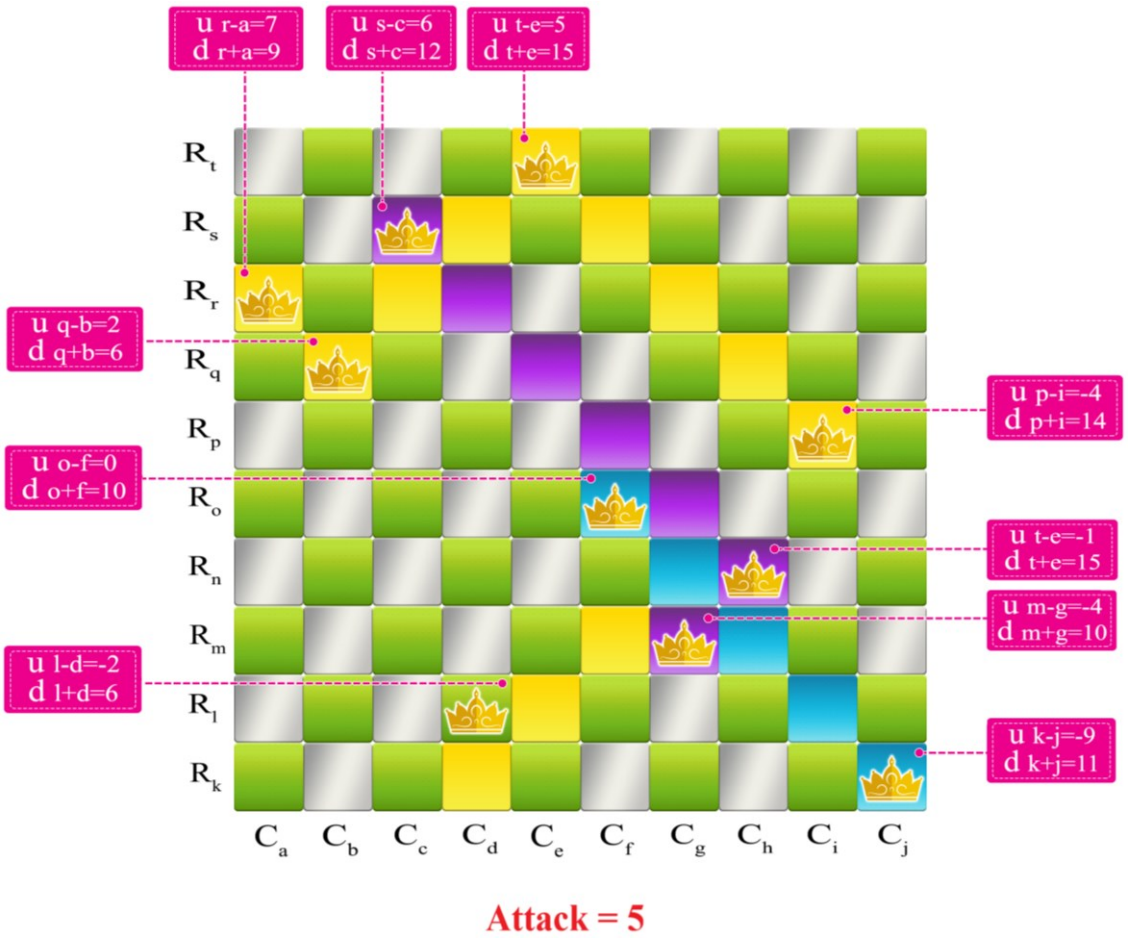

Figure. 12. Displacement of the Queens relative to the shape selected in the first step

Then, the R_2 C_4 remains unchanged and displacement be as follow (As be seen in Figure 13):

$R_7C_2 \rightarrow R_7$ C9 $\quad R_5C_6 \rightarrow R_5C_8 \quad R_3C_7 \rightarrow R_3C_4$

$R_6C_9 \rightarrow R_6C_2 \quad R_4C_8 \rightarrow R_4C_9 \quad R_2C_4 \rightarrow R_2C_7$

or

$R_qC_b \rightarrow R_q\ C_i \quad R_pC_i \rightarrow R_pC_b \quad R_oC_f \rightarrow R_oC_h$

$R_nC_h \rightarrow R_nC_f \quad R_mC_g \rightarrow R_mC_d \quad R_lC_d \rightarrow R_lC_g$

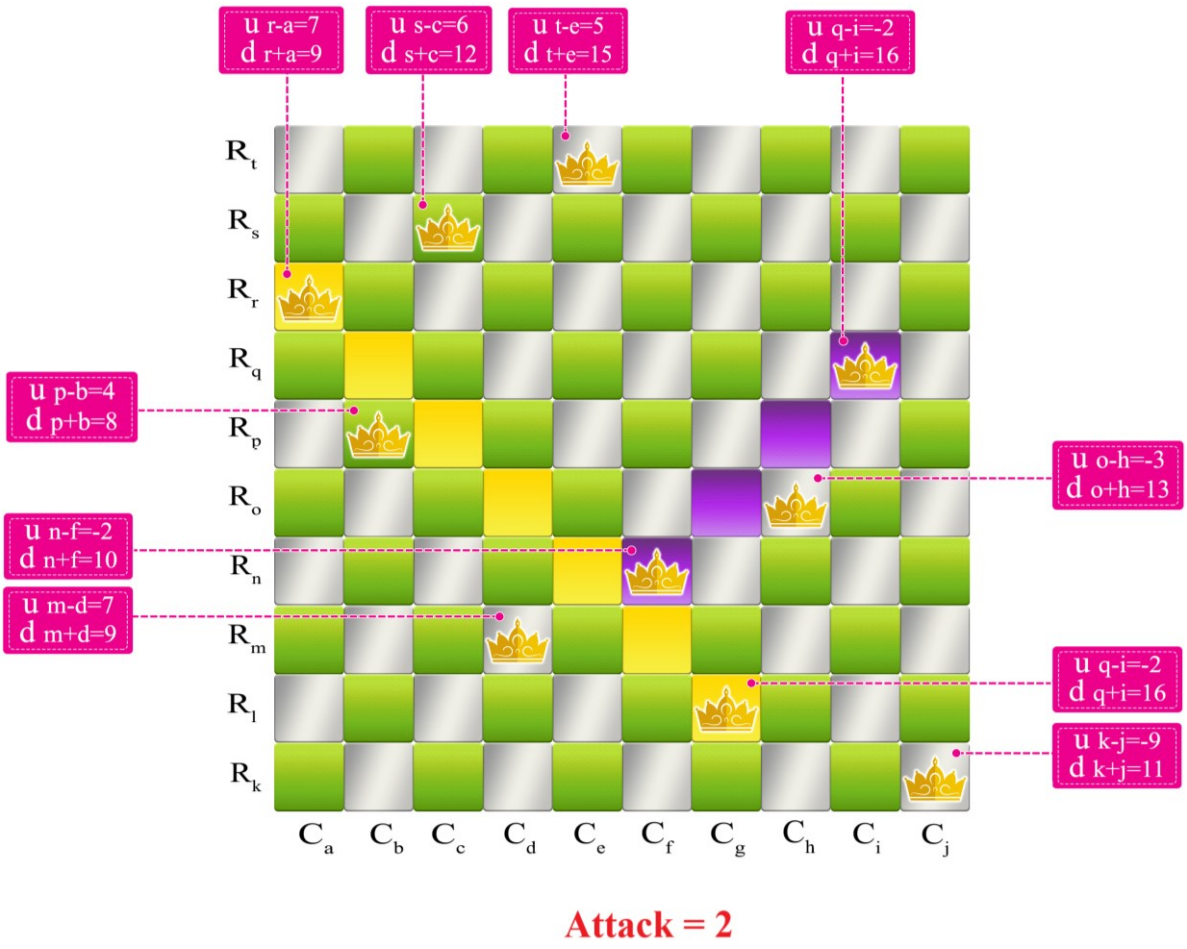

Figure 13. The Queen's last move with the least attack

So at this stage, the R_1 C_{10} remains unchanged.

Step 4:

At this step, according to the following equation, "YES" (resolved Queen) is sent to the environment and changes the polarization of the membrane to (-), which stops all other rules from being implemented.

$[D_{cnt(2)}, \ldots, D_{cnt(2N)}, U_{cnt(-N+1)}, \ldots, U_{cnt(N+1)}] \begin{matrix} 0 \\ 1 \end{matrix} \rightarrow [\,] \begin{matrix} - \\ 1 \end{matrix}$ yes; If all $D_{cnt} \leq 2$ and $U_{cnt(p)} \leq 2$

$q = 2, \ldots, 2N, p = -N + 1, \ldots, N + 1.$

This step runs when all ascending and descending Queen counters are equal to or less than two limits ($U_{cnt(p)} \leq 2, D_{cnt(q)} \leq 2$), which means that in ascending and descending diameters there is the least collision. But concerning the first step, there is no collision in the rows and columns.

But if there are more attacks on the board and no progress or more clashes, step four will send "NO" instead of "YES" as follows:

$[\text{Cnt No} \rightarrow +\text{Cnt No}]\begin{matrix}0\\1\end{matrix}$; if for all m, n, w, v, … $\in \{1, \ldots, N\}$, m $\neq$ w and

$Colli_{Removed}(R_m.C_n) + Colli_{Removed}(R_w.C_v) + \ldots \leq Colli_{Placed}(R_m.C_v) + Colli_{Placed}(R_w.C_n) + \cdots$

$[\text{Cnt No}]\begin{matrix}0\\1\end{matrix} \rightarrow [\,]\overline{}_1$ No; if Cnt No = User _ Const

Step 5:

It was at this step, after sending a "YES" to the previous stage that the early Queens were properly positioned other types of Queen by relationship $\frac{x}{2}+1$ where x Indicates the number of rows in the designated places according to this relation. The location of the other Queens is as follows (As to be seen in Figure 14):

$B_{ij} \leftarrow A_{(1+\frac{x}{2})j}$

where A and B are each a Queen.

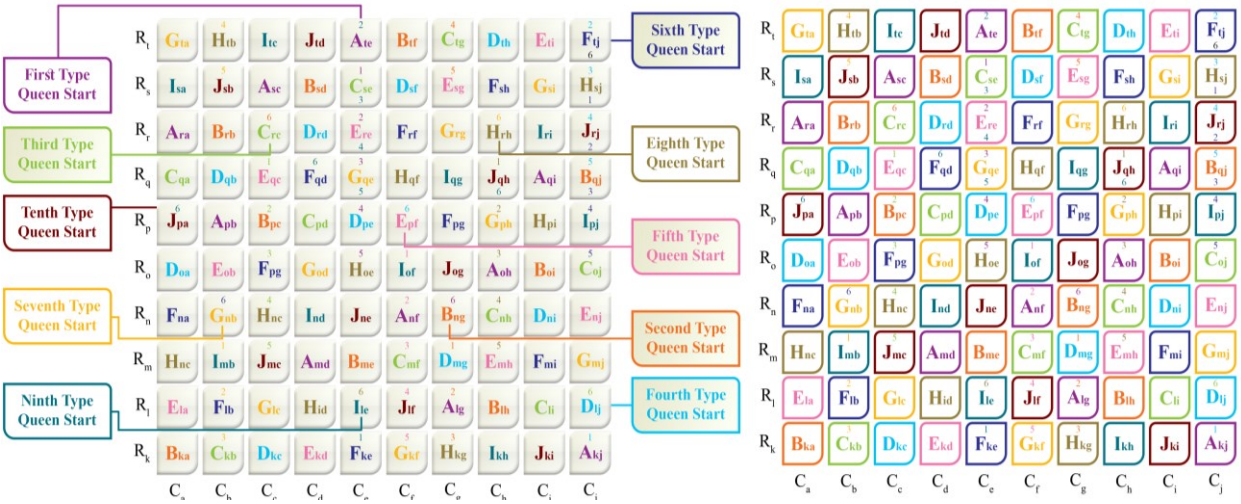

Figure 14. Placement of the other type of Queen according to the formula given in step 5

After introducing the proposed technique and describing its implementation steps, the flowchart presented in Figure 15 shows the step-by-step implementation of the n-Queen's method on the PV array.

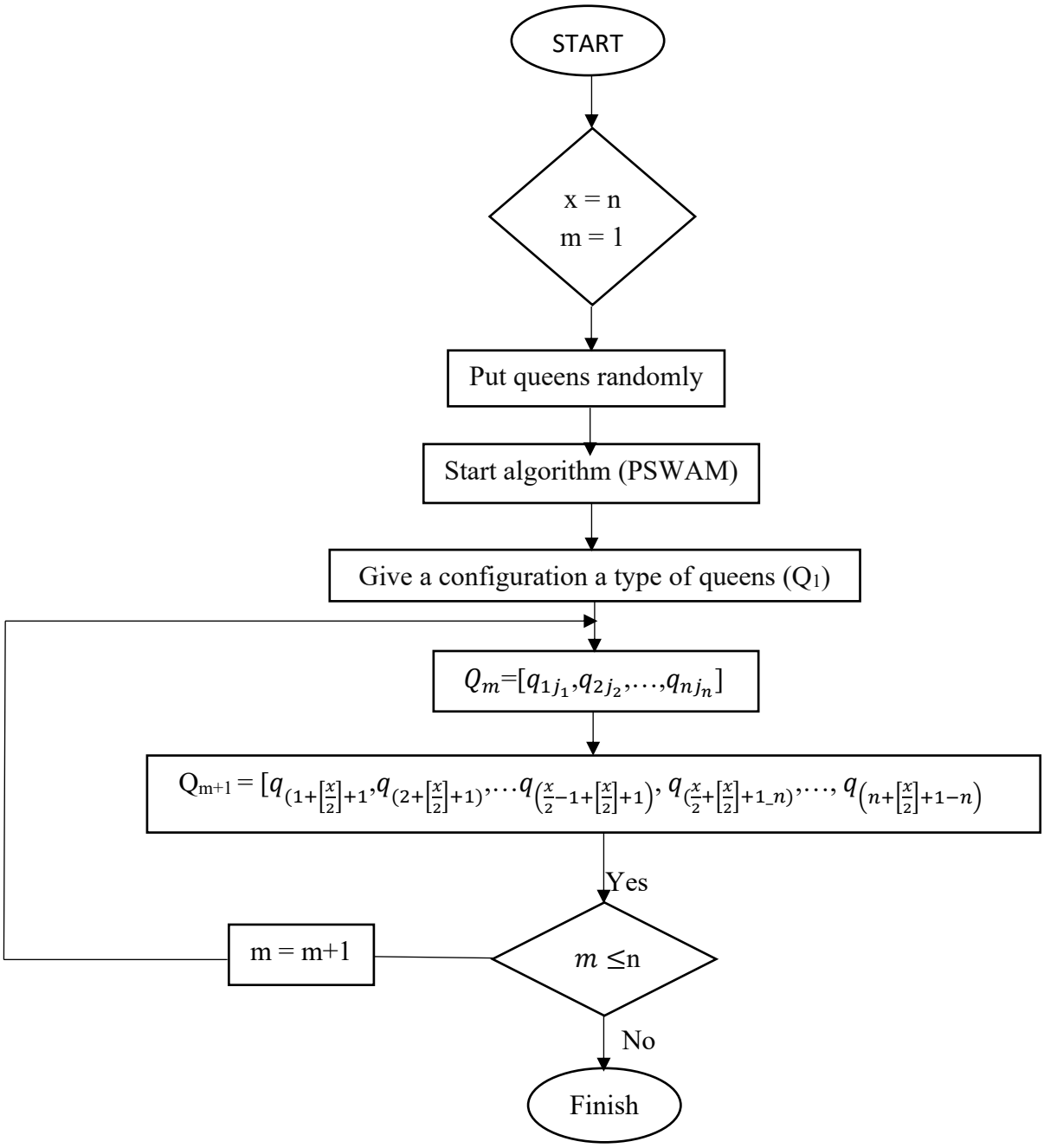

Figure 15. Flowchart of PV array reconfiguration by the n-Queen's technique

Figure 16 illustrates the arrangement of the Queens in 6 states is shown in order. So, in section (a) the Queens are randomly positioned. In section (c), where the Queen attack begins, the Queen is replaced with the next Queen, and in this section, the first type of Queens reach their final state, and if the number of attacks does not reach the minimum, it will return to the section (a) again. The other types of Queens are classified as second, third, fourth, etc. depending on the relationship $(x/2 + 1)$ that x indicates the number of rows, in their respective positions.

The following is a general overview of the stages of initial and late Queen depletion.

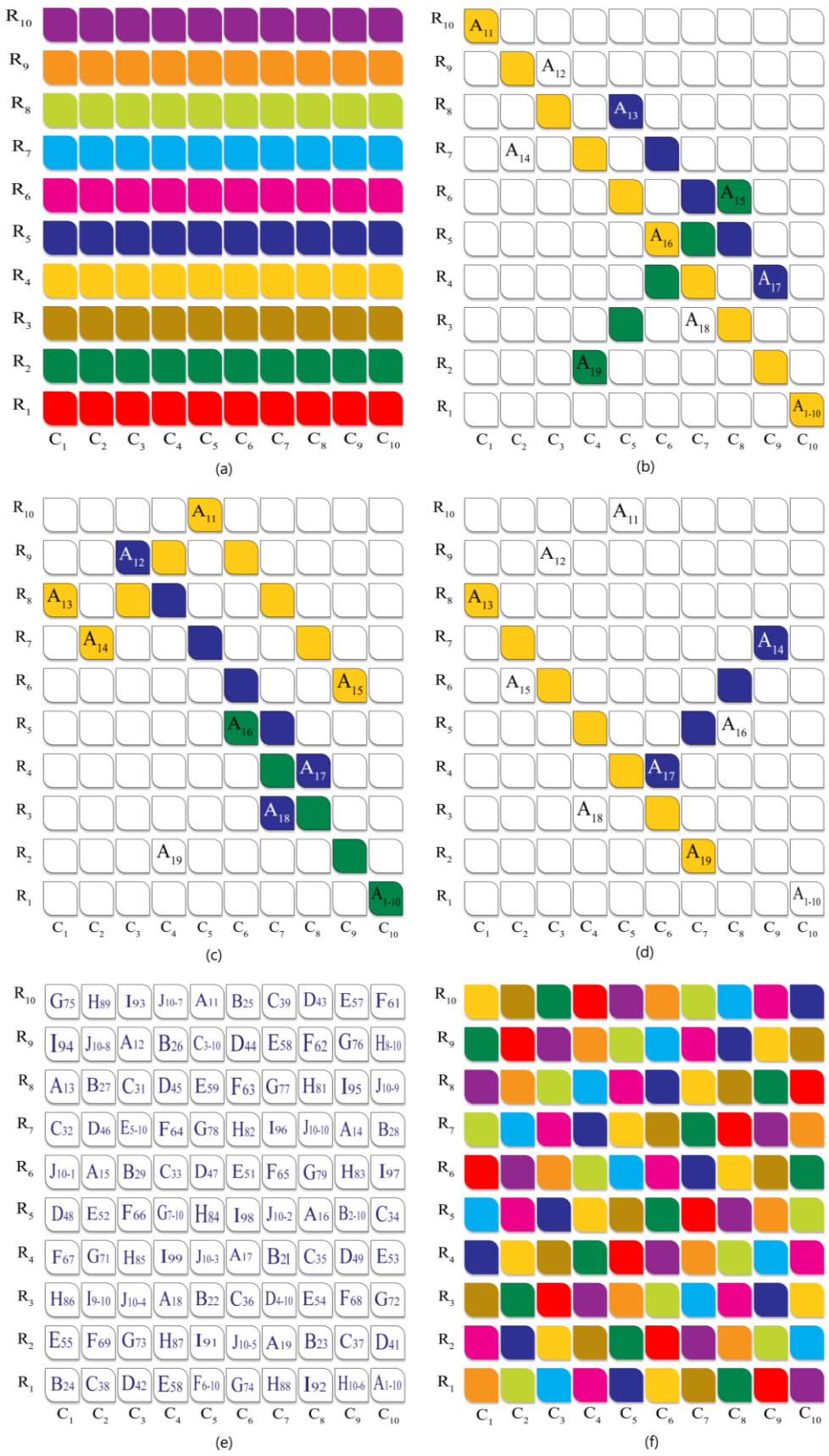

Figure 16. (a) Queens placement without rearrangement (b) Position of the first type of Queens is random (c) The Queens with the largest number of rows and columns will be replaced (d)

The place of the Queen's changes from where the attack begins (e) Other types of Queens are in their places (f) The final shape obtained from the placement of the Queens after rearrangement

3. Simulation results

In this paper, the reconfiguration of modules in the PV arrays is performed using the 8-queen's technique. The proposed procedure is implemented on the different 7 cases of the PV arrays under various shade conditions. However, for presenting the efficiency of the 8-Queen's technique, other solutions such as Magic Square Puzzle, d Distance, SuDoKu, Optimal SuDoKu, and improved SuDoKu are applied to the studied cases and the results are evaluated via a comparison approach.

The cases studied in this paper are described as follows:

Case 1: A 6 × 6 TCT PV array under a 4 × 4 shading condition
Case 2: A 6 × 6 TCT PV array under a scattered shading in all rows
Case 3: A 9 × 9 TCT PV array under a 4 × 4 shading condition
Case 4: A 9 × 9 TCT PV array under a 6 × 3 shading condition
Case 5: A 10 × 12 TCT PV array under a 4 × 4 shading condition
Case 6: A 20 × 20 TCT PV array under a 6 × 6 shading condition
Case 7: A 4 × 4 TCT PV array under a 2 × 4 shading condition

The electrical parameters and standard test condition (STC) specifications of the PV panels used in all seven cases are introduced in Table 4. So, under these conditions, only the size of the panels and the shadow conditions have changed in each case.

Table 4. Standard test condition specifications of the PV panels

Parameter	Values
Maximum rated power (W)	213.15 W
Open circuit voltage (V_{oc})	36.3 V
Short circuit current (I_{sc})	7.84 A
Voltage at maximum power point (V_{mp})	29 V
Current at maximum power point (I_{mp})	7.35 A

3.1. Case 1:

As seen in Figure 17(a), in this case, a 6 × 6 TCT PV array is under a 4 × 4 shading condition and receive radiations of $1000\ W/m^2$, $300\ W/m^2$, $200\ W/m^2$. In addition to the 8-Queen's technique, reconfiguring the PV modules and spreading the shadow, in this case, is also done by Magic Square puzzle and d Distance methods (As seen in Figure 17). To locate GMPP, it is necessary to calculate the current generated by the PV array in each row. So, in this case, in order to track the GMPP, the generated current in each row of the PV array after distribution of shadows via the Magic Square puzzle, d Distance, and 8-Queen's solutions is calculated as follows:

$$I_{row1} = B_{11}\, I_{11} + B_{22}\, I_{22} + B_{33}\, I_{33} + B_{44}\, I_{44} + B_{55}\, I_{55} + B_{66}\, I_{66} \quad (1)$$

$$B_{1,j} = \frac{G_{1,j}}{G_0} \quad (2)$$

where j is the column index, $G_{1,j}$ shows the irradiance in the panel labeled $1j$, G_0 is the full irradiance, and I_{1j} demonstrate the limited current for full irradiance of the panel labeled $1j$. If I_m be considered the current limit of the panel for full irradiance ($B_{i,j} = 1$) under standard temperature conditions. Assume that the current generated by each module at STC is I_m (7) and the current of each row in the TCT array is calculated as:

$$I_{row1} = I_{row2} = 6I_m \quad (3)$$

$$I_{row3} = I_{row4} = I_{row5} = I_{row6} = (2)I_m + (2 \times\ 0.3)\ I_m + (2 \times\ 0.2)\ I_m = ٣I_m \quad (4)$$

The current of each row in reconfiguration by the Magic Square Puzzle:

$$I_{row1} = I_{row5} = 6I_m \quad (5)$$

$$I_{row2} = (2)I_m + (1 \times\ 0.3)\ I_m + (3 \times\ 0.2)\ I_m = 3.1I_m \quad (6)$$

$$I_{row3} = I_{row4} = (2)I_m + (2 \times\ 0.3)\ I_m + (2 \times\ 0.2)\ I_m = 3I_m \quad (7)$$

$$I_{row6} = (2)I_m + (3 \times\ 0.3)\ I_m + (1 \times\ 0.2)\ I_m = 2.9I_m \quad (8)$$

The current of each row in reconfiguration by the d Distance:

$$I_{row1} = (2)I_m + (2 \times\ 0.3)\ I_m + (2 \times\ 0.2)\ I_m = 3I_m \quad (9)$$

$$I_{row2} = (3)I_m + (1 \times\ 0.3)\ I_m + (2 \times\ 0.2)\ I_m = 3.7I_m \quad (10)$$

$$I_{row3} = I_{row4} = I_{row5} = (4)I_m + (1 \times\ 0.3)\ I_m + (1 \times\ 0.2)\ I_m = 4.5I_m \quad (11)$$

$$I_{row6} = (3)I_m + (2 \times\ 0.3)\ I_m + (1 \times\ 0.2)\ I_m = 3.8I_m \quad (12)$$

The current of each row in reconfiguration by the 8-Queen's:

$$I_{row1} = I_{row6} = (4)I_m + (1 \times\ 0.3)\ I_m + (1 \times\ 0.2)\ I_m = 4.5I_m \quad (13)$$

$$I_{row2} = I_{row3} = (3)I_m + (2 \times\ 0.3)\ I_m + (1 \times\ 0.2)\ I_m = 3.8I_m \quad (14)$$

$$I_{row4} = I_{row5} = (3)I_m + (2 \times\ 0.2)\ I_m + (1 \times\ 0.3)\ I_m = 3.7I_m \quad (15)$$

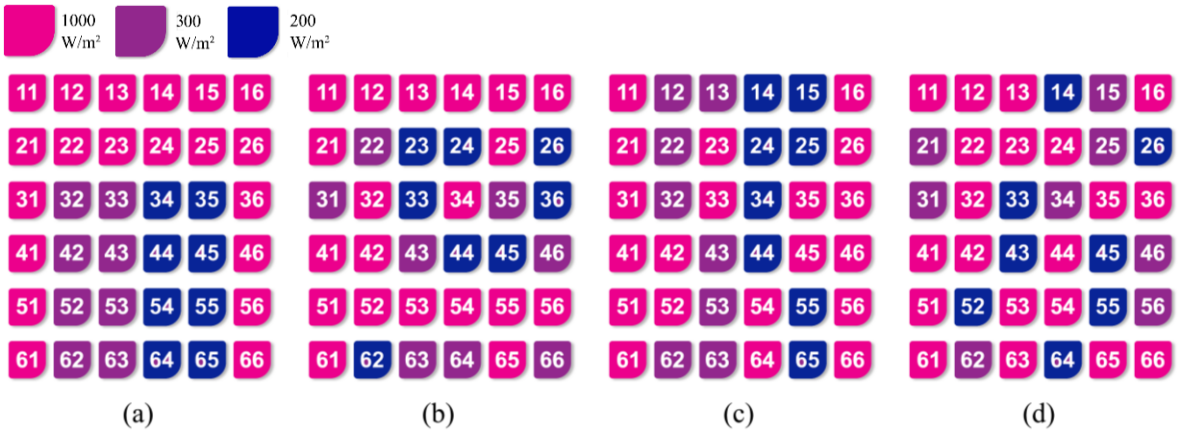

Figure 17. PV arrays reconfiguration in case 1; (a) TCT arrangement (b) Magic Square puzzle (c) d Distance (d) 8-Queen's technique

Figures 18 illustrate the P-V and I-V characteristic curves for reconfiguration of the PV arrays by the mentioned methods in case 1, respectively. The corresponding current, voltage, and power for adjusting the TCT interconnected, Magic Square puzzle, d Distance, and 8-Queen's techniques are given in Table 5.

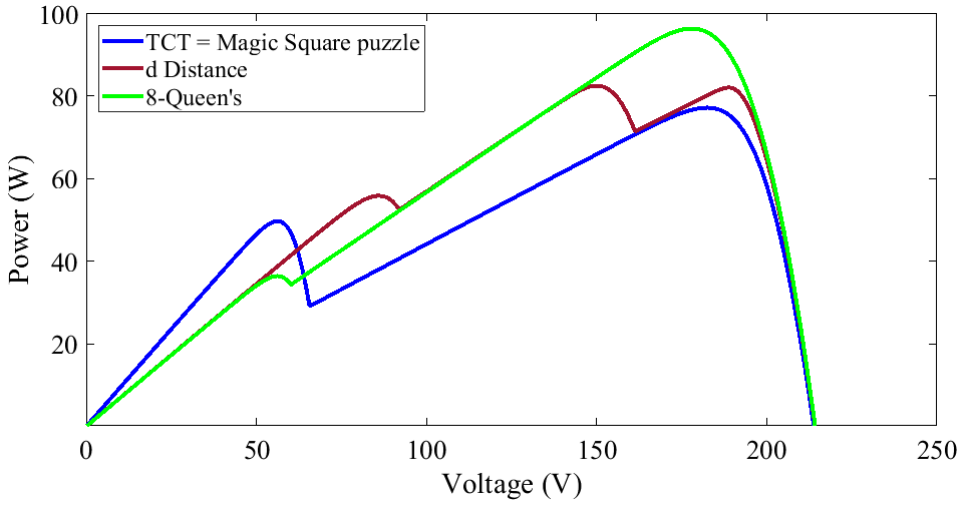

(a)

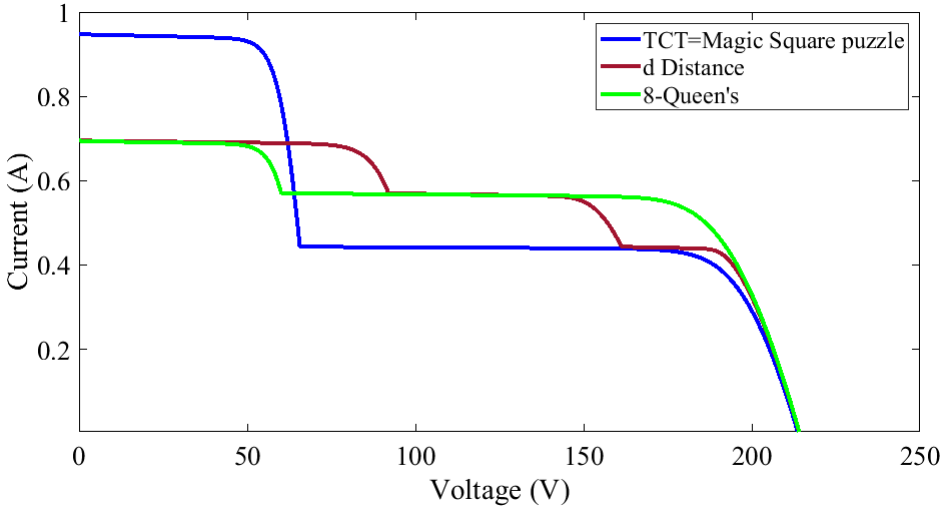

(b)

Figure 18. Simulation performed for the I group shadow conditions (a) P-V characteristics (b) I-V characteristics

Table 5. Current, voltage and power values for adjusting the TCT interconnected, Magic Square puzzle, d Distance, and 8-Queen's techniques in case 1

TCT interconnected				Magic Square puzzle				d Distance				8-Queen's			
Row bypassed	Current	Voltage	Power	Row bypassed	Current	Voltage	Power	Row bypassed	Current	Voltage	Power	Row bypassed	Current	Voltage	Power
Irow6	$3I_m$	$6V_m$	$\mathbf{18V_mI_m}$	Irow6	$3.1\ I_m$	$5V_m$	$15.5V_mI_m$	Irow6	$3.8I_m$	$4V_m$	$15.2V_mI_m$	Irow6	$۴.5I_m$	$4V_m$	$18V_mI_m$
Irow5	$3I_m$	$6V_m$	$\mathbf{18V_mI_m}$	Irow5	$۶I_m$	$۳V_m$	$\mathbf{۱۸V_mI_m}$	Irow5	$4.5I_m$	$3V_m$	$13.5V_mI_m$	Irow5	$۳.7I_m$	$6V_m$	$\mathbf{22.2V_mI_m}$
Irow4	$3I_m$	$6V_m$	$\mathbf{18V_mI_m}$	Irow4	$3I_m$	$4V_m$	$12V_mI_m$	Irow4	$4.5I_m$	$3V_m$	$13.5V_mI_m$	Irow4	$۳.7I_m$	$6V_m$	$\mathbf{22.2V_mI_m}$
Irow3	$3I_m$	$6V_m$	$\mathbf{18V_mI_m}$	Irow3	$3I_m$	$4V_m$	$12V_mI_m$	Irow3	$۴.5I_m$	$3V_m$	$13.5V_mI_m$	Irow3	$۳.8I_m$	$5V_m$	$19V_mI_m$
Irow2	$6I_m$	$2V_m$	$12V_mI_m$	Irow۲	$2.9I_m$	$6V_m$	$17.5V_mI_m$	Irow2	$3.7I_m$	$5V_m$	$\mathbf{18.5V_mI_m}$	Irow2	$۳.8I_m$	$5V_m$	$19V_mI_m$
Irow1	$6I_m$	$2V_m$	$12V_mI_m$	Irow۱	$۶I_m$	$۳V_m$	$\mathbf{۱۸V_mI_m}$	Irow1	$3I_m$	$6V_m$	$\mathbf{18\ V_mI_m}$	Irow1	$4.5I_m$	$4V_m$	$18V_mI_m$

The results presented in Figure 18 and Table 5 shows that the highest GMPP value i.e. 22.2 I_mV_m was obtained of the 8-Queen's technique. Finally, the comparison of the results presented for case 1 emphasizes the efficiency of the suggested technique with the highest power generation compared to other solutions.

3.2. Case 2:

In this case, a 6 × 6 TCT PV array is under a scattered shading in all rows and receive and receive radiations of $1000\ W/m^2$, $300\ W/m^2$, $200\ W/m^2$ (As seen in Figure 19(a)). In this case, reconfiguring of the PV modules is performed in TCT interconnected and by Magic Square puzzle, d Distance, and 8-Queen's techniques. Figure 19 shows how the PV modules are reconfigured by each of the mentioned techniques in this case. In this case, the generated current in each row related to the TCT interconnections can be calculated as follows:

$$I_{row1} = 5.2I_m \tag{16}$$

$$I_{row2} = I_{row3} = (4)I_m + (2 \times\ 0.3)\ I_m = 4.6I_m \tag{17}$$

$$I_{row4} = (3)I_m + (2 \times\ 0.3)\ I_m + (1 \times\ 0.2)\ I_m = 3.8I_m \tag{18}$$

$$I_{row5} = I_{row6} = (3)I_m + (3 \times\ 0.2)\ I_m = 3.6I_m \tag{19}$$

The current of each row in reconfiguration by the Magic Square Puzzle:

$$I_{row1} = I_{row5} = (3)I_m + (1 \times\ 0.3)\ I_m + (2 \times\ 0.2)\ I_m = 3.7I_m \tag{20}$$

$$I_{row2} = (4)I_m + (2 \times\ 0.3)\ I_m = 4.6I_m \tag{21}$$

$$I_{row3} = (5)I_m + (1 \times\ 0.2)\ I_m = 5.2I_m \tag{22}$$

$$I_{row4} = (4)I_m + (1 \times\ 0.2)\ I_m + (1 \times\ 0.3)\ I_m = 4.5I_m \tag{23}$$

$$I_{row6} = (3)I_m + (1 \times\ 0.2)\ I_m + (2 \times\ 0.3)\ I_m = 3.8I_m \tag{24}$$

The current of each row in reconfiguration by the d Distance:

$$I_{row1} = I_{row5} = (3)I_m + (2 \times\ 0.3)\ I_m + (1 \times\ 0.2)\ I_m = 3.8I_m \tag{25}$$

$$I_{row2} = I_{row3} = (4)I_m + (1 \times\ 0.3)\ I_m + (1 \times\ 0.2)\ I_m = 4.5I_m \tag{26}$$

$$I_{row4} = (5)I_m + (1 \times\ 0.2)\ I_m = 5.2I_m \tag{27}$$

$$I_{row6} = (3)I_m + (1 \times\ 0.2)\ I_m + (2 \times\ 0.3)\ I_m = 3.8I_m \tag{28}$$

The current of each row in reconfiguration by the 8-Queen's:

$$I_{row1} = I_{row3} = (4)I_m + (1 \times\ 0.3)\ I_m + (1 \times\ 0.2)\ I_m = 4.5I_m \tag{29}$$

$$I_{row2} = (3)I_m + (1 \times\ 0.3)\ I_m + (2 \times\ 0.2)\ I_m = 3.7I_m \tag{30}$$

$$I_{row4} = (4)I_m + (2 \times\ 0.2)\ I_m = 4.4I_m \tag{31}$$

$$I_{row5} = (4)I_m + (2 \times\ 0.3)\ I_m = 4.6I_m \tag{32}$$

$$I_{row6} = (3)I_m + (2 \times\ 0.3)\ I_m + (1 \times\ 0.2)\ I_m = 3.8I_m \tag{33}$$

Figure 19. PV arrays reconfiguration in case 2; (a) TCT arrangement (b) Magic Square puzzle (c) d Distance arrangement (d) 8-Queen's technique

Figures 20 show the P-V and I-V characteristic curves for reconfiguration of the PV arrays by mentioned methods in case 2, respectively. The corresponding current, voltage, and power for adjusting the TCT interconnected, Magic Square puzzle, d Distance, and 8-Queen's techniques are given in Table 6.

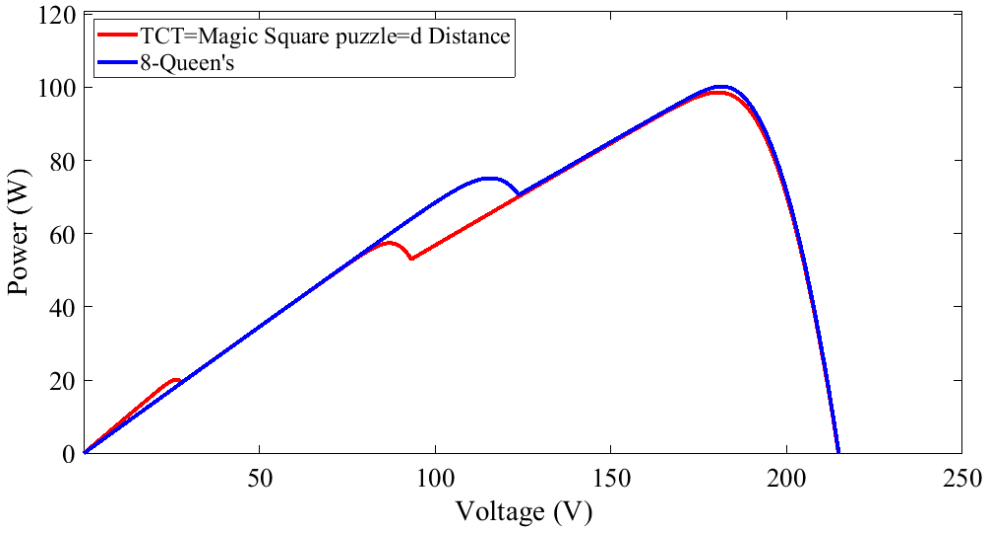

(a)

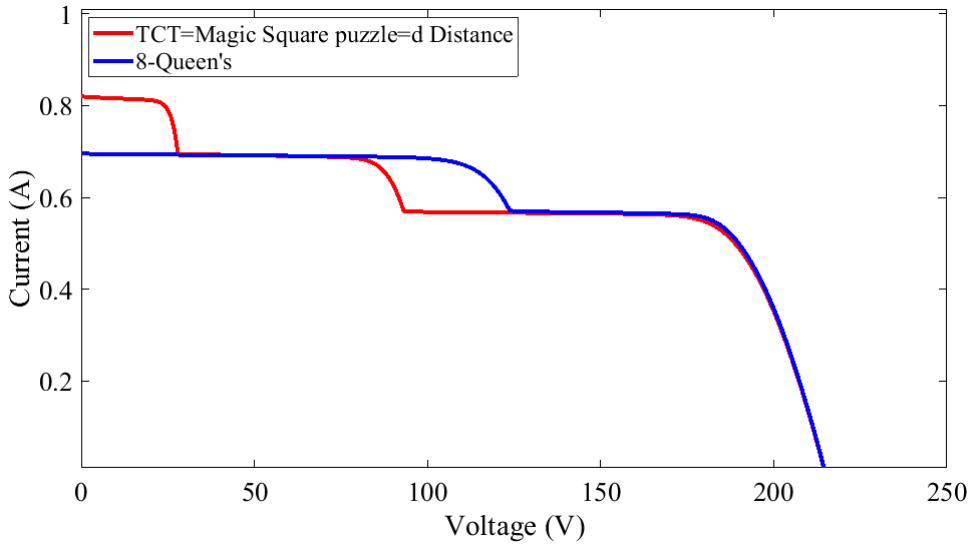

(b)

Figure 20. Simulation performed for the II group shadow conditions (a) P-V characteristics (b) I-V characteristics

Table 6. Current, voltage and power values for adjusting the TCT interconnected, Magic Square puzzle, d Distance, and 8-Queen's techniques in case 2

TCT interconnected				Magic Square puzzle				d Distance				8-Queen's			
Row bypassed	Current	Voltage	Power	Row bypassed	Current	Voltage	Power	Row bypassed	Current	Voltage	Power	Row bypassed	Current	Voltage	Power
Irow6	$3.9I_m$	$6V_m$	$11.V_mI_m$	Irow6	$3.7I_m$	$5V_m$	$\mathbf{18.5V_mI_m}$	Irow6	$3.8I_m$	$5V_m$	$\mathbf{19V_mI_m}$	Irow6	$3.7I_m$	$6V_m$	$\mathbf{22.2V_mI_m}$
Irow5	$3.9I_m$	$6V_m$	$11.7V_mI_m$	Irow5	$3.8I_m$	$4V_m$	$15.2V_mI_m$	Irow5	$3.7I_m$	$4V_m$	$13.6V_mI_m$	Irow5	$4.4I_m$	$4V_m$	$17.6V_mI_m$
Irow4	$3.8I_m$	$5V_m$	$\mathbf{14.8V_mI_m}$	Irow4	$4.5I_m$	$3V_m$	$13.5V_mI_m$	Irow4	$5.3I_m$	$2V_m$	$10.6V_mI_m$	Irow4	$4.6I_m$	$2V_m$	$9.2V_mI_m$
Irow3	$4.6I_m$	$4V_m$	$8.8V_mI_m$	Irow3	$5.3I_m$	$1V_m$	$5.3V_mI_m$	Irow3	$۴.5I_m$	$3V_m$	$13.5V_mI_m$	Irow3	$4.5I_m$	$3V_m$	$13.5V_mI_m$
Irow2	$4.6I_m$	$4V_m$	$8.8V_mI_m$	Irow۲	$3.8I_m$	$4V_m$	$15.2V_mI_m$	Irow2	$4.5I_m$	$3V_m$	$13.5V_mI_m$	Irow2	$۳.8I_m$	$5V_m$	$19V_mI_m$
Irow1	$5.3I_m$	$3V_m$	$5.2V_mI_m$	Irow۱	$3.7I_m$	$5V_m$	$\mathbf{۱۸.5V_mI_m}$	Irow1	$3.7I_m$	$4V_m$	$13.6V_mI_m$	Irow1	$4.5I_m$	$3V_m$	$13.5V_mI_m$

The results presented in Figure 20 and Table 6 shows that the highest GMPP value i.e. 22.2 I_mV_m was obtained of the 8-Queen's technique. Finally, the comparison of the results presented for case 2 emphasizes the efficiency of the suggested technique with the highest power generation compared to other methods.

3.3. Case 3:

As shown in Figure 21(a), in this case, a 9 × 9 TCT PV array is under shaded conditions with dimensions of 4 × 4 square and receive radiations of 1000 W/m^2, 300 W/m^2, 200 W/m^2. In this case, reconfiguring of the PV modules is performed in TCT interconnected and via Sudoku, optimal Sudoku, improved Sudoku, and 8-Queen's techniques. The reconfiguration of PV modules related to arrays in case 3 by the aforementioned solutions is represented in Figure 21. Locating the GMPP and calculating the amount of current generated in each row of this PV array is based on the equations used for case 1 (Equations 1-15). Figures 22 show the P-V and I-V characteristic curves for reconfiguration of the PV arrays by mentioned methods in case 3, respectively. The relative current, voltage, and power for adjusting the TCT interconnected, Sudoku, optimal Sudoku, improved Sudoku, and 8-Queen's techniques are given in Table 7.

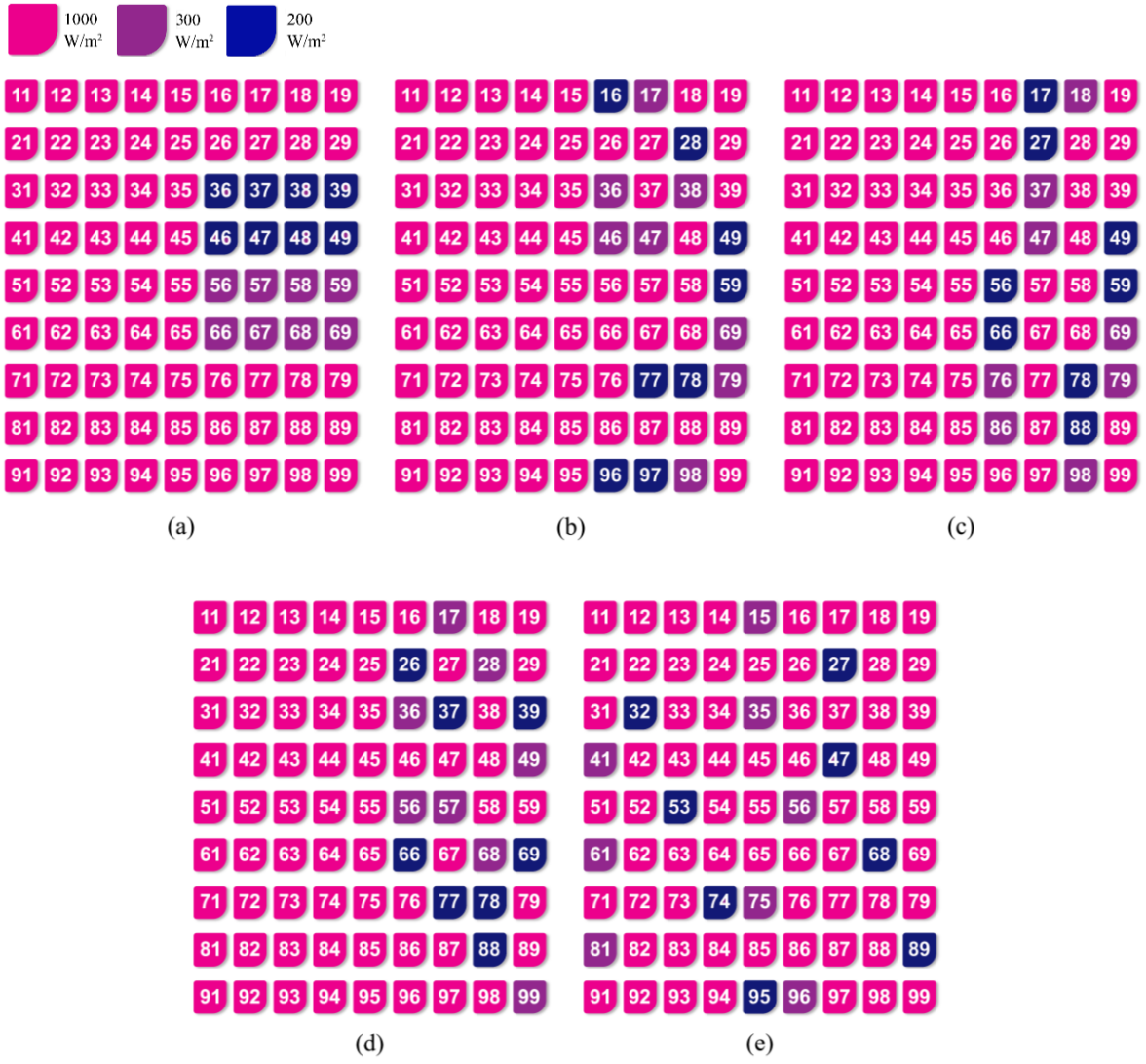

Figure. 21. PV arrays reconfiguration in case 3; (a) TCT arrangement (b) Sudoku arrangement (c) Optimal Sudoku arrangement (d) Improved Sudoku (e) 8-Queen's technique

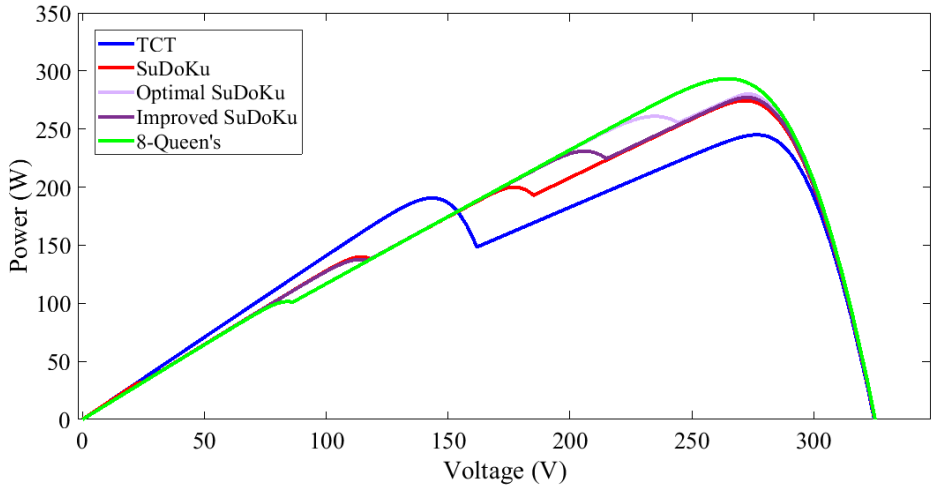

(a)

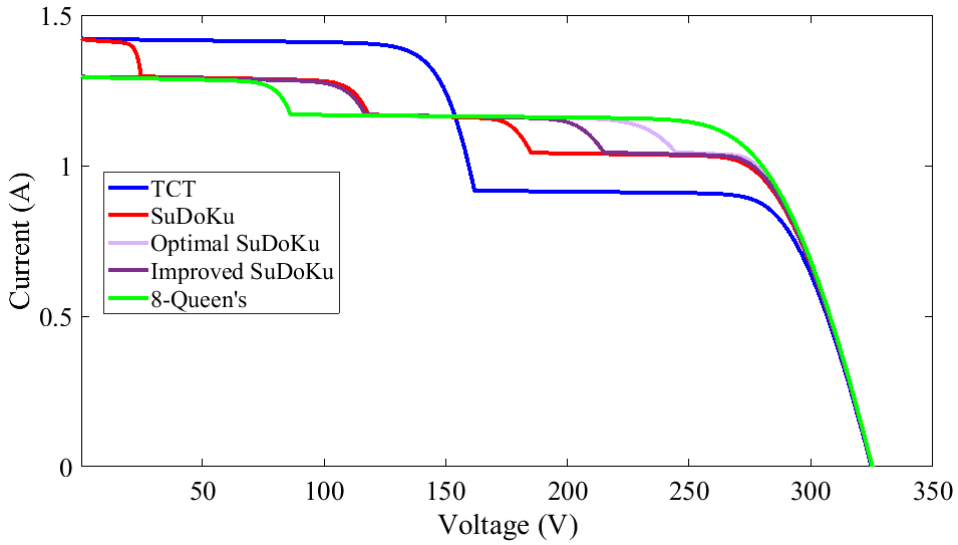

(b)

Figure 22. Simulation performed for the III group shadow conditions (a) P-V characteristics (b) I-V characteristics

Table 7. Current, voltage and power values for adjusting the TCT interconnected, Sudoku, optimal Sudoku, improved Sudoku, and 8-Queen's techniques in case 3

TCT interconnected				Sudoku arrangement				Optimal Sudoku arrangement				Improved Sudoku arrangement				8-Queen's arrangement			
Row bypassed	Current	Voltage	Power	Row bypassed	Current	Voltage	Power	Row bypassed	Current	Voltage	Power	Row bypassed	Current	Voltage	Power	Row bypassed	Current	Voltage	Power
Irow9	$9I_m$	$5V_m$	$45V_mI_m$	Irow9	$6.8I_m$	$8V_m$	$54.4V_mI_m$	Irow9	$8.2I_m$	$6V_m$	$49.2V_mI_m$	Irow9	$8.2I_m$	$5V_m$	$41V_mI_m$	Irow9	$7.5I_m$	$9V_m$	$\mathbf{67.5V_mI_m}$
Irow8	$9I_m$	$5V_m$	$45V_mI_m$	Irow8	$9I_m$	$3V_m$	$27V_mI_m$	Irow8	$7.5I_m$	$8V_m$	$60V_mI_m$	Irow8	$8.3I_m$	$4V_m$	$33.2V_mI_m$	Irow8	$7.5I_m$	$9V_m$	$\mathbf{67.5V_mI_m}$
Irow7	$9I_m$	$5V_m$	$45V_mI_m$	Irow7	$6.8I_m$	$8V_m$	$54.4V_mI_m$	Irow7	$6.7I_m$	$9V_m$	$\mathbf{60.3V_mI_m}$	Irow7	$7.6I_m$	$6V_m$	$45.6V_mI_m$	Irow7	$7.5I_m$	$9V_m$	$\mathbf{67.5V_mI_m}$
Irow6	$5.8I_m$	$9V_m$	$\mathbf{52.2V_mI_m}$	Irow6	$8.2I_m$	$5V_m$	$41V_mI_m$	Irow6	$7.5I_m$	$8V_m$	$60V_mI_m$	Irow6	$6.8I_m$	$9V_m$	$\mathbf{61.2V_mI_m}$	Irow6	$7.5I_m$	$9V_m$	$\mathbf{67.5V_mI_m}$
Irow5	$5.8I_m$	$9V_m$	$\mathbf{52.2V_mI_m}$	Irow5	$8.3I_m$	$4V_m$	$33.2V_mI_m$	Irow5	$7.6I_m$	$7V_m$	$53.2V_mI_m$	Irow5	$7.4I_m$	$8V_m$	$59.2V_mI_m$	Irow5	$7.5I_m$	$9V_m$	$\mathbf{67.5V_mI_m}$
Irow4	$6.2I_m$	$7V_m$	$43.4V_mI_m$	Irow4	$6.7I_m$	$9V_m$	$\mathbf{60.3V_mI_m}$	Irow4	$7.5I_m$	$8V_m$	$60V_mI_m$	Irow4	$8.2I_m$	$5V_m$	$41V_mI_m$	Irow4	$7.5I_m$	$9V_m$	$\mathbf{67.5V_mI_m}$
Irow3	$6.2I_m$	$7V_m$	$43.4V_mI_m$	Irow3	$7.4I_m$	$7V_m$	$51.8V_mI_m$	Irow3	$8.2I_m$	$6V_m$	$49.2V_mI_m$	Irow3	$6.8I_m$	$9V_m$	$\mathbf{61.2V_mI_m}$	Irow3	$7.5I_m$	$9V_m$	$\mathbf{67.5V_mI_m}$
Irow2	$9I_m$	$5V_m$	$45V_mI_m$	Irow2	$8.3I_m$	$4V_m$	$33.2V_mI_m$	Irow2	$8.3I_m$	$5V_m$	$41.5V_mI_m$	Irow2	$7.5I_m$	$7V_m$	$52.2V_mI_m$	Irow2	$8.3I_m$	$8V_m$	$66.4V_mI_m$
Irow1	$9I_m$	$5V_m$	$45V_mI_m$	Irow1	$7.5I_m$	$6V_m$	$45V_mI_m$	Irow1	$7.5I_m$	$8V_m$	$60V_mI_m$	Irow1	$8.2I_m$	$5V_m$	$41V_mI_m$	Irow1	$8.2I_m$	$7V_m$	$57.4V_mI_m$

Based on the results presented in Figure 22 and Table 7, it is observed that the highest GMPP value i.e. 67.5 I_mV_m was obtained of the suggested technique.

3.4.Case 4:

In case 4, at the bottom section of the PV array, there is a partial shadow with a size of 3×6 and receive different irradiance levels of $1000\ W/m^2$, $300\ W/m^2$, $200\ W/m^2$, as shown in Figure 23(a). In this case, partial shade is distributed by the Sudoku, optimal Sudoku, improved Sudoku, and 8-Queen's methods (As seen in Figure 23). The theoretical GMPP, simulated by drawing the I-V and P-V specifications, is shown in Figure 24. The location of GMPP for the TCT interconnected, Sudoku, optimal Sudoku, improved Sudoku, and 8-Queen's arrangements are calculated theoretically and are presented in Table 8. According to the presented results in Table 8, the highest GMPPT is obtained by the 8-Queen's technique i.e. 66.6 $I_m V_m$.

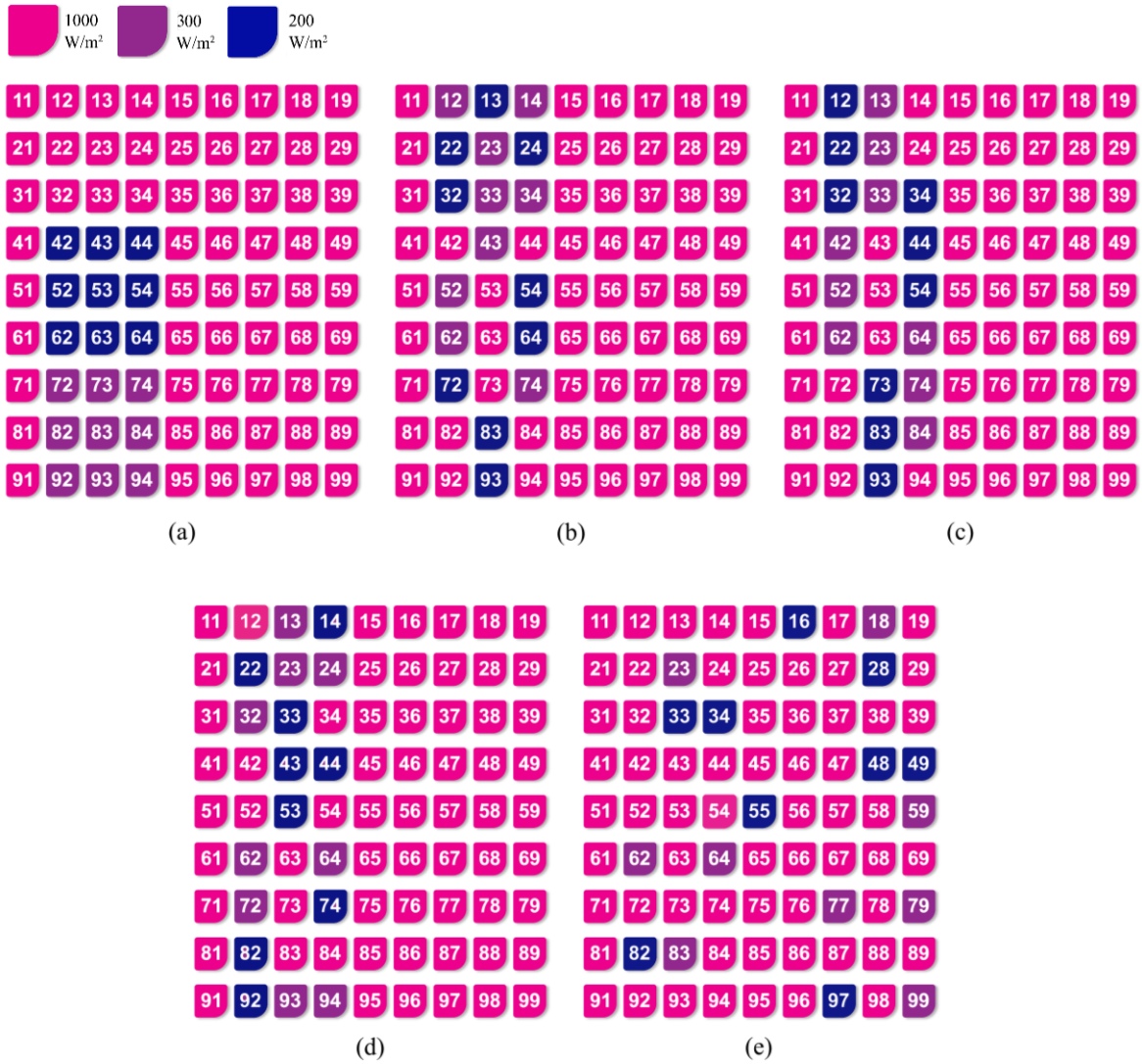

Figure 23. PV arrays reconfiguration in case 4; (a) TCT arrangement (b) Sudoku (c) Optimal Sudoku (d) Improved Sudoku (e) 8-Queen's technique

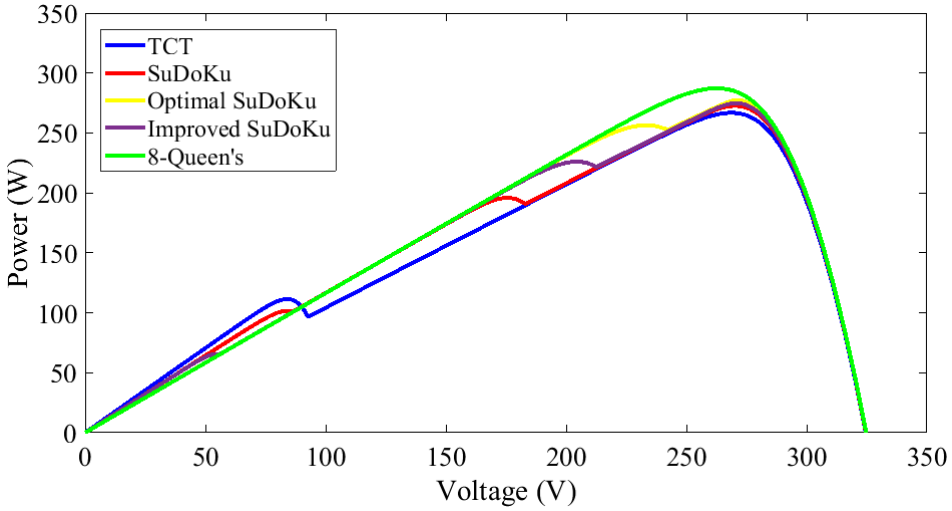

(a)

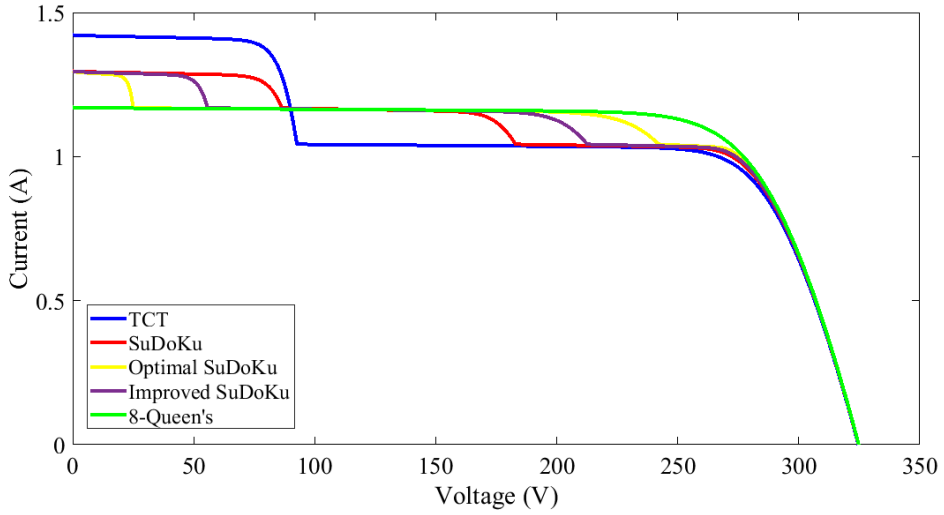

(b)

Figure 24. Simulation performed for the IV group shadow conditions (a) P-V characteristics (b) I-V characteristics

Table 8. Current, voltage and power values for adjusting the TCT interconnected, Sudoku, optimal Sudoku, improved Sudoku, and 8-Queen's techniques in case 4

TCT interconnected				Sudoku arrangement				Optimal Sudoku arrangement				Improved Sudoku arrangement				8-Queen's arrangement			
Row bypassed	Current	Voltage	Power	Row bypassed	Current	Voltage	Power	Row bypassed	Current	Voltage	Power	Row bypassed	Current	Voltage	Power	Row bypassed	Current	Voltage	Power
Irow9	$6.9I_m$	$7V_m$	$48.3V_mI_m$	Irow9	$8.2I_m$	$5V_m$	$41V_mI_m$	Irow9	$8.2I_m$	$6V_m$	$49.2V_mI_m$	Irow9	$6.8I_m$	$9V_m$	$\mathbf{61.2V_mI_m}$	Irow9	$7.5I_m$	$8V_m$	$60V_mI_m$
Irow8	$6.9I_m$	$7V_m$	$48.3V_mI_m$	Irow8	$8.2I_m$	$6V_m$	$41V_mI_m$	Irow8	$7.5I_m$	$8V_m$	$60V_mI_m$	Irow8	$8.2I_m$	$5V_m$	$41V_mI_m$	Irow8	$7.5I_m$	$8V_m$	$60V_mI_m$
Irow7	$6.9I_m$	$7V_m$	$48.3V_mI_m$	Irow7	$7.5I_m$	$7V_m$	$52.5V_mI_m$	Irow7	$7.5I_m$	$8V_m$	$60V_mI_m$	Irow7	$7.5I_m$	$7V_m$	$52.5V_mI_m$	Irow7	$7.6I_m$	$7V_m$	$53.2V_mI_m$
Irow6	$6.6I_m$	$9V_m$	$\mathbf{59.4V_mI_m}$	Irow6	$7.5I_m$	$7V_m$	$52.5V_mI_m$	Irow6	$7.6I_m$	$7V_m$	$53.2V_mI_m$	Irow6	$7.6I_m$	$6V_m$	$45.6V_mI_m$	Irow6	$7.6I_m$	$7V_m$	$53.2V_mI_m$
Irow5	$6.6I_m$	$9V_m$	$\mathbf{59.4V_mI_m}$	Irow5	$7.5I_m$	$7V_m$	$52.5V_mI_m$	Irow5	$7.5I_m$	$8V_m$	$60V_mI_m$	Irow5	$8.2I_m$	$5V_m$	$41V_mI_m$	Irow5	$7.5I_m$	$8V_m$	$60V_mI_m$
Irow4	$6.6I_m$	$9V_m$	$\mathbf{59.4V_mI_m}$	Irow4	$8.3I_m$	$4V_m$	$33.2V_mI_m$	Irow4	$7.5I_m$	$8V_m$	$60V_mI_m$	Irow4	$7.4I_m$	$8V_m$	$45.6V_mI_m$	Irow4	$7.4I_m$	$9V_m$	$\mathbf{66.6V_mI_m}$
Irow3	$9I_m$	$5V_m$	$54V_mI_m$	Irow3	$6.8I_m$	$8V_m$	$54.4V_mI_m$	Irow3	$6.7I_m$	$9V_m$	$\mathbf{60.3V_mI_m}$	Irow3	$7.5I_m$	$7V_m$	$52.5V_mI_m$	Irow3	$7.4I_m$	$9V_m$	$\mathbf{66.6V_mI_m}$
Irow2	$9I_m$	$5V_m$	$54V_mI_m$	Irow2	$6.7I_m$	$9V_m$	$\mathbf{60.3V_mI_m}$	Irow2	$7.5I_m$	$8V_m$	$60V_mI_m$	Irow2	$6.8I_m$	$9V_m$	$\mathbf{61.2V_mI_m}$	Irow2	$7.5I_m$	$8V_m$	$60V_mI_m$
Irow1	$9I_m$	$5V_m$	$54V_mI_m$	Irow1	$6.8I_m$	$8V_m$	$54.4V_mI_m$	Irow1	$7.5I_m$	$8V_m$	$60V_mI_m$	Irow1	$7.5I_m$	$7V_m$	$52.5V_mI_m$	Irow1	$7.5I_m$	$8V_m$	$60V_mI_m$

3.5.Case 5:

In this case, a 9 × 9 TCT PV array is under PSC with the size of 4 × 4 and receive the radiations of 1000 W/m^2, 400 W/m^2, 100 W/m^2. In this case, reconfiguring of the PV modules is performed in TCT interconnected and via Sudoku, optimal Sudoku, improved Sudoku, and 8-Queen's techniques. The reconfiguration of PV modules related to arrays in case 5 by the aforementioned solutions is represented in Figure 25. The P-V and I-V characteristic curves for reconfiguration of the PV arrays by mentioned methods in case 5 are shown in Figure 26, respectively. The relative current, voltage, and power for adjusting the TCT interconnected and 8-Queen's techniques are given in Table 9.

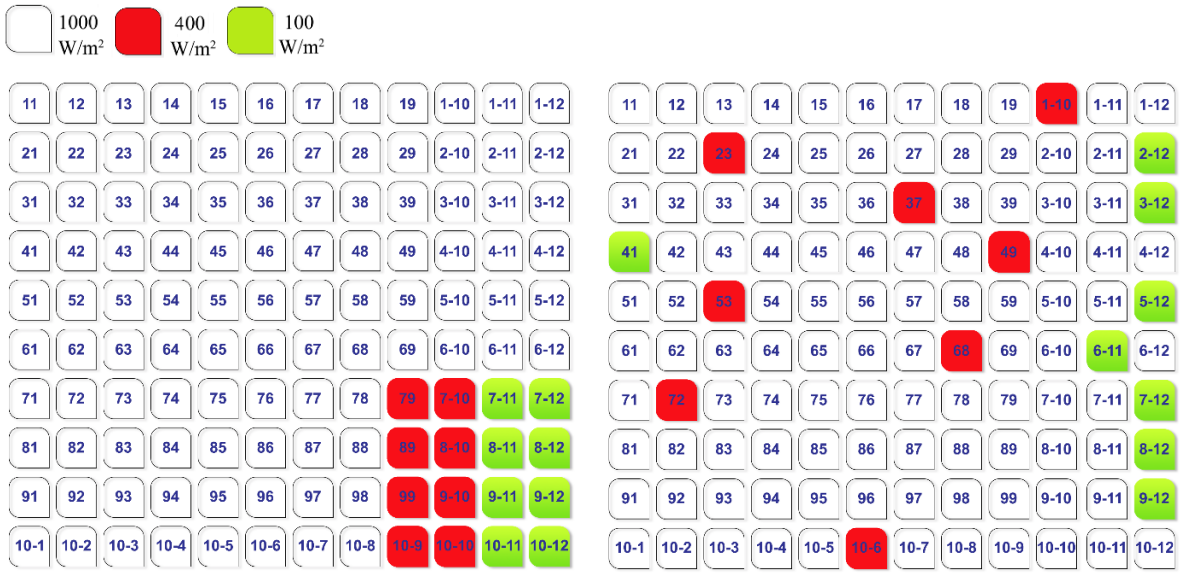

(a) (b)

Figure 25. PV arrays reconfiguration in case 5; (a) TCT arrangement (b) 8-Queen's technique

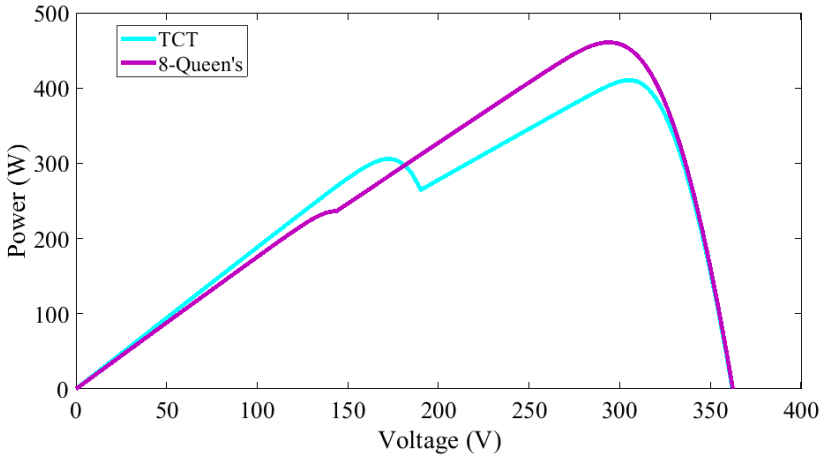

(a)

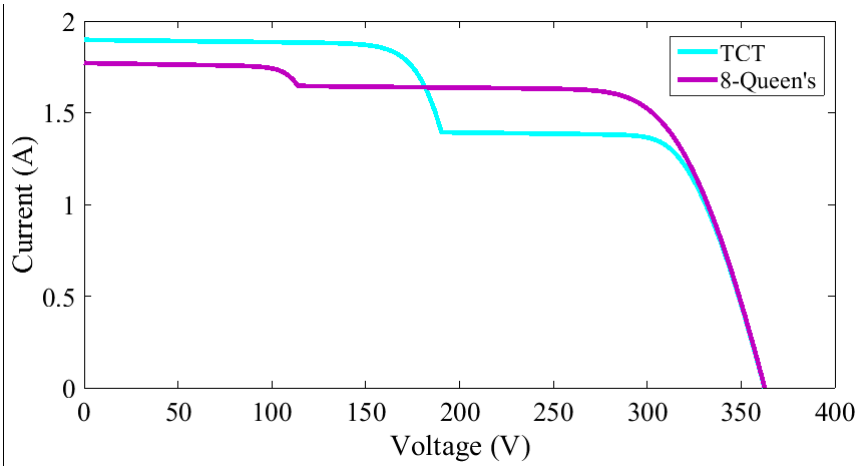

(b)

Figure 26. Simulation performed for the V group shadow conditions (a) P-V characteristics (b) I-V characteristics

Table 9. Current, voltage, and power values for adjusting the TCT interconnected and 8-Queen's techniques in case 5

TCT interconnected				8-Queen's technique			
Row bypassed	Current	Voltage	Power	Row bypassed	Current	Voltage	Power
Irow10	$9I_m$	$12V_m$	$108V_mI_m$	Irow10	$11.4I_m$	$8V_m$	$91.2V_mI_m$
Irow9	$9I_m$	$12V_m$	$108V_mI_m$	Irow9	$11.1I_m$	$10V_m$	$111V_mI_m$
Irow8	$9I_m$	$12V_m$	$108V_mI_m$	Irow8	$11.1I_m$	$10V_m$	$111V_mI_m$
Irow7	$9I_m$	$١٢V_m$	$١٠٨V_mI_m$	Irow7	$10.5I_m$	$12V_m$	$\mathbf{126V_mI_m}$
Irow6	$12I_m$	$١٠V_m$	$\mathbf{١٢٠V_mI_m}$	Irow6	$10.5I_m$	$12V_m$	$\mathbf{126V_mI_m}$
Irow5	$12I_m$	$١٠V_m$	$\mathbf{١٢٠V_mI_m}$	Irow5	$10.5I_m$	$12V_m$	$\mathbf{126V_mI_m}$
Irow4	$12I_m$	$١٠V_m$	$\mathbf{١٢٠V_mI_m}$	Irow4	$10.5I_m$	$12V_m$	$\mathbf{126V_mI_m}$
Irow3	$12I_m$	$١٠V_m$	$\mathbf{١٢٠V_mI_m}$	Irow3	$10.5I_m$	$12V_m$	$\mathbf{126V_mI_m}$
Irow2	$12I_m$	$١٠V_m$	$\mathbf{١٢٠V_mI_m}$	Irow2	$10.5I_m$	$12V_m$	$\mathbf{126V_mI_m}$
Irow1	$12I_m$	$١٠V_m$	$\mathbf{١٢٠V_mI_m}$	Irow1	$11.4I_m$	$8V_m$	$91.2V_mI_m$

The results presented in Figure 26 and Table 9 shows that the highest GMPP value i.e. $126\,I_mV_m$ was obtained of the 8-Queen's technique. Given that other methods used for reconfiguring could not be applied to rectangular PV arrays, the results presented in Table 9 show the capability of 8-Queen's technique in the reconfiguration of the rectangular PV array.

3.6.Case 6:

To illustrate the ability of the 8-Queen's technique in the reconfiguration of large-sized PV arrays, case 6 is considered as a large dimension TCT PV array in the size of 20×20. As shown in Figure 27(a), in this case, the shadow with the size of 6×6 affects the PV array. Thus, shadow-less modules receive the irradiance of $1000\,W/m^2$ and shadowed modules receive the irradiance of $300\,W/m^2$ and $200\,W/m^2$ differently. Figure 27 shows how the shadow is distributed in the PV array of case 6 by the 8-Queen's technique.

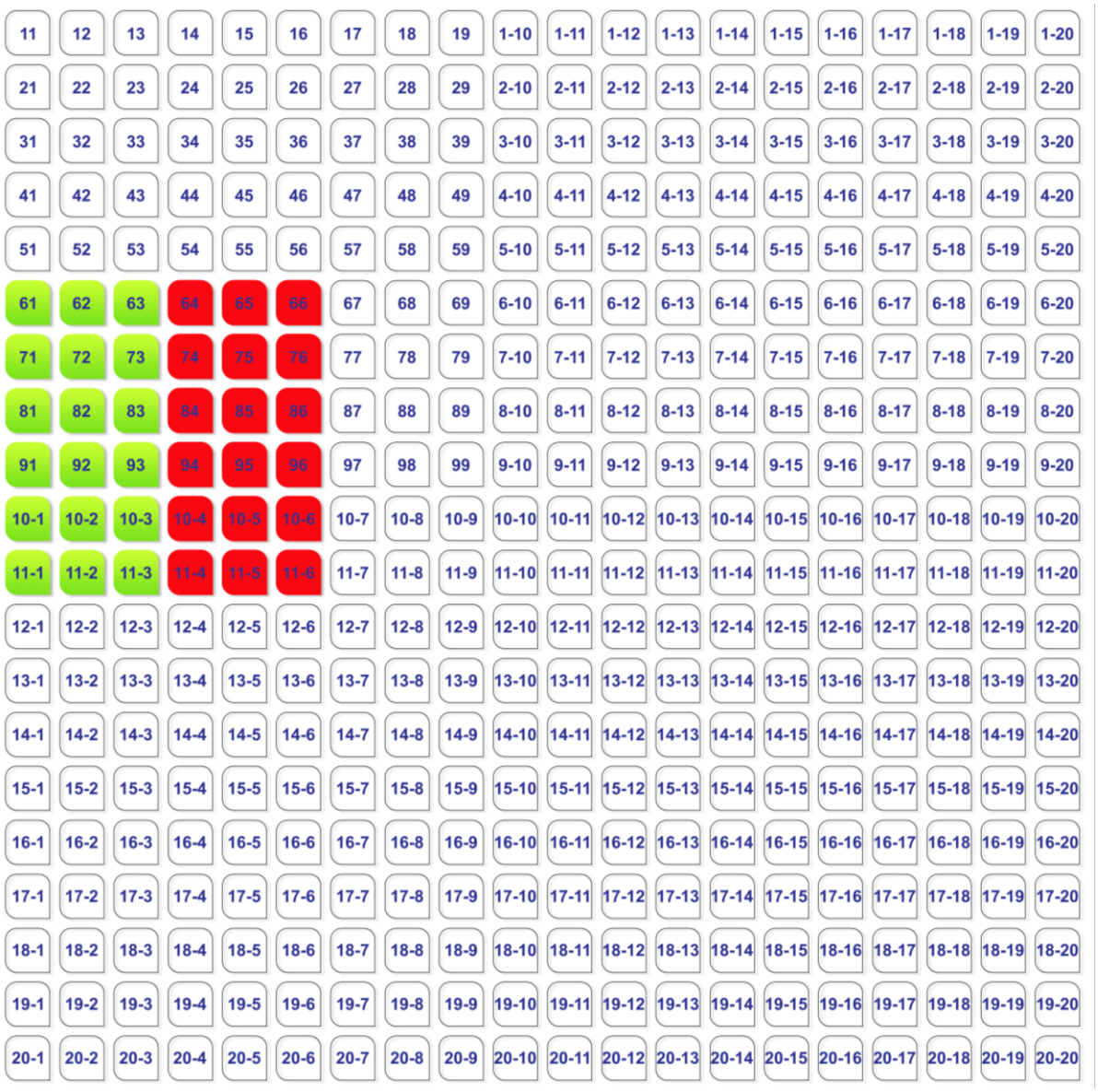
11 12 13 14 15 16 17 18 19 1-10 1-11 1-12 1-13 1-14 1-15 1-16 1-17 1-18 1-19 1-20
21 22 23 24 25 26 27 28 29 2-10 2-11 2-12 2-13 2-14 2-15 2-16 2-17 2-18 2-19 2-20
31 32 33 34 35 36 37 38 39 3-10 3-11 3-12 3-13 3-14 3-15 3-16 3-17 3-18 3-19 3-20
41 42 43 44 45 46 47 48 49 4-10 4-11 4-12 4-13 4-14 4-15 4-16 4-17 4-18 4-19 4-20
51 52 53 54 55 56 57 58 59 5-10 5-11 5-12 5-13 5-14 5-15 5-16 5-17 5-18 5-19 5-20
61 62 63 64 65 66 67 68 69 6-10 6-11 6-12 6-13 6-14 6-15 6-16 6-17 6-18 6-19 6-20
71 72 73 74 75 76 77 78 79 7-10 7-11 7-12 7-13 7-14 7-15 7-16 7-17 7-18 7-19 7-20
81 82 83 84 85 86 87 88 89 8-10 8-11 8-12 8-13 8-14 8-15 8-16 8-17 8-18 8-19 8-20
91 92 93 94 95 96 97 98 99 9-10 9-11 9-12 9-13 9-14 9-15 9-16 9-17 9-18 9-19 9-20
10-1 10-2 10-3 10-4 10-5 10-6 10-7 10-8 10-9 10-10 10-11 10-12 10-13 10-14 10-15 10-16 10-17 10-18 10-19 10-20
11-1 11-2 11-3 11-4 11-5 11-6 11-7 11-8 11-9 11-10 11-11 11-12 11-13 11-14 11-15 11-16 11-17 11-18 11-19 11-20
12-1 12-2 12-3 12-4 12-5 12-6 12-7 12-8 12-9 12-10 12-11 12-12 12-13 12-14 12-15 12-16 12-17 12-18 12-19 12-20
13-1 13-2 13-3 13-4 13-5 13-6 13-7 13-8 13-9 13-10 13-11 13-12 13-13 13-14 13-15 13-16 13-17 13-18 13-19 13-20
14-1 14-2 14-3 14-4 14-5 14-6 14-7 14-8 14-9 14-10 14-11 14-12 14-13 14-14 14-15 14-16 14-17 14-18 14-19 14-20
15-1 15-2 15-3 15-4 15-5 15-6 15-7 15-8 15-9 15-10 15-11 15-12 15-13 15-14 15-15 15-16 15-17 15-18 15-19 15-20
16-1 16-2 16-3 16-4 16-5 16-6 16-7 16-8 16-9 16-10 16-11 16-12 16-13 16-14 16-15 16-16 16-17 16-18 16-19 16-20
17-1 17-2 17-3 17-4 17-5 17-6 17-7 17-8 17-9 17-10 17-11 17-12 17-13 17-14 17-15 17-16 17-17 17-18 17-19 17-20
18-1 18-2 18-3 18-4 18-5 18-6 18-7 18-8 18-9 18-10 18-11 18-12 18-13 18-14 18-15 18-16 18-17 18-18 18-19 18-20
19-1 19-2 19-3 19-4 19-5 19-6 19-7 19-8 19-9 19-10 19-11 19-12 19-13 19-14 19-15 19-16 19-17 19-18 19-19 19-20
20-1 20-2 20-3 20-4 20-5 20-6 20-7 20-8 20-9 20-10 20-11 20-12 20-13 20-14 20-15 20-16 20-17 20-18 20-19 20-20

(a)

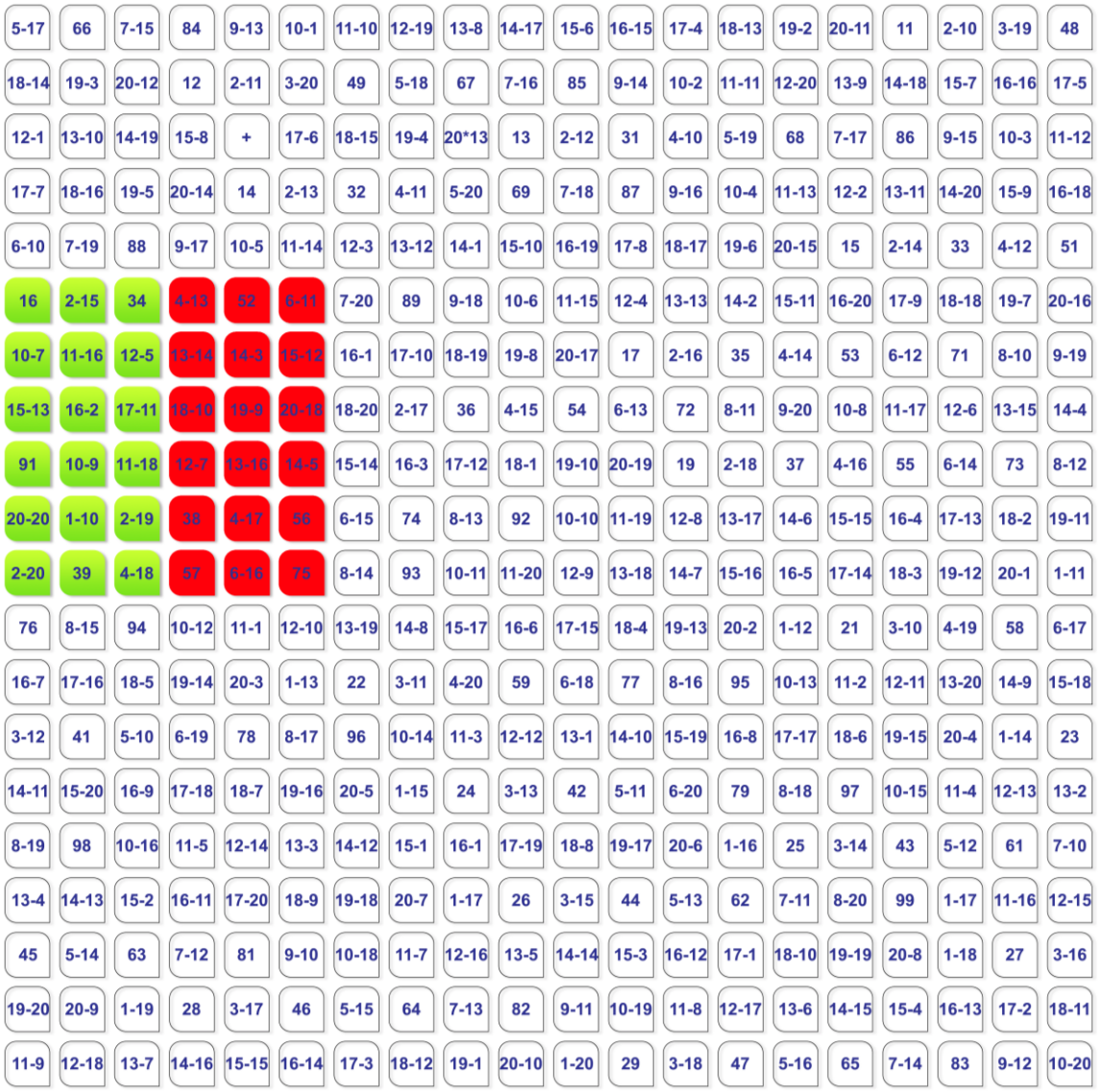
5-17 66 7-15 84 9-13 10-1 11-10 12-19 13-8 14-17 15-6 16-15 17-4 18-13 19-2 20-11 11 2-10 3-19 48
18-14 19-3 20-12 12 2-11 3-20 49 5-18 67 7-16 85 9-14 10-2 11-11 12-20 13-9 14-18 15-7 16-16 17-5
12-1 13-10 14-19 15-8 + 17-6 18-15 19-4 20*13 13 2-12 31 4-10 5-19 68 7-17 86 9-15 10-3 11-12
17-7 18-16 19-5 20-14 14 2-13 32 4-11 5-20 69 7-18 87 9-16 10-4 11-13 12-2 13-11 14-20 15-9 16-18
6-10 7-19 88 9-17 10-5 11-14 12-3 13-12 14-1 15-10 16-19 17-8 18-17 19-6 20-15 15 2-14 33 4-12 51
16 2-15 34 4-13 52 6-11 7-20 89 9-18 10-6 11-15 12-4 13-13 14-2 15-11 16-20 17-9 18-18 19-7 20-16
10-7 11-16 12-5 13-14 14-3 15-12 16-1 17-10 18-19 19-8 20-17 17 2-16 35 4-14 53 6-12 71 8-10 9-19
15-13 16-2 17-11 18-10 19-9 20-18 18-20 2-17 36 4-15 54 6-13 72 8-11 9-20 10-8 11-17 12-6 13-15 14-4
91 10-9 11-18 12-7 13-16 14-5 15-14 16-3 17-12 18-1 19-10 20-19 19 2-18 37 4-16 55 6-14 73 8-12
20-20 1-10 2-19 38 4-17 56 6-15 74 8-13 92 10-10 11-19 12-8 13-17 14-6 15-15 16-4 17-13 18-2 19-11
2-20 39 4-18 57 6-16 75 8-14 93 10-11 11-20 12-9 13-18 14-7 15-16 16-5 17-14 18-3 19-12 20-1 1-11
76 8-15 94 10-12 11-1 12-10 13-19 14-8 15-17 16-6 17-15 18-4 19-13 20-2 1-12 21 3-10 4-19 58 6-17
16-7 17-16 18-5 19-14 20-3 1-13 22 3-11 4-20 59 6-18 77 8-16 95 10-13 11-2 12-11 13-20 14-9 15-18
3-12 41 5-10 6-19 78 8-17 96 10-14 11-3 12-12 13-1 14-10 15-19 16-8 17-17 18-6 19-15 20-4 1-14 23
14-11 15-20 16-9 17-18 18-7 19-16 20-5 1-15 24 3-13 42 5-11 6-20 79 8-18 97 10-15 11-4 12-13 13-2
8-19 98 10-16 11-5 12-14 13-3 14-12 15-1 16-1 17-19 18-8 19-17 20-6 1-16 25 3-14 43 5-12 61 7-10
13-4 14-13 15-2 16-11 17-20 18-9 19-18 20-7 1-17 26 3-15 44 5-13 62 7-11 8-20 99 1-17 11-16 12-15
45 5-14 63 7-12 81 9-10 10-18 11-7 12-16 13-5 14-14 15-3 16-12 17-1 18-10 19-19 20-8 1-18 27 3-16
19-20 20-9 1-19 28 3-17 46 5-15 64 7-13 82 9-11 10-19 11-8 12-17 13-6 14-15 15-4 16-13 17-2 18-11
11-9 12-18 13-7 14-16 15-15 16-14 17-3 18-12 19-1 20-10 1-20 29 3-18 47 5-16 65 7-14 83 9-12 10-20

(b)

(c)

Figure 27. PV arrays reconfiguration in case 5; (a) TCT arrangement, (b) Shadow on the proposed method (8-Queen), (c) Shadow distribution by the 8-Queen's technique

As the ability to apply on the large-size PV arrays has been cited as one of the most important capabilities of the 8-Queen's technique in the literature, Figure 27(c) shows this fact. It is noticeable that the proposed technique was able to spread the desired shadow well in all rows of the PV array. Figure 28 illustrates the P-V and I-V characteristic curves for reconfiguration of the PV arrays in case 6, respectively. The corresponding current, voltage, and power for adjusting the TCT interconnected and 8-Queen's technique are given in Table 10.

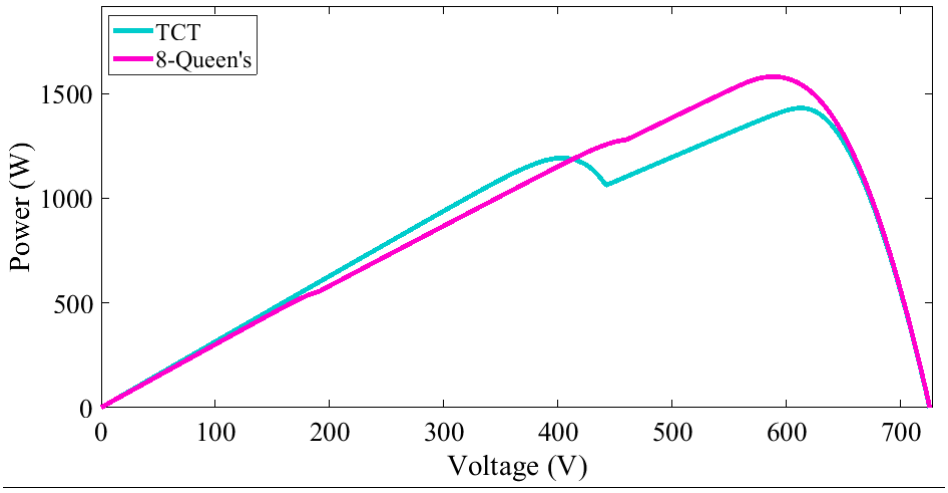

(a)

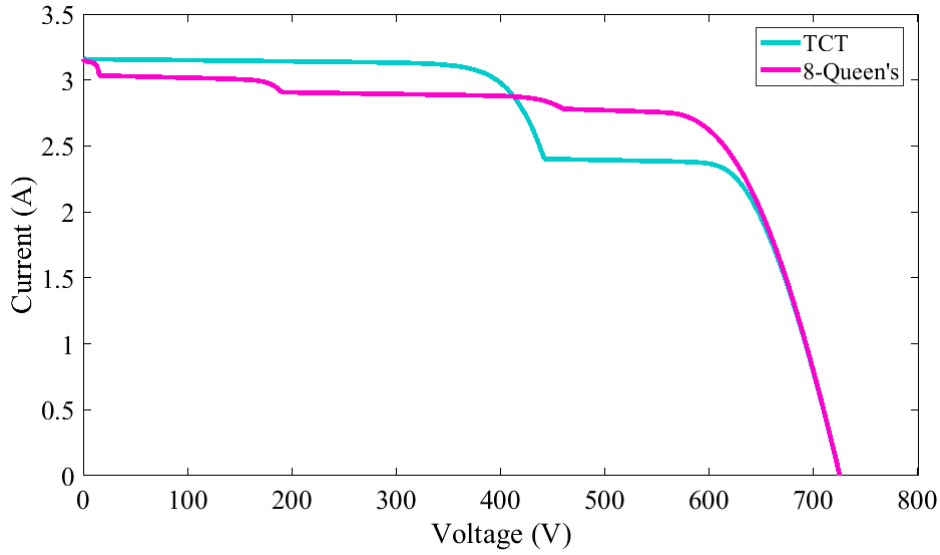

(b)

Figure 28. Simulation performed for the VI group shadow conditions (a) P-V characteristics (b) I-V characteristics

Table 10. Current, voltage, and power values for adjusting the TCT interconnected and 8-Queen's technique in case 6

TCT interconnected				8-Queen's technique			
Row bypassed	Current	Voltage	Power	Row bypassed	Current	Voltage	Power
Irow20	$20I_m$	$12V_m$	**$320V_mI_m$**	Irow20	$18.5I_m$	$16V_m$	$296V_mI_m$
Irow19	$20I_m$	$12V_m$	**$320V_mI_m$**	Irow19	$19.4I_m$	$13V_m$	$252.2V_mI_m$
Irow18	$20I_m$	$12V_m$	**$320V_mI_m$**	Irow18	$19.4I_m$	$13V_m$	$252.2V_mI_m$
Irow17	$20I_m$	$12V_m$	**$320V_mI_m$**	Irow17	$19.1I_m$	$14V_m$	$267.4V_mI_m$
Irow16	$20I_m$	$12V_m$	**$320V_mI_m$**	Irow16	$19.1I_m$	$14V_m$	$267.4V_mI_m$
Irow15	$20I_m$	$12V_m$	**$320V_mI_m$**	Irow15	$18.5I_m$	$16V_m$	$296V_mI_m$
Irow14	$20I_m$	$12V_m$	**$320V_mI_m$**	Irow14	$18.8I_m$	$15V_m$	$282V_mI_m$
Irow13	$20I_m$	$12V_m$	**$320V_mI_m$**	Irow13	$18.8I_m$	$15V_m$	$282V_mI_m$
Irow12	$20I_m$	$12V_m$	**$320V_mI_m$**	Irow12	$18.5I_m$	$16V_m$	$296V_mI_m$
Irow11	$15.5I_m$	$20V_m$	$310V_mI_m$	Irow11	$18.2I_m$	$17V_m$	$309.4V_mI_m$

Irow10	$15.5I_m$	$20V_m$	$310V_mI_m$	Irow10	$18.2I_m$	$17V_m$	$309.4V_mI_m$
Irow9	$15.5I_m$	$20V_m$	$310V_mI_m$	Irow9	$19.1I_m$	$14V_m$	$267.4V_mI_m$
Irow8	$15.5I_m$	$20V_m$	$310V_mI_m$	Irow8	$20I_m$	$12V_m$	$240V_mI_m$
Irow7	$15.5I_m$	$20V_m$	$310V_mI_m$	Irow7	$19.4I_m$	$13V_m$	$252.2V_mI_m$
Irow6	$15.5I_m$	$20V_m$	$310V_mI_m$	Irow6	$18.8I_m$	$15V_m$	$282V_mI_m$
Irow5	$20I_m$	$12V_m$	$\mathbf{320V_mI_m}$	Irow5	$18.2I_m$	$17V_m$	$309.4V_mI_m$
Irow4	$20I_m$	$12V_m$	$\mathbf{320V_mI_m}$	Irow4	$17.9I_m$	$18V_m$	$322.2V_mI_m$
Irow3	$20I_m$	$12V_m$	$\mathbf{320V_mI_m}$	Irow3	$17.6I_m$	$19V_m$	$334V_mI_m$
Irow2	$20I_m$	$12V_m$	$\mathbf{320V_mI_m}$	Irow2	$17.3I_m$	$20V_m$	$\mathbf{346V_mI_m}$
Irow1	$20I_m$	$12V_m$	$\mathbf{320V_mI_m}$	Irow1	$18.2I_m$	$17V_m$	$309.4V_mI_m$

The results presented in Figure 28 and Table 10 represents that the highest GMPP value i.e. 346 I_mV_m was obtained of the 8-Queen's technique. It should be noted that the other solutions used in this paper for comparison with the 8-Queen's technique do not apply to the reconfiguration of large-size PV arrays such as case 6.

3.7.Case 7:

To present the capability of the 8-Queen's technique in the reconfiguration of very small-sized PV arrays, this case is considered as a small dimension TCT PV array in the size of 4×4. As shown in Figure 29(a), in this case, the shadow with the size of 2×4 affects the PV array. Thus, shadow-less modules receive the irradiance of 1000 W/m^2 and shadowed modules receive the irradiance of 300 W/m^2 and 200 W/m^2 differently. Figure 29 shows how the shadow is scattered in the PV array of case 7 by the 8-Queen's technique.

Figure 29. PV arrays reconfiguration in case 7; (a) TCT arrangement, (b) Magic Square puzzle, (c) d Distance arrangement, (d) 8-Queen's technique

Figure 29(d) shows the high ability of the 8-Queen's technique to reconfiguration shaded modules in this case. As mentioned in the literature, other conventional Sudoku-based techniques were not able to do this. Figure 30 shows the P-V and I-V characteristic curves for reconfiguration PV array modules in Case 7, respectively. The related current, voltage, and power for the TCT interconnected, Magic Square, d Distance, and the 8-Queen's technique are given in Table 11.

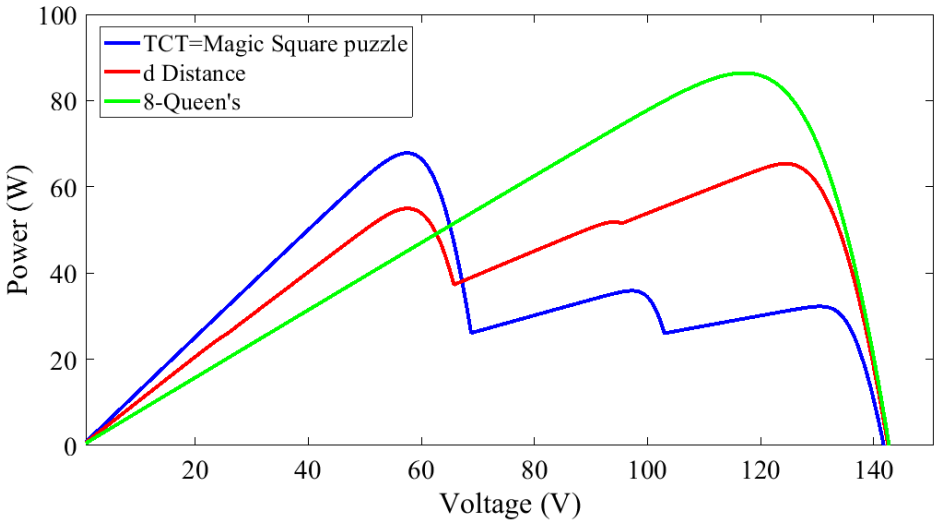

(a)

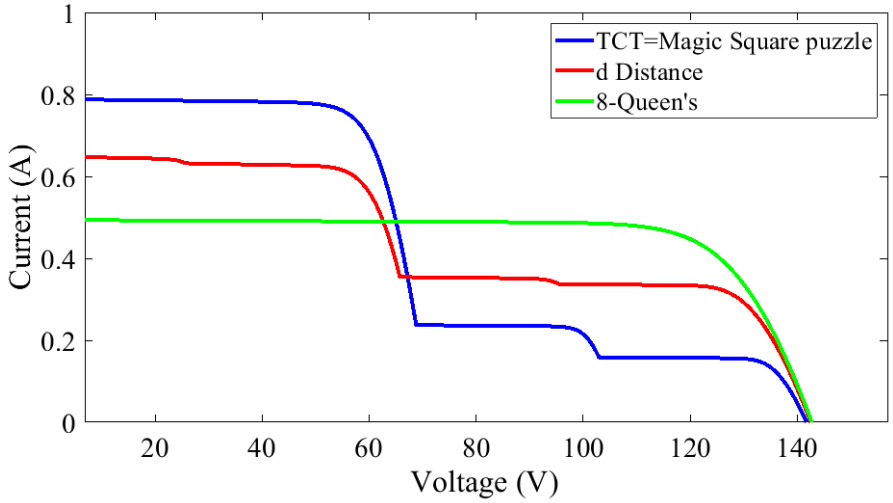

(b)

Figure 30. Simulation performed for the VII group shadow conditions (a) P-V characteristics (b) I-V characteristics

Table 11. Current, voltage and power values for adjusting the TCT interconnected, Magic Square puzzle, d Distance, and 8-Queen's techniques in case 7

TCT interconnected				Magic Square puzzle				d Distance				8-Queen's arrangement			
Row bypassed	Current	Voltage	Power	Row bypassed	Current	Voltage	Power	Row bypassed	Current	Voltage	Power	Row bypassed	Current	Voltage	Power
Irow4	$4I_m$	$1V_m$	$\mathbf{4V_mI_m}$	Irow4	$4I_m$	$1V_m$	$4V_mI_m$	Irow4	$3.3I_m$	$2V_m$	$6.6V_mI_m$	Irow4	$2.7I_m$	$3V_m$	$\mathbf{8.1V_mI_m}$
Irow3	$0.8I_m$	$4V_m$	$3.2V_mI_m$	Irow3	$0.8I_m$	$4V_m$	$3.2V_mI_m$	Irow3	$1.8I_m$	$4V_m$	$\mathbf{7.2V_mI_m}$	Irow3	$2.7I_m$	$3V_m$	$\mathbf{8.1V_mI_m}$
Irow2	$1.2I_m$	$3V_m$	$3.6V_mI_m$	Irow2	$1.2I_m$	$4V_m$	$\mathbf{4.8V_mI_m}$	Irow2	$1.7I_m$	$4V_m$	$6.8V_mI_m$	Irow2	$2.7I_m$	$3V_m$	$\mathbf{8.1V_mI_m}$
Irow1	$4I_m$	$1V_m$	$\mathbf{4V_mI_m}$	Irow1	$4I_m$	$1V_m$	$4V_mI_m$	Irow1	$3.2I_m$	$2V_m$	$6.4V_mI_m$	Irow1	$2.7I_m$	$3V_m$	$\mathbf{8.1V_mI_m}$

The results presented in Figure 30 and Table 11 show that the proposed 8-Queen's technique was well able to implement the process of reconfiguring the modules of the PV array with dimensions of 4×4. Among the comparative methods used in this paper, only techniques TCT interconnected, Magic Square puzzle, and d Distance were able to be implemented on this PV array, which the results showed the highest GMPP value of $8.1V_mI_m$ volts for the 8-Queen's technique.

4. Results evaluation

In this paper, 7 cases of the TCT PV arrays in different dimensions were evaluated under various shaded conditions for reconfiguring the modules by different solutions in order to distribute the shadows in the rows and extract the maximum production power. The results obtained in each case emphasize the superiority of the proposed technique of this paper in producing the highest output power. In addition, in this paper, the results of each method in MPPT are analyzed by different performance evaluation indicators. The FF, power efficiency (η), and Mismatch Losses (ML) perform these assessments in this paper. Each of these indicators is defined as follows:

A. Fill Factor (FF):

FF is a parameter that determines the maximum output power of a solar cell about open circuit voltage and short circuit current. The FF is expressed as follows:

$$FF\ (\%) = \frac{P_m}{I_{SC} \times V_{OC}} \times 100 \tag{34}$$

where P_m is the maximum extracted power, V_{OC} shows the open-circuit voltage, and I_{SC} represent the short circuit current.

B. Power efficiency (η):

Power efficiency (η) is the ratio between the maximum output power and the solar energy input (P_{in}), and is calculated as follows:

$$\eta\ (\%) = \frac{P_m}{P_{in}} \times 100\% \tag{35}$$

C. Mismatch losses:

ML represents the difference between the maximum power under uniform radiation and the GMPP under PSC. The ML can be calculated as follows:

$$\text{ML}\ (\%) = \frac{MPP_{uniform} - GMPP_{PSCs}}{GMPP_{PSCs}} \times 100\% \tag{36}$$

where MPP_{uni} shows the maximum power under uniform radiation and $GMPP_{PSCs}$ demonstrate the GMPP under PSC.

Accordingly, the results of evaluations to extract the maximum production output power of the studied PV arrays in cases 1-7 by performance evaluation indicators are presented in Figures 31-37, respectively.

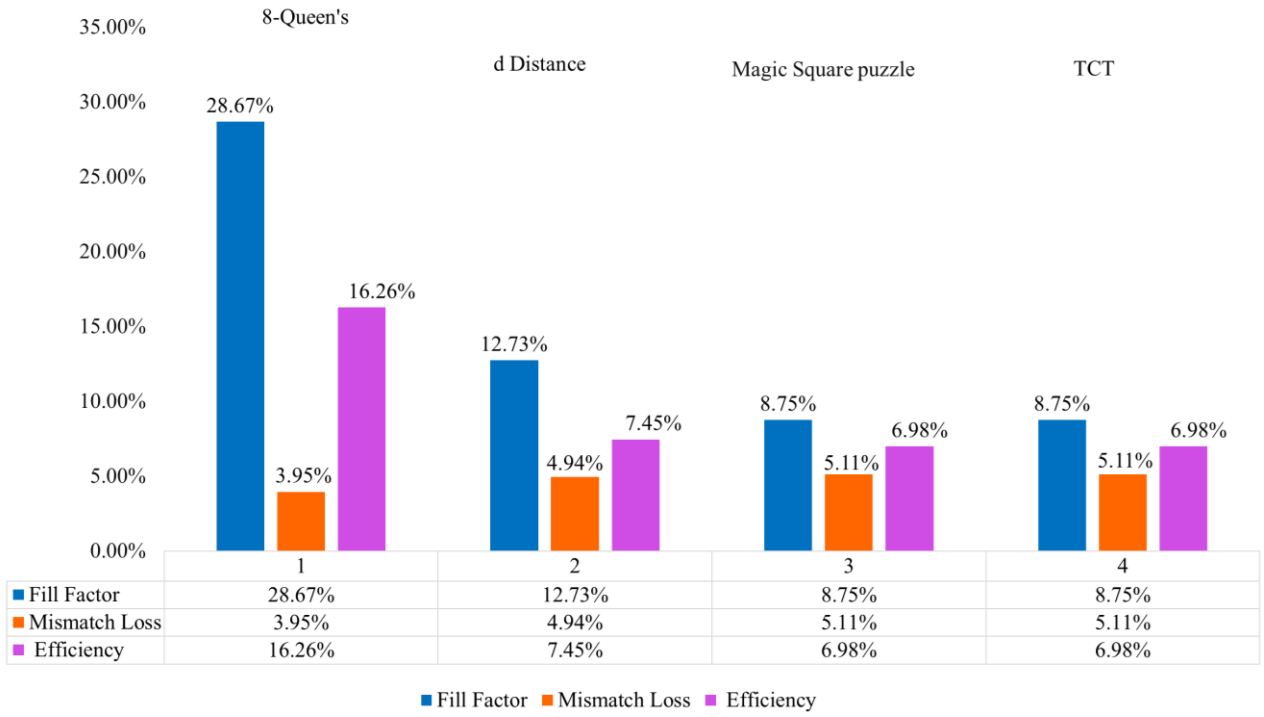

Figure 31. Result evaluations for extracting maximum power point of the PV array in case 1

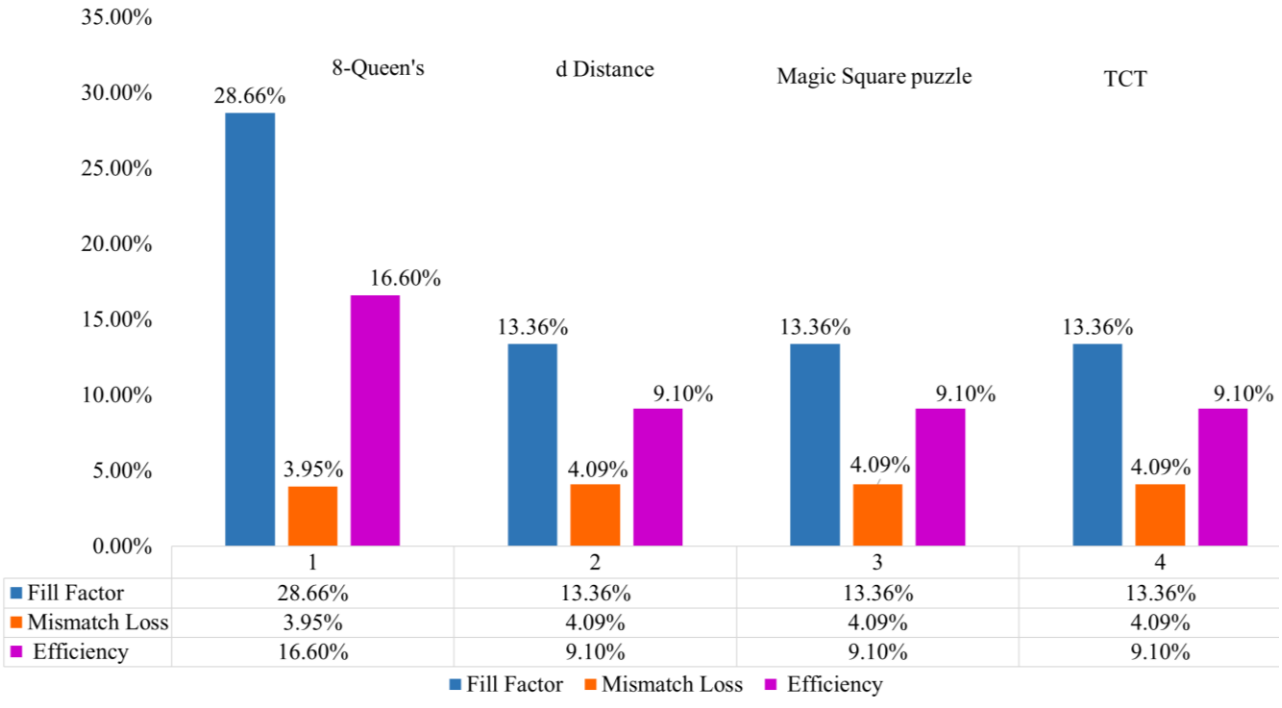

Figure 32. Result evaluations for extracting maximum power point of the PV array in case 2

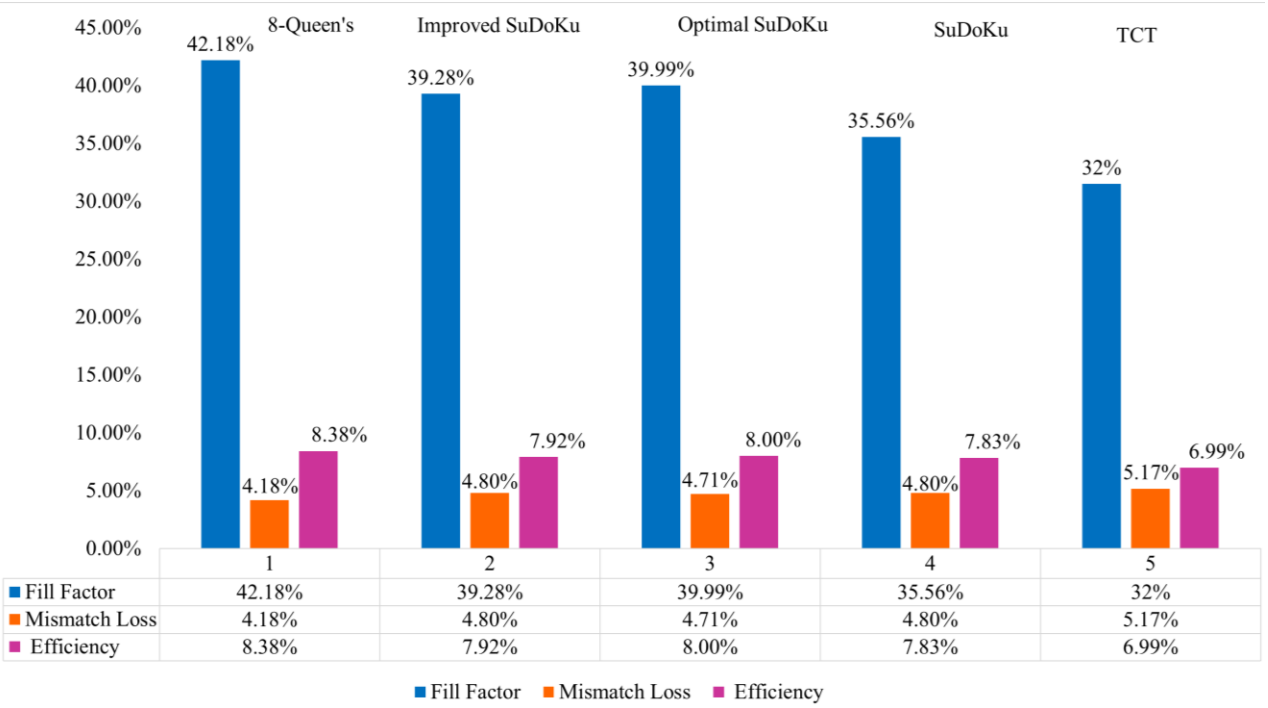

	1	2	3	4	5
Fill Factor	42.18%	39.28%	39.99%	35.56%	32%
Mismatch Loss	4.18%	4.80%	4.71%	4.80%	5.17%
Efficiency	8.38%	7.92%	8.00%	7.83%	6.99%

Figure 33. Result evaluations for extracting maximum power point of the PV array in case 3

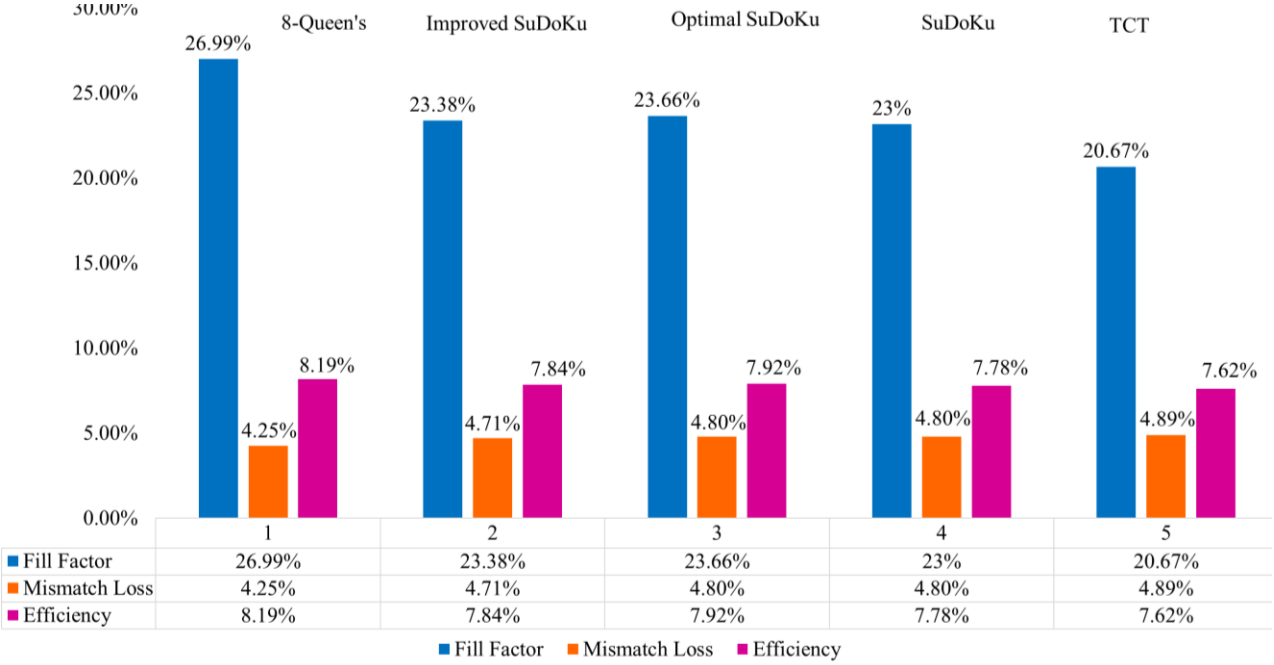

	1	2	3	4	5
Fill Factor	26.99%	23.38%	23.66%	23%	20.67%
Mismatch Loss	4.25%	4.71%	4.80%	4.80%	4.89%
Efficiency	8.19%	7.84%	7.92%	7.78%	7.62%

Figure 34. Result evaluations for extracting maximum power point of the PV array in case 4

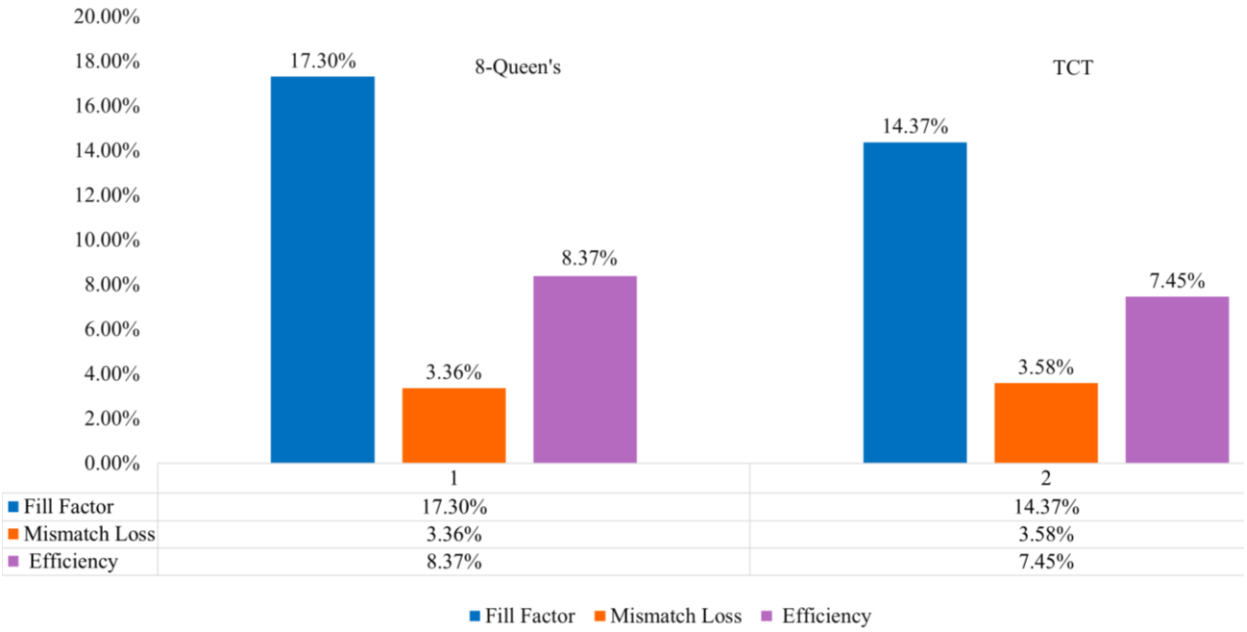

Figure 35. Result evaluations for extracting maximum power point of the PV array in case 5

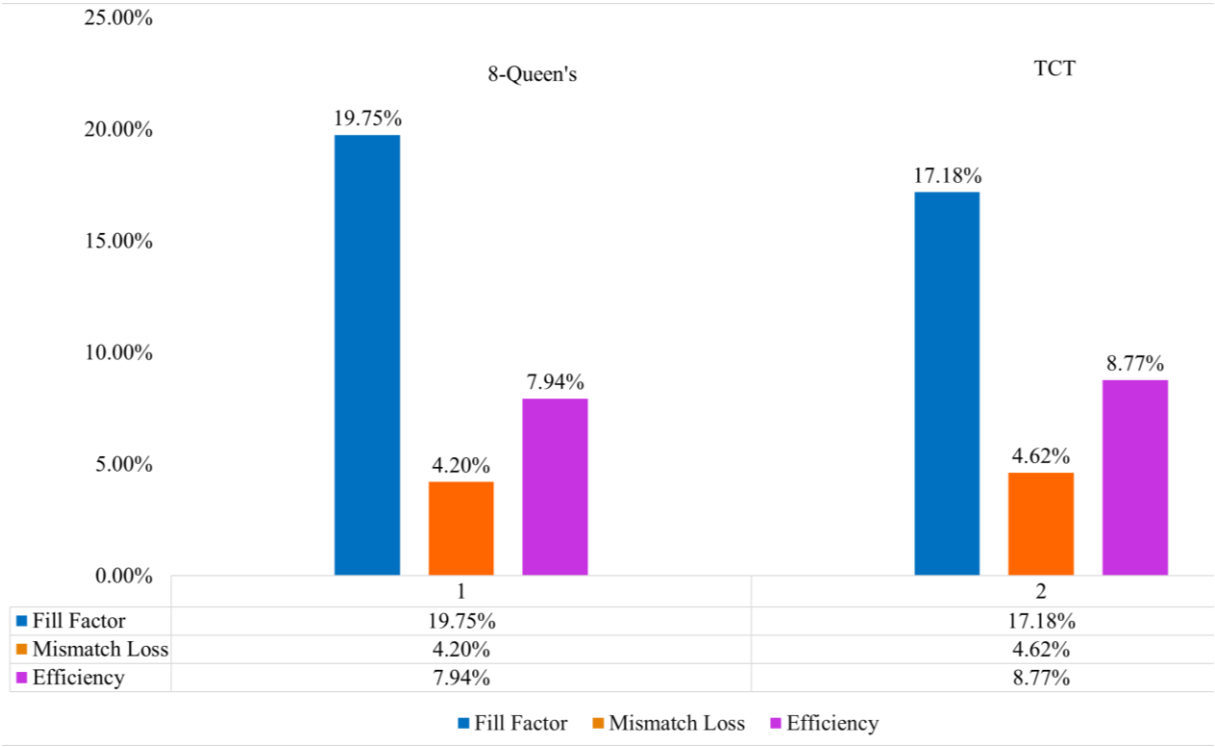

Figure 36. Result evaluations for extracting maximum power point of the PV array in case 6

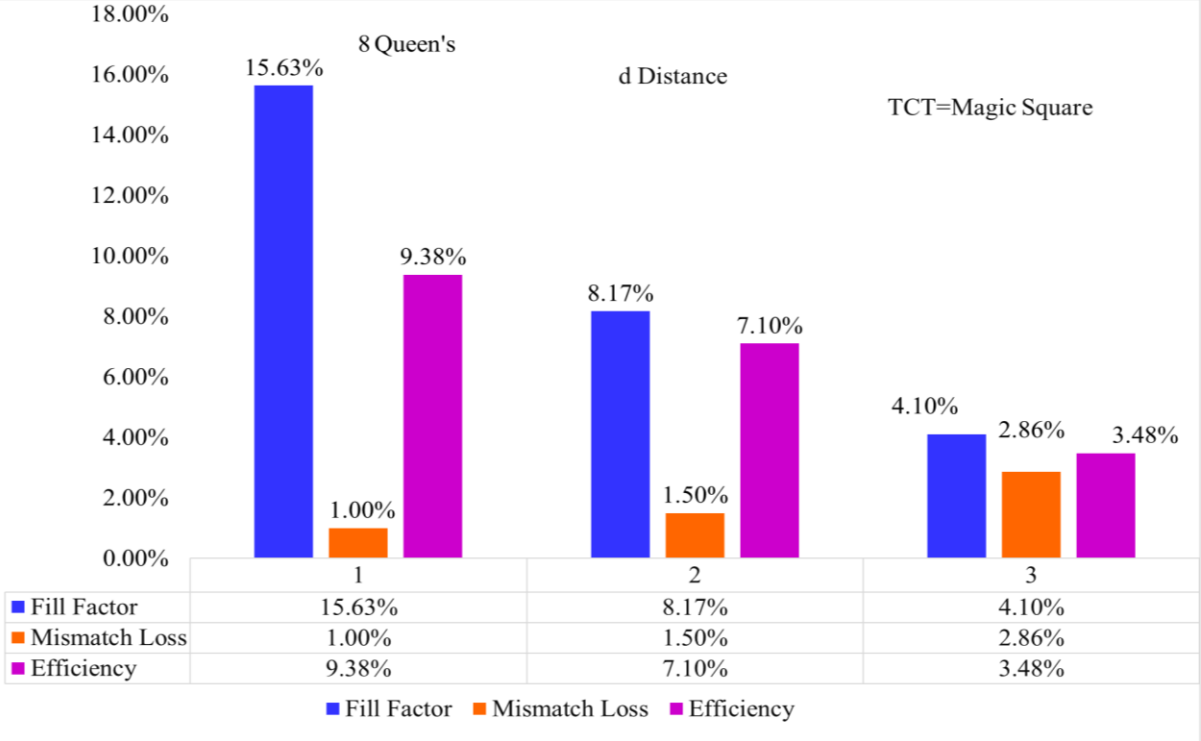

Figure 37. Result evaluations for extracting maximum power point of the PV array in case 7

Evaluation of results was performed for all cases studied. Each of the methods used to distribute the shadow in the TCT PV array provided some output power. It was observed that among the utilized methods, the 8-Queen's technique was able to show its effectiveness compared to other methods used by extracting the output power values of $22.2I_mV_m, 22.2I_mV_m, 67.5I_mV_m, 66.6I_mV_m, 126I_mV_m, 346I_mV_m,$ and $8.1I_mV_m$, respectively, for cases 1-7. In evaluating the performance of each method, it was also observed that the proposed technique had the best performance with the lowest ML per case and with maximum efficiency values of 16.26%, 16.6%, 8.38%, 8.19%, 8.37%, 8.77%, and 9.38% for cases 1-7, respectively. In addition, the very high-performance speed and the application and presentation of the best reconfiguration results on large-size and rectangular PV arrays were other capabilities of the 8-Queen's technique in this paper.

The presented results showed the effectiveness of the 8-Queen's method. In addition, no need for switching and no effect on increasing power losses are other salient features of the proposed static-based 8-Queen's method. However, the important point to consider is evaluating the behavior and performance of this method on real-world PV arrays. As such, real-world PV arrays typically contain measurement errors. The PV arrays reconfiguration process is performed by all available techniques based on the voltage and current parameters obtained from the PV system, and the combination of these values with the measurement error reduces the performance accuracy of the method used and interfere with the reconfiguration results.

In this paper, in order to analysis the efficiency of the proposed procedure in reconfiguring the modules of real-world PV arrays, samples of voltage and current parameters with measurement errors are utilized. Measurement errors were modeled once by decreasing and increasing the voltage values by 5% and 10% and again by decreasing and increasing the current values by 5% and 10%. This test was done optionally on the first case to analysis the efficiency of the 8-Queen's method in reconfiguration and access to GMPP in real-world samples. Table 12 shows

the GMPP results obtained for reconfiguration under measurement error on the voltage parameters in the first case PV model. Table 13 shows the GMPP results obtained for reconfiguration under measurement error on the current parameters in the first case PV model.

Table 12. The results of the obtained GMPP for the reconfiguration under measurement error on the voltage parameters in the first case study

Error type	Row bypassed	Current	Voltage	Power
Decrease 5 %	Irow9	$7.13I_m$	$8.55V_m$	$\mathbf{60.96I_mV_m}$
	Irow8	$7.13I_m$	$8.55V_m$	$\mathbf{60.96I_mV_m}$
	Irow7	$7.13I_m$	$8.55V_m$	$\mathbf{60.96I_mV_m}$
	Irow6	$7.13I_m$	$8.55V_m$	$\mathbf{60.96I_mV_m}$
	Irow5	$7.13I_m$	$8.55V_m$	$\mathbf{60.96I_mV_m}$
	Irow4	$7.13I_m$	$8.55V_m$	$\mathbf{60.96I_mV_m}$
	Irow3	$7.13I_m$	$8.55V_m$	$\mathbf{60.96I_mV_m}$
	Irow2	$7.89I_m$	$7.55V_m$	$59.56I_mV_m$
	Irow1	$7.79I_m$	$6.55V_m$	$51.02I_mV_m$
Increase 5 %	Irow9	$٧٫٨٧I_m$	$٩.45V_m$	$\mathbf{74.37I_mV_m}$
	Irow8	$٧٫٨٧I_m$	$٩.45V_m$	$\mathbf{74.37I_mV_m}$
	Irow7	$٧٫٨٧I_m$	$٩.45V_m$	$\mathbf{74.37I_mV_m}$
	Irow6	$٧٫٨٧I_m$	$٩.45V_m$	$\mathbf{74.37I_mV_m}$
	Irow5	$٧٫٨٧I_m$	$٩.45V_m$	$\mathbf{74.37I_mV_m}$
	Irow4	$٧٫٨٧I_m$	$٩.45V_m$	$\mathbf{74.37I_mV_m}$
	Irow3	$٧٫٨٧I_m$	$٩.45V_m$	$\mathbf{74.37I_mV_m}$
	Irow2	$8.٧١I_m$	$٨.45V_m$	$73.59I_mV_m$
	Irow1	$8.٤١I_m$	$٧.45V_m$	$64.4\ I_mV_m$
Decrease 10 %	Irow9	$٦٫٧٥I_m$	$8.1V_m$	$\mathbf{54.67I_mV_m}$
	Irow8	$٦٫٧٥I_m$	$8.1V_m$	$\mathbf{54.67I_mV_m}$
	Irow7	$٦٫٧٥I_m$	$8.1V_m$	$\mathbf{54.67I_mV_m}$
	Irow6	$٦٫٧٥I_m$	$8.1V_m$	$\mathbf{54.67I_mV_m}$
	Irow5	$٦٫٧٥I_m$	$8.1V_m$	$\mathbf{54.67I_mV_m}$
	Irow4	$٦٫٧٥I_m$	$8.1V_m$	$\mathbf{54.67I_mV_m}$
	Irow3	$٦٫٧٥I_m$	$8.1V_m$	$\mathbf{54.67I_mV_m}$
	Irow2	$٧٫٤٧I_m$	$7.2V_m$	$53.78I_mV_m$
	Irow1	$٧٫٣٨I_m$	$6.3V_m$	$46.49I_mV_m$
Increase 10 %	Irow9	$٨٫٢٥I_m$	$٩.9V_m$	$\mathbf{81.67I_mV_m}$
	Irow8	$٨٫٢٥I_m$	$٩.9V_m$	$\mathbf{81.67I_mV_m}$
	Irow7	$٨٫٢٥I_m$	$٩.9V_m$	$\mathbf{81.67I_mV_m}$
	Irow6	$٨٫٢٥I_m$	$٩.9V_m$	$\mathbf{81.67I_mV_m}$
	Irow5	$٨٫٢٥I_m$	$٩.9V_m$	$\mathbf{81.67I_mV_m}$
	Irow4	$٨٫٢٥I_m$	$٩.9V_m$	$\mathbf{81.67I_mV_m}$
	Irow3	$٨٫٢٥I_m$	$٩.9V_m$	$\mathbf{81.67I_mV_m}$
	Irow2	$٩.١٣I_m$	$٨.8V_m$	$80.34I_mV_m$
	Irow1	$٩.٠٢I_m$	$٧.7V_m$	$69.45I_mV_m$

Table 13. The results of the obtained GMPP for the reconfiguration under measurement error on the current parameters in the first case study

Error type	Row bypassed	Current	Voltage	Power
Decrease 5 %	Irow9	$7.13I_m$	$9V_m$	$\mathbf{64.17I_mV_m}$
	Irow8	$7.13I_m$	$9V_m$	$\mathbf{64.17I_mV_m}$
	Irow7	$7.13I_m$	$٩V_m$	$\mathbf{64.17I_mV_m}$
	Irow6	$7.13I_m$	$9V_m$	$\mathbf{64.17I_mV_m}$
	Irow5	$7.13I_m$	$9V_m$	$\mathbf{64.17I_mV_m}$
	Irow4	$7.13I_m$	$9V_m$	$\mathbf{64.17I_mV_m}$
	Irow3	$7.13I_m$	$9V_m$	$\mathbf{64.17I_mV_m}$
	Irow2	$7.89I_m$	$8V_m$	$63.12I_mV_m$
	Irow1	$7.79I_m$	$7V_m$	$54.53I_mV_m$
Increase 5 %	Irow9	$٧٫٨٧I_m$	$٩V_m$	$\mathbf{٧٠٫٨٣I_mV_m}$
	Irow8	$٧٫٨٧I_m$	$٩V_m$	$\mathbf{٧٠٫٨٣I_mV_m}$
	Irow7	$٧٫٨٧I_m$	$٩V_m$	$\mathbf{٧٠٫٨٣I_mV_m}$
	Irow6	$٧٫٨٧I_m$	$٩V_m$	$\mathbf{٧٠٫٨٣I_mV_m}$

	Irow5	۷/۸۷I_m	۹V_m	**۷۰/۸۳I_mV_m**
	Irow4	۷/۸۷I_m	۹V_m	**۷۰/۸۳I_mV_m**
	Irow3	۷/۸۷I_m	۹V_m	**۷۰/۸۳I_mV_m**
	Irow2	8.۷۱I_m	۸V_m	۶۹/۶I_mV_m
	Irow1	8.۶۱I_m	۷V_m	۶۰/۲I_mV_m
Decrease 10 %	Irow9	۶/۷۵I_m	۹V_m	**۶۰/۷۵I_mV_m**
	Irow8	۶/۷۵I_m	۹V_m	**۶۰/۷۵I_mV_m**
	Irow7	۶/۷۵I_m	۹V_m	**۶۰/۷۵I_mV_m**
	Irow6	۶/۷۵I_m	۹V_m	**60.۷۵I_mV_m**
	Irow5	۶/۷۵I_m	۹V_m	**۶۰/۷۵I_mV_m**
	Irow4	۶/۷۵I_m	۹V_m	**۶۰/۷۵I_mV_m**
	Irow3	۶/۷۵I_m	۹V_m	**۶۰/۷۵I_mV_m**
	Irow2	۷/۴۷I_m	۸V_m	۵۹/۷۶I_mV_m
	Irow1	۷/۳۸I_m	۷V_m	۵۱/۶۶I_mV_m
Increase 10 %	Irow9	۸/۲۵I_m	۹V_m	**۷۴.۲۵I_mV_m**
	Irow8	۸/۲۵I_m	۹V_m	**۷۴.۲۵I_mV_m**
	Irow7	۸/۲۵I_m	۹V_m	**۷۴.2۵I_mV_m**
	Irow6	۸/۲۵I_m	۹V_m	**۷۴.۲۵I_mV_m**
	Irow5	۸/۲۵I_m	۹V_m	**۷۴.2۵I_mV_m**
	Irow4	۸/۲۵I_m	۹V_m	**۷۴.۲۵I_mV_m**
	Irow3	۸/۲۵I_m	۹V_m	**۷۴.2۵I_mV_m**
	Irow2	۹.۱۳I_m	۸V_m	۷۳.۰۴I_mV_m
	Irow1	۹.۰۲I_m	۷V_m	۶۳.۱۴I_mV_m

From the results presented in Tables 12 and 13, it can be seen that the change in voltage and current values also changes the value obtained for GMPP. However, it can be seen that the 8-Queen's method, in a situation where voltage and current parameters suffer from measurement error, can provide the highest GMPP values than other techniques that used clean voltage and current measurements. It should be noted that the proposed technique can be employed for the real-world PV arrays and can be considered as a suitable tool for the solar energy efficiency of the PV panels under PSCs.

5. Conclusions

Partial shading is one of the most important problems that make it difficult to extract maximum power from photovoltaic (PV) arrays. This issue has raised many challenges so far and various methods have been proposed to solve this problem. However, in this paper, a static-based technique for reconfiguration of the PV modules to increase maximum output power under partial shading conditions (PSC) was presented. The proposed procedure is called 8-Queen's and is based on the movement of the Queens on the chessboard and solves the problem in such a way that none of the Queens can attack the other. The 8-Queen's procedure was applied to 7 cases of the PV arrays with the TCT inter-connection and different PSCs for maximum power point tracking (MPPT). In addition, the PV modules related to the TCT PV arrays of all 7 cases were reconfigured using other reconfiguration methods such as Magic Square puzzle, d Distance, Sudoku, optimal Sudoku, and improved Sudoku. The results of used methods in the MPPT were analyzed through various evaluation indicators such as global maximum power point (GMPP), fill factor, power efficiency, and mismatch losses (ML). Finally, the obtained highest values of GMPP i.e. $22.2I_mV_m, 22.2I_mV_m, 67.5I_mV_m, 66.6I_mV_m, 126I_mV_m, 346I_mV_m,$ and $8.1I_mV_m$ for cases 1-7, respectively, by the 8-Queen's technique, emphasized the ability and high performance of this method than the other selected methods. In addition, the 8-Queen's technique compared to the

other methods had minimum values of ML i.e. 3.95%, 3.95%, 4.18%, 4.25%, 3.365, 4.20%, and 1% for cases 1-7, respectively, that indicating the superiority of the suggested procedure.

It should be noted that the 8-Queen's technique can also be employed as a state-of-the-art solution for reconfiguration of the PV arrays in the real world. According to the results and modeling of real-world PV arrays, it is recommended to use the proposed method to achieve the maximum power point and optimal operation of real PV systems. Thus, the algorithm of the proposed 8-Queen's method is prepared as a code and is installed in the PV system using a microcontroller to perform the process of reconfiguration PV array modules under PSCs.

References

[1] Sadeghian O, Moradzadeh A, Mohammadi-Ivatloo B, Abapour M, Anvari-Moghaddam A, Shiun Lim J, et al. A comprehensive review on energy saving options and saving potential in low voltage electricity distribution networks: Building and public lighting. Sustainable Cities and Society 2021;72:103064. https://doi.org/10.1016/j.scs.2021.103064.

[2] Moradzadeh A, Mohammadi-Ivatloo B, Abapour M, Anvari-Moghaddam A, Gholami Farkoush S, Rhee S-B. A practical solution based on convolutional neural network for non-intrusive load monitoring. Journal of Ambient Intelligence and Humanized Computing 2021;12:9775–89. https://doi.org/10.1007/s12652-020-02720-6.

[3] Pillai DS, Prasanth Ram J, Siva Sai Nihanth M, Rajasekar N. A simple, sensorless and fixed reconfiguration scheme for maximum power enhancement in PV systems. Energy Conversion and Management 2018;172:402–17. https://doi.org/10.1016/j.enconman.2018.07.016.

[4] Shahsavari A, Akbari M. Potential of solar energy in developing countries for reducing energy-related emissions. Renewable and Sustainable Energy Reviews 2018;90:275–91. https://doi.org/10.1016/j.rser.2018.03.065.

[5] Mellit A, Tina GM, Kalogirou SA. Fault detection and diagnosis methods for photovoltaic systems: A review. Renewable and Sustainable Energy Reviews 2018;91:1–17. https://doi.org/10.1016/j.rser.2018.03.062.

[6] Madeti SR, Singh SN. A comprehensive study on different types of faults and detection techniques for solar photovoltaic system. Solar Energy 2017;158:161–85. https://doi.org/10.1016/j.solener.2017.08.069.

[7] Ram JP, Babu TS, Rajasekar N. A comprehensive review on solar PV maximum power point tracking techniques. Renewable and Sustainable Energy Reviews 2017;67:826–47. https://doi.org/10.1016/j.rser.2016.09.076.

[8] Djellouli A, Lakdja F, Rachid M. Control and Management of Hybrid Renewable Energy System. Smart Innovation, Systems and Technologies, vol. 150, 2019, p. 1–10. https://doi.org/10.1007/978-3-030-22964-1_1.

[9] Li Y, Ding K, Zhang J, Chen F, Chen X, Wu J. A fault diagnosis method for photovoltaic arrays based on fault parameters identification. Renewable Energy 2019;143:52–63. https://doi.org/10.1016/j.renene.2019.04.147.

[10] Drif M, Pérez PJ, Aguilera J, Aguilar JD. A new estimation method of irradiance on a partially shaded PV generator in grid-connected photovoltaic systems. Renewable

Energy 2008;33:2048–56. https://doi.org/10.1016/j.renene.2007.12.010.

[11] Braun H, Buddha ST, Krishnan V, Tepedelenlioglu C, Spanias A, Banavar M, et al. Topology reconfiguration for optimization of photovoltaic array output. Sustainable Energy, Grids and Networks 2016;6:58–69. https://doi.org/10.1016/j.segan.2016.01.003.

[12] Karatepe E, Boztepe M, Çolak M. Development of a suitable model for characterizing photovoltaic arrays with shaded solar cells. Solar Energy 2007;81:977–92. https://doi.org/10.1016/j.solener.2006.12.001.

[13] Sai Krishna G, Moger T. Improved SuDoKu reconfiguration technique for total-cross-tied PV array to enhance maximum power under partial shading conditions. Renewable and Sustainable Energy Reviews 2019;109:333–48. https://doi.org/10.1016/j.rser.2019.04.037.

[14] Sanseverino ER, Ngoc TN, Cardinale M, Li Vigni V, Musso D, Romano P, et al. Dynamic programming and Munkres algorithm for optimal photovoltaic arrays reconfiguration. Solar Energy 2015;122:347–58. https://doi.org/10.1016/j.solener.2015.09.016.

[15] Akrami M, Pourhossein K. A novel reconfiguration procedure to extract maximum power from partially-shaded photovoltaic arrays. Solar Energy 2018;173:110–9. https://doi.org/10.1016/j.solener.2018.06.067.

[16] Sai Krishna G, Moger T. Reconfiguration strategies for reducing partial shading effects in photovoltaic arrays: State of the art. Solar Energy 2019;182:429–52. https://doi.org/10.1016/j.solener.2019.02.057.

[17] Ajmal AM, Sudhakar Babu T, Ramachandaramurthy VK, Yousri D, Ekanayake JB. Static and dynamic reconfiguration approaches for mitigation of partial shading influence in photovoltaic arrays. Sustainable Energy Technologies and Assessments 2020;40:100738. https://doi.org/10.1016/j.seta.2020.100738.

[18] Belhachat F, Larbes C. PV array reconfiguration techniques for maximum power optimization under partial shading conditions: A review. Solar Energy 2021;230:558–82. https://doi.org/10.1016/j.solener.2021.09.089.

[19] Yang B, Ye H, Wang J, Li J, Wu S, Li Y, et al. PV arrays reconfiguration for partial shading mitigation: Recent advances, challenges and perspectives. Energy Conversion and Management 2021;247:114738. https://doi.org/10.1016/j.enconman.2021.114738.

[20] Salameh ZM, Dagher F. The effect of electrical array reconfiguration on the performance of a pv-powered volumetric water pump. IEEE Transactions on Energy Conversion 1990;5:653–8. https://doi.org/10.1109/60.63135.

[21] Salameh ZM, Liang C. Optimum switching points for array reconfiguration controller. IEEE Conference on Photovoltaic Specialists, vol. 2, IEEE; 1990, p. 971–6. https://doi.org/10.1109/PVSC.1990.111762.

[22] Velasco-Quesada G, Guinjoan-Gispert F, Pique-Lopez R, Roman-Lumbreras M, Conesa-Roca A. Electrical PV Array Reconfiguration Strategy for Energy Extraction Improvement in Grid-Connected PV Systems. IEEE Transactions on Industrial Electronics 2009;56:4319–31. https://doi.org/10.1109/TIE.2009.2024664.

[23] Srinivasan A, Devakirubakaran S, Sundaram BM, Balachandran PK, Cherukuri SK,

Winston DP, et al. L-Shape Propagated Array Configuration With Dynamic Reconfiguration Algorithm for Enhancing Energy Conversion Rate of Partial Shaded Photovoltaic Systems. IEEE Access 2021;9:97661–74. https://doi.org/10.1109/ACCESS.2021.3094736.

[24] Etezadinejad M, Asaei B, Farhangi S, Anvari-Moghaddam A. An Improved and Fast MPPT Algorithm for PV Systems under Partially Shaded Conditions. IEEE Transactions on Sustainable Energy 2021:1–1. https://doi.org/10.1109/TSTE.2021.3130827.

[25] Shams El-Dein MZ, Kazerani M, Salama MMA. Optimal photovoltaic array reconfiguration to reduce partial shading losses. IEEE Transactions on Sustainable Energy 2013;4:145–53. https://doi.org/10.1109/TSTE.2012.2208128.

[26] Nguyen D, Lehman B. An Adaptive Solar Photovoltaic Array Using Model-Based Reconfiguration Algorithm. IEEE Transactions on Industrial Electronics 2008;55:2644–54. https://doi.org/10.1109/TIE.2008.924169.

[27] Dzung Nguyen, Lehman B. A reconfigurable solar photovoltaic array under shadow conditions. 2008 Twenty-Third Annual IEEE Applied Power Electronics Conference and Exposition, IEEE; 2008, p. 980–6. https://doi.org/10.1109/APEC.2008.4522840.

[28] Alahmad M, Chaaban MA, Lau S kit, Shi J, Neal J. An adaptive utility interactive photovoltaic system based on a flexible switch matrix to optimize performance in real-time. Solar Energy 2012;86:951–63. https://doi.org/10.1016/j.solener.2011.12.028.

[29] Tabanjat A, Becherif M, Hissel D. Reconfiguration solution for shaded PV panels using switching control. Renewable Energy 2015;82:4–13. https://doi.org/10.1016/j.renene.2014.09.041.

[30] Parlak KŞ. PV array reconfiguration method under partial shading conditions. International Journal of Electrical Power and Energy Systems 2014;63:713–21. https://doi.org/10.1016/j.ijepes.2014.06.042.

[31] Pillai DS, Rajasekar N, Ram JP, Chinnaiyan VK. Design and testing of two phase array reconfiguration procedure for maximizing power in solar PV systems under partial shade conditions (PSC). Energy Conversion and Management 2018;178:92–110. https://doi.org/10.1016/j.enconman.2018.10.020.

[32] Storey JP, Wilson PR, Bagnall D. Improved optimization strategy for irradiance equalization in dynamic photovoltaic arrays. IEEE Transactions on Power Electronics 2013;28:2946–56. https://doi.org/10.1109/TPEL.2012.2221481.

[33] La Manna D, Li Vigni V, Riva Sanseverino E, Di Dio V, Romano P. Reconfigurable electrical interconnection strategies for photovoltaic arrays: A review. Renewable and Sustainable Energy Reviews 2014;33:412–26. https://doi.org/10.1016/j.rser.2014.01.070.

[34] Spagnuolo G, Petrone G, Lehman B, Ramos Paja CA, Zhao Y, Orozco Gutierrez ML. Control of Photovoltaic Arrays: Dynamical Reconfiguration for Fighting Mismatched Conditions and Meeting Load Requests. IEEE Industrial Electronics Magazine 2015;9:62–76. https://doi.org/10.1109/MIE.2014.2360721.

[35] Liu Y, Pang Z, Cheng Z. Research on an adaptive solar photovoltaic array using shading degree model-based reconfiguration algorithm. 2010 Chinese Control and Decision

Conference, CCDC 2010, IEEE; 2010, p. 2356–60. https://doi.org/10.1109/CCDC.2010.5498823.

[36] Karakose M, Baygin M, Parlak KS. A new real-time reconfiguration approach based on neural network in partial shading for PV arrays. 2014 International Conference on Renewable Energy Research and Application (ICRERA), IEEE; 2014, p. 633–7. https://doi.org/10.1109/ICRERA.2014.7016462.

[37] Bouselham L, Hajji M, Hajji B, Bouali H. A New MPPT-based ANN for Photovoltaic System under Partial Shading Conditions. Energy Procedia 2017;111:924–33. https://doi.org/10.1016/j.egypro.2017.03.255.

[38] Karakose M, Baygin M. Image processing based analysis of moving shadow effects for reconfiguration in PV arrays. 2014 IEEE International Energy Conference (ENERGYCON), IEEE; 2014, p. 683–7. https://doi.org/10.1109/ENERGYCON.2014.6850500.

[39] Karakose M, Baygin M, Parlak KS, Baygin N, Akin E. A novel reconfiguration method using image processing based moving shadow detection, optimization, and analysis for PV Arrays*. Journal of Information Science and Engineering 2018;34:1307–28. https://doi.org/10.6688/JISE.201809_34(5).0012.

[40] Wang Y-J, Hsu P-C. An investigation on partial shading of PV modules with different connection configurations of PV cells. Energy 2011;36:3069–78. https://doi.org/10.1016/j.energy.2011.02.052.

[41] Mahmoud Y, El-Saadany EF. Enhanced Reconfiguration Method for Reducing Mismatch Losses in PV Systems. IEEE Journal of Photovoltaics 2017;7:1746–54. https://doi.org/10.1109/JPHOTOV.2017.2752708.

[42] Jazayeri M, Jazayeri K, Uysal S. Adaptive photovoltaic array reconfiguration based on real cloud patterns to mitigate effects of non-uniform spatial irradiance profiles. Solar Energy 2017;155:506–16. https://doi.org/10.1016/j.solener.2017.06.052.

[43] Srinivasa Rao P, Saravana Ilango G, Nagamani C. Maximum power from PV arrays using a fixed configuration under different shading conditions. IEEE Journal of Photovoltaics 2014;4:679–86. https://doi.org/10.1109/JPHOTOV.2014.2300239.

[44] Yadav AS, Pachauri RK, Chauhan YK, Choudhury S, Singh R. Performance enhancement of partially shaded PV array using novel shade dispersion effect on magic-square puzzle configuration. Solar Energy 2017;144:780–97. https://doi.org/10.1016/j.solener.2017.01.011.

[45] Yadav AS, Pachauri RK, Chauhan YK. Comprehensive investigation of PV arrays with puzzle shade dispersion for improved performance. Solar Energy 2016;129:256–85. https://doi.org/10.1016/j.solener.2016.01.056.

[46] Rani BI, Ilango GS, Nagamani C. Enhanced Power Generation From PV Array Under Partial Shading Conditions by Shade Dispersion Using Su Do Ku Configuration. IEEE Transactions on Sustainable Energy 2013;4:594–601. https://doi.org/10.1109/TSTE.2012.2230033.

[47] Potnuru SR, Pattabiraman D, Ganesan SI, Chilakapati N. Positioning of PV panels for reduction in line losses and mismatch losses in PV array. Renewable Energy 2015;78:264–75. https://doi.org/10.1016/j.renene.2014.12.055.

[48] Nihanth MSS, Ram JP, Pillai DS, Ghias AMYM, Garg A, Rajasekar N. Enhanced power production in PV arrays using a new skyscraper puzzle based one-time reconfiguration procedure under partial shade conditions (PSCs). Solar Energy 2019;194:209–24. https://doi.org/10.1016/j.solener.2019.10.020.

[49] Yadav K, Kumar B, D. S. Mitigation of Mismatch Power Losses of PV Array under Partial Shading Condition using novel Odd Even Configuration. Energy Reports 2020;6:427–37. https://doi.org/10.1016/j.egyr.2020.01.012.

[50] Reddy SS, Yammani C. A novel Magic-Square puzzle based one-time PV reconfiguration technique to mitigate mismatch power loss under various partial shading conditions. Optik 2020;222:165289. https://doi.org/10.1016/j.ijleo.2020.165289.

[51] Vijayalekshmy S, Bindu GR, Rama Iyer S. A novel Zig-Zag scheme for power enhancement of partially shaded solar arrays. Solar Energy 2016;135:92–102. https://doi.org/10.1016/j.solener.2016.05.045.

[52] Rezazadeh S, Moradzadeh A, Hashemzadeh SM, Pourhossein K, Mohammadi-Ivatloo B, Hosseini SH. A novel prime numbers-based PV array reconfiguration solution to produce maximum energy under partial shade conditions. Sustainable Energy Technologies and Assessments 2021;47:101498. https://doi.org/10.1016/j.seta.2021.101498.

[53] Cherukuri SK, Balachandran PK, Kaniganti KR, Buddi MK, Butti D, Devakirubakaran S, et al. Power Enhancement in Partial Shaded Photovoltaic System Using Spiral Pattern Array Configuration Scheme. IEEE Access 2021;9:123103–16. https://doi.org/10.1109/ACCESS.2021.3109248.

[54] Palpandian M, Winston DP, Kumar BP, Kumar CS, Babu TS, Alhelou HH. A New Ken-Ken Puzzle Pattern Based Reconfiguration Technique for Maximum Power Extraction in Partial Shaded Solar PV Array. IEEE Access 2021;9:65824–37. https://doi.org/10.1109/ACCESS.2021.3076608.

[55] Venkateswari R, Rajasekar N. Power enhancement of PV system via physical array reconfiguration based Lo Shu technique. Energy Conversion and Management 2020;215:112885. https://doi.org/10.1016/j.enconman.2020.112885.

[56] Zhang X, Li C, Li Z, Yin X, Yang B, Gan L, et al. Optimal mileage-based PV array reconfiguration using swarm reinforcement learning. Energy Conversion and Management 2021;232:113892. https://doi.org/10.1016/j.enconman.2021.113892.

[57] Sahu HS, Nayak SK, Mishra S. Maximizing the Power Generation of a Partially Shaded PV Array. IEEE Journal of Emerging and Selected Topics in Power Electronics 2016;4:626–37. https://doi.org/10.1109/JESTPE.2015.2498282.

[58] Malathy S, Ramaprabha R. Reconfiguration strategies to extract maximum power from photovoltaic array under partially shaded conditions. Renewable and Sustainable Energy Reviews 2018;81:2922–34. https://doi.org/10.1016/j.rser.2017.06.100.

[59] Dhanalakshmi B, Rajasekar N. Dominance square based array reconfiguration scheme for power loss reduction in solar PhotoVoltaic (PV) systems. Energy Conversion and Management 2018;156:84–102. https://doi.org/10.1016/j.enconman.2017.10.080.

[60] Bell J, Stevens B. A survey of known results and research areas for n-queens. Discrete Mathematics 2009;309:1–31. https://doi.org/10.1016/j.disc.2007.12.043.

[61] Topor RW. Fundamental solutions of the eight queens problem. Bit 1982;22:42–52. https://doi.org/10.1007/BF01934394.

[62] https://www.geeksforgeeks.org/n-queen-problem-backtracking-3/ 2021. https://doi.org/https://www.geeksforgeeks.org/n-queen-problem-backtracking-3/.

[63] Alhassan A. Build and Conquer: Solving N Queens Problem using Iterative Compression. 2019 International Conference on Computer, Control, Electrical, and Electronics Engineering (ICCCEEE), IEEE; 2019, p. 1–5. https://doi.org/10.1109/ICCCEEE46830.2019.9070976.

[64] Azuma Y, Sakagami H, Kise K. An efficient parallel hardware scheme for solving the N-queens problem. Proceedings - 2018 IEEE 12th International Symposium on Embedded Multicore/Many-Core Systems-on-Chip, MCSoC 2018, IEEE; 2018, p. 16–22. https://doi.org/10.1109/MCSoC2018.2018.00015.

[65] Guldal S, Baugh V, Allehaibi S. N-Queens solving algorithm by sets and backtracking. Conference Proceedings - IEEE SOUTHEASTCON, vol. 2016- July, IEEE; 2016, p. 1–8. https://doi.org/10.1109/SECON.2016.7506688.

[66] Engelhardt MR. A group-based search for solutions of the n-queens problem. Discrete Mathematics 2007;307:2535–51. https://doi.org/10.1016/j.disc.2007.01.007.

[67] Osaba E, Diaz F, Carballedo R, Onieva E, Lopez P. A study on the impact of heuristic initialization functions in a genetic algorithm solving the N-queens problem. GECCO 2014 - Companion Publication of the 2014 Genetic and Evolutionary Computation Conference, New York, New York, USA: ACM Press; 2014, p. 1473–4. https://doi.org/10.1145/2598394.2602269.

[68] Aghazadeh Heris JE, Oskoei MA. Modified genetic algorithm for solving n-queens problem. 2014 Iranian Conference on Intelligent Systems, ICIS 2014, IEEE; 2014, p. 1–5. https://doi.org/10.1109/IranianCIS.2014.6802550.

[69] Martinjak I, Golub M. Comparison of Heuristic Algorithms for the N-Queen Problem. 2007 29th International Conference on Information Technology Interfaces, IEEE; 2007, p. 759–64. https://doi.org/10.1109/ITI.2007.4283867.

[70] Wang Y-R, Lin H-L, Yang L. Swarm Refinement PSO for Solving N-queens Problem. 2012 Third International Conference on Innovations in Bio-Inspired Computing and Applications, IEEE; 2012, p. 29–33. https://doi.org/10.1109/IBICA.2012.43.

[71] Khan S, Bilal M, Sharif M, Sajid M, Baig R. Solution of n-Queen problem using ACO. INMIC 2009 - 2009 IEEE 13th International Multitopic Conference, 2009. https://doi.org/10.1109/INMIC.2009.5383157.

[72] Le TN, Pham CK. A new N - Parallel updating method of the hopfield - Type neural network for N - Queens problem. Proceedings of the International Joint Conference on Neural Networks, vol. 2, IEEE; 2005, p. 788–91. https://doi.org/10.1109/IJCNN.2005.1555952.

[73] Wang RL, Tang Z, Cao QP. A new updating procedure in the Hopfield-type network and its application to N-Queens problem. IEICE Transactions on Fundamentals of Electronics, Communications and Computer Sciences 2002;E85-A:2368–72.

[74] Jesus de Souza F, Luis de Mello F. N-Queens Problem Resolution Using the Quantum Computing Model. IEEE Latin America Transactions 2017;15:534–40.

https://doi.org/10.1109/TLA.2017.7867605.

[75] Ohta M. Chaotic neural networks with reinforced self-feedbacks and its application to N-Queen problem. Mathematics and Computers in Simulation 2002;59:305–17. https://doi.org/10.1016/S0378-4754(01)00367-6.

[76] Ohta M. On the self-feedback controlled chaotic neural network and its application to N-Queen problem. IJCNN'99. International Joint Conference on Neural Networks. Proceedings (Cat. No.99CH36339), vol. 1, IEEE; 1999, p. 713–6. https://doi.org/10.1109/IJCNN.1999.831589.

[77] Paun G. P systems with Active Membranes: Attacking NP-Complete Problems. Journal of Automata, Languages and Combinatorics 2001;6:75–90.

[78] Maroosi A, Muniyandi RC. Accelerated execution of P systems with active membranes to solve the N-queens problem. Theoretical Computer Science 2014;551:39–54. https://doi.org/10.1016/j.tcs.2014.05.004.

[79] Gutiérrez-Naranjo MA, Martínez-del-Amor MA, Pérez-Hurtado I, Pérez-Jiménez MJ. Solving the N-Queens puzzle with P systems. 7th Brainstorming Week on Membrane Computing 2009;I:199–210.

[80] Bussey WH. A Note on the Problem of the Eight Queens. The American Mathematical Monthly 1922;29:252. https://doi.org/10.2307/2299223.

[81] Sosic R, Gu J. Fast search algorithms for the n-queens problem. IEEE Transactions on Systems, Man, and Cybernetics 1991;21:1572–6. https://doi.org/10.1109/21.135698.

[82] Schrage G. The eight queens problem as a strategy game. International Journal of Mathematical Education in Science and Technology 1986;17:143–8. https://doi.org/10.1080/0020739860170203.

[83] Pratt K. Closed-form expressions for the n-queens problem and related problems. International Mathematics Research Notices 2019;2019:1098–107. https://doi.org/10.1093/imrn/rnx119.

[84] Song B, Pérez-Jiménez MJ, Pan L. Computational efficiency and universality of timed P systems with membrane creation. Soft Computing 2015;19:3043–53. https://doi.org/10.1007/s00500-015-1732-3.

[85] Alhazov A, Leporati A, Mauri G, Porreca AE, Zandron C. Space complexity equivalence of P systems with active membranes and Turing machines. Theoretical Computer Science 2014;529:69–81. https://doi.org/10.1016/j.tcs.2013.11.015.

[86] Shiiba T, Fujiwara A. Solving Subset Sum Problem Using en P System with Active Membranes. Proceedings - 2016 Joint 8th International Conference on Soft Computing and Intelligent Systems and 2016 17th International Symposium on Advanced Intelligent Systems, SCIS-ISIS 2016, IEEE; 2016, p. 886–91. https://doi.org/10.1109/SCIS-ISIS.2016.0192.